Journal of Computational Physics 257 (2014) 1228–1259

Contents lists available at ScienceDirect

Journal of Computational Physics

www.elsevier.com/locate/jcp

Mimetic scalar products of discrete differential forms

F. Brezzi [a,c,b], A. Buffa [b], G. Manzini [b,c,d,*]

[a] King Abdulaziz University (KAU), Jeddah, Saudi Arabia
[b] Istituto di Matematica Applicata e Tecnologie Informatiche, Consiglio Nazionale delle Ricerche (IMATI-CNR), via Ferrata 1, I-27100 Pavia, Italy
[c] Centro di Simulazione Numerica Avanzata (CeSNA) – IUSS Pavia, v.le Lungo Ticino Sforza 56, I-27100 Pavia, Italy
[d] Los Alamos National Laboratory, Theoretical Division, Group T-5, MS B284, Los Alamos, NM 87545, USA

ARTICLE INFO

Article history:
Received 16 August 2012
Received in revised form 28 June 2013
Accepted 4 August 2013
Available online 28 August 2013

Keywords:
Discrete differential form
Mimetic finite difference method
Polyhedral mesh

ABSTRACT

We propose a strategy for the systematic construction of the mimetic inner products on cochain spaces for the numerical approximation of partial differential equations on unstructured polygonal and polyhedral meshes. The mimetic inner products are locally built in a recursive way on each k-cell and, then, globally assembled. This strategy is similar to the implementation of the finite element methods. The effectiveness of this approach is documented by deriving mimetic discretizations and testing their behavior on a set of problems related to the Maxwell equations.

Published by Elsevier Inc.

1. Introduction

The mimetic discretizations are based on the idea that some fundamental properties of the partial differential equations that have to be approximated can be incorporated in the formulation of the numerical methods. Such approach for the design of numerical schemes is intimately connected with the nature of the equations that we deal with and with their geometric structures. In fact, in many physical theories we can associate some of the simplest geometrical objects like points, lines, surfaces and volumes to the basic physical variables used in the mathematical formulation and establish a natural correspondence in the formal structure of such theories [24,70,85,86]. This fact is also the very profound reason for the success of mimetic discretizations like the *Support Operator Method* (SOM) [61,80,81], the *Mimetic Finite Difference* (MFD) method [31,32], and the very recent development of the *Virtual Finite Element* (VEM) method [10]. These methods have been successful in the numerical resolution of a wide range of scientific and engineering problems, such as continuum mechanics [68], electromagnetism [60,63], gas dynamics [35], linear diffusion [3,8,17,31,37,64,65,71], convection–diffusion [11,38], steady Stokes equations [12,13,16], elasticity [9], elliptic obstacle [4], Reissner–Mindlin plates [19], eigenvalues [36] and two-phase flows in porous media [1,66]. High-order mimetic discretizations for elliptic problems are also found in [7, 14,15,18,39–42,54,77].

As originally pointed out in [31], a mimetic method can be directly formulated in a variational way on the degrees of freedom through a *consistency condition*, which is an exactness property on a well-defined family of polynomials, and a *stability condition*, which ensures the well-posedness of the method. However, there is no need to determine the shape functions associated with such degrees of freedom and this feature provides a great flexibility of the mimetic discretizations, which can be easily formulated on general polygonal and polyhedral unstructured meshes. Moreover, the two minimal assumptions of consistency and stability mentioned above do not determine a single numerical scheme but a family of numerical schemes, see, for example, [32].

* Corresponding author at: Los Alamos National Laboratory, Theoretical Division, Group T-5, MS B284, Los Alamos, NM 87545, USA.
E-mail address: gmanzini@lanl.gov (G. Manzini).

0021-9991/$ – see front matter Published by Elsevier Inc.
http://dx.doi.org/10.1016/j.jcp.2013.08.017

In this work, we will reformulate the design and construction of such mimetic discretizations by using a few basic concepts from algebraic topology such as chains and cochains, boundary and coboundary operators, projection and reconstruction of differential forms, and inner products on cochain spaces. In particular, we shall identify the cochains with the numerical unknowns: pointwise scalar functions, line integrals, surface integrals, and volume integrals are all possible degrees of freedom. These degrees of freedom are the values taken by the discrete fields used to approximate the solution of partial differential equations, i.e., grid functions defined at the vertices, the edges, the faces and the elements of a mesh. This viewpoint is in agreement with the approximation of scalar functions by linear conforming Galerkin finite elements in H^1, of vector-valued function by edge elements and face elements in respectively $H(\mathrm{curl})$ and $H(\mathrm{div})$, and scalar functions by cell averages in L^2 as in the lowest-order discontinuous Galerkin method and in cell-centered finite volume methods. Thus, the main contribution of this paper is not the introduction of new mimetic spaces, but rather the unified presentation of such discretization spaces in the setting of differential forms.

These grid functions and all their linear combinations span the linear spaces of cochains and the coboundary operators are the most natural definition of discrete differential operators. The duality relation between the boundary and the coboundary operators incorporates a discrete version of the Stokes Theorem in the numerical formulation, which, therefore, embodies the core of a discrete exterior calculus.

Each cochain space is equipped with an inner product, which provides, in the language of differential geometry, a discrete representation of the Hodge star operator. Such representation is substantial in describing the properties of the material with which we are dealing, even when the problem is set in the vacuum. We require that these scalar products mimic the L^2-inner product for scalar functions and vector-valued functions. We formally derive all the mimetic inner products through the *reconstruction operators* that give back a differential form from a cochain. To this purpose, we introduce the concept of *complete set of reconstructions* and of *admissible reconstruction*. An admissible reconstruction is a member of a family of possible reconstructions, each one producing an acceptable mimetic inner product. We emphasize that these reconstructions never need to be computed in the implementation of the method, but are only theoretical tools that allows us to describe and analyze the properties that we want to set on our inner products. Since from any scalar product we derive a mimetic method, we normally deal with a family of methods instead of a single numerical method. However, every scalar product of a given family returns the same result when (at least) one of its two arguments is locally originated by the projection of a scalar or vector-valued function that is constant on each polygonal or polyhedral cell. This remarkable fact is the key point in our construction, ensuring the approximation properties of the methods.

Most of the ideas here considered are not at all new. The reconstruction of differential forms from cochains on meshes of simplexes dates back to the work of Whitney on discrete forms on simplex meshes in the context of the Whitney's Geometric Integration Theory [88]. Dodziuk [47] developed a finite difference framework for harmonic functions based on Hodge theory. Hyman and Scovel [57], and, more recently, Bochev and Hyman [22] developed a systematic topological approach to the design of finite difference methods. In a series of papers published since mid-nineties [58–62,79], Hyman, Shashkov, and collaborators derived discrete approximations of the divergence, gradient and curl using discrete analogs of the integral identities satisfied by the differential operators. It was developed a discrete analog of vector calculus on logically rectangular, non-orthogonal, non-smooth grids, the *Support Operator Method*, which was successfully applied to elliptic problems on rough grids with non-smooth non-isotropic diffusion coefficients. By constructing the adjoints to the natural discrete operators, they also developed a set of discrete first-order operators with complementary domains and ranges that can be combined with the original operators. An alternative approach that makes also use of topological and mimetic concepts is found in the works on covolumes methods (and applications to Maxwell's equations) by Yee [89], Nicolaides and co-authors [74–76] and Gross and Kotiuga [52,53]; Nicolaides and Trapp [73] and Trapp [87] proposed a unified formulation for covolume methods and SOM based on a reformulation of an underlying mimetic inner product. Using similar topological concepts, Mattiussi [69] observed similarities between numerical methods of very different nature, such as finite volumes, finite differences, and finite elements. Bossavit explored the connections between Whitney forms and mixed finite elements (Nedelec elements) [24–28] and its application to computational electromagnetism. Finite element techniques have been recently recast in the framework of Whitney forms and formalized in the *Finite Element Exterior Calculus* by Arnold and collaborators [5,6]. In this respect, we also mention the work by Hiptmair in [55,56] and the extensions proposed in [33,34]. Finally, it is worth mentioning that there also exist different approaches in finite volumes that are based on reconstructions from degrees of freedom [20,21,50,51,67] and duality relations [2,45,48].

The outline of the paper is as follows. In Section 2 we discuss the general mimetic framework for the discretization of differential forms. In Section 3 we discuss the construction of the mimetic inner products for a single element. In Section 4 we show examples of how this technology can be used to derive new numerical schemes, which are consistent and compatible, for partial differential equations. In Section 5 we offer the final remarks and conclusion.

2. Mimetic discretizations of differential forms

2.1. Chains, cochains and mimetic differential operators

2.1.1. Mesh notation and regularity

Let Ω be a three-dimensional polyhedral domain. The numerical treatment of a boundary value problem defined on the domain Ω requires a *sequence of mesh partitions* $\{\Omega_h\}$ of Ω for decreasing values of h, a characteristic length size. Each Ω_h

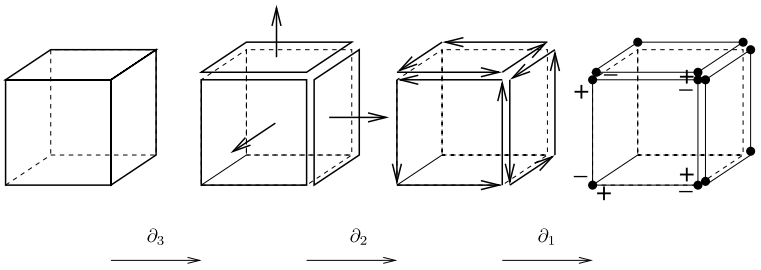

Fig. 1. The action of the boundary operators ∂_3, ∂_2 and ∂_1 on the chains $\mathcal{P}_{\mathsf{P}}$, $\mathcal{F}_{\mathsf{P}}$, $\mathcal{E}_{\mathsf{P}}$, $\mathcal{V}_{\mathsf{P}}$. Orientations are also shown.

is a decomposition of Ω formed by *vertices*, *edges*, *faces*, and *elements*. Each vertex v is a three-dimensional point of $\overline{\Omega}$, the closure of Ω in $\mathbb{R}^3$; each edge e is a straight segment; each face f is a two-dimensional bounded connected region that lies on a planar surface; each element P is a polyhedron. These geometric objects are oriented and so is Ω_h; in particular, we assume that the orientation of every edge and every face is fixed once and for all. The numerical methods for the approximation of the PDEs are usually defined on a sequence of meshes $\{\Omega_h\}$ of Ω. We require that all the meshes of $\{\Omega_h\}$ satisfy a few regularity conditions to avoid pathological situations, i.e., that "unreasonable" elements or faces take part in the sequence. To this end, we assume that:

(HG) there exists a strictly positive integer number $\mathcal{N}^s$, which is independent of h, such that
- (i) every polyhedron P of Ω_h admits a simplicial subdecomposition $\mathcal{S}^h_{\mathsf{P}}$ formed by less than $\mathcal{N}^s$ simplexes;
- (ii) $\mathcal{S}^h$, the mesh of simplexes collecting all polyhedron decompositions $\mathcal{S}^h_{\mathsf{P}}$, is a *regular and conforming* partition of Ω in the sense of Ciarlet [43].

Assumption (HG) is normally used to prove the convergence of the mimetic approximations. According to such conditions, polyhedral elements with very general shapes (also non-convex) are admissible, since the major restriction is that any element can be split into few regular simplexes in a general conforming way. Nonetheless, the existence of $\mathcal{S}^h$ is only a theoretical requirement and the practical implementation of the mimetic methods does not really need it.

Remark 2.1. It turns out that $\mathcal{S}^h$ is also a *three-dimensional simplicial complex*, see [72] for an extensive exposition of these concepts. In fact, the collection of the subdecompositions $\mathcal{S}^h_{\mathsf{P}}$ for $\mathsf{P} \in \mathcal{P}$ into regular tetrahedra (3-simplexes) induces a conforming decomposition of each mesh face into regular triangles (2-simplexes), and this latter induces a conforming decomposition of mesh edges into line segments (1-simplexes). Therefore, (i) every k-simplex in $\mathcal{S}^h$ for $1 \leqslant k \leqslant n = 3$ is formed by simplexes of lower dimension that are again in $\mathcal{S}^h$, and (ii) the intersection of any two distinct simplexes of any dimension of $\mathcal{S}^h$ is either a simplex of $\mathcal{S}^h$ or is empty.

2.1.2. Chains and the boundary operator

According to standard definitions in algebraic topology, we say that each vertex v is a 0-cell, each edge e is a 1-cell, each face f is a 2-cell, and each polyhedral element P is a 3-cell. The linear combinations of the k-cells with real coefficients forms the linear space of the *k-chains of* Ω_h, which is denoted by $\mathcal{C}_k(\Omega_h)$. For the sake of exposition, we also use the equivalent notation $\mathcal{V} \equiv \mathcal{C}_0(\Omega_h)$, $\mathcal{E} \equiv \mathcal{C}_1(\Omega_h)$, $\mathcal{F} \equiv \mathcal{C}_2(\Omega_h)$ and $\mathcal{P} \equiv \mathcal{C}_3(\Omega_h)$ and $\mathcal{T} = (\mathcal{V}, \mathcal{E}, \mathcal{F}, \mathcal{P})$.

A precise hierarchical structure exists for these geometric objects: any polyhedral element is bounded by a finite set of faces, any face is bounded by a set of edges and any edge connects a couple of vertices. We express this fundamental concept through the *boundary operator* $\partial_k : \mathcal{C}_k(\Omega_h) \to \mathcal{C}_{k-1}(\Omega_h)$. We assume that ∂_k is an *additive* operator so that its extension to the k-chains is straightforward once it has been defined on the basic geometric objects v, e, f and P. According to Fig. 1, we consider:

- $k = 0$, the boundary of a vertex is zero. Formally, $\partial_0 \mathsf{v} = 0$ for every $\mathsf{v} \in \mathcal{V}$;
- $k = 1$, the boundary of an edge is the formal difference between the vertices connected by that edge. We say that $\partial_1 \mathsf{e} = \mathsf{v}_2 - \mathsf{v}_1$ for every edge $\mathsf{e} \in \mathcal{E}$ that connects the couple of vertices v_1 and v_2 and is oriented from v_1 to v_2;
- $k = 2$, the boundary of a face is the formal linear combination of the oriented edges forming the polygonal line that encloses the face. We say that $\partial_2 \mathsf{f} = \sum_{i=1}^{N^{\mathcal{E}}_{\mathsf{f}}} s_{\mathsf{f},i} \mathsf{e}_i$ for every face $\mathsf{f} \in \mathcal{F}$ defined by the $N^{\mathcal{E}}_{\mathsf{f}}$ consecutive edges $\{\mathsf{e}_1, \mathsf{e}_2, \ldots, \mathsf{e}_{N^{\mathcal{E}}_{\mathsf{f}}}\}$. The symbol $s_{\mathsf{f},i}$ is the sign associated with the i-th edge, its value is either $+1$ or -1, and reflects the reciprocal orientation of the edge e_i and the face f;
- $k = 3$, the boundary of a polyhedral element is the linear combination of the oriented planar faces the union of which encloses the element. We say that $\partial \mathsf{P} = \sum_{i=1}^{N^{\mathcal{F}}_{\mathsf{P}}} s_{\mathsf{P},i} \mathsf{f}_i$ for every $\mathsf{P} \in \mathcal{P}$, defined by the $N^{\mathcal{F}}_{\mathsf{P}}$ faces $\{\mathsf{f}_1, \mathsf{f}_2, \ldots, \mathsf{f}_{N^{\mathcal{F}}_{\mathsf{P}}}\}$. The symbol $s_{\mathsf{P},i}$ is the sign associated with the i-th face, its value is either $+1$ or -1, and reflects the reciprocal orientation of the face f_i and the element P.

2.1.3. Cochains and the coboundary operator

On the algebraic topological structure $(\mathcal{V}, \mathcal{E}, \mathcal{F}, \mathcal{P})$ we consider the grid functions $(\mathcal{V}^h, \mathcal{E}^h, \mathcal{F}^h, \mathcal{P}^h)$ where:

- $\mathcal{V}^h$ is the set of *vertex functions* whose values are associated with the vertices of the mesh. A vertex function can be interpreted as the collection of the values of a scalar function at each mesh vertex;
- $\mathcal{E}^h$ is the set of *edge functions* whose values are associated with the edges of the mesh. An edge function can be interpreted as the collection of the line integrals of the tangential component of a vector-valued function along each mesh edge;
- $\mathcal{F}^h$ is the set of *face functions* whose values are associated with the faces of the mesh. A face function can be interpreted as the collection of the surface integrals of the normal component of a vector-valued function over each mesh face;
- $\mathcal{P}^h$ is the set of *element functions* whose values are associated with the polyhedral elements of the mesh. An element function can be interpreted as the collection of the volume integrals of a scalar function over each mesh element.

Remark 2.2. On a general mesh structure, a proper definition of edge variables and face variables require an orientation of edges and faces. Such orientation is the same that was considered in the definition of the boundary operator.

Each set of grid functions, e.g. $\mathcal{V}^h$, $\mathcal{E}^h$, $\mathcal{F}^h$ and $\mathcal{P}^h$, is isomorphic to a finite-dimensional linear space over $\mathbb{R}$ once we have introduced (in the obvious way) the sum of two elements of the same space and the multiplication by a real number. We say that the linear combinations of the grid functions form the linear space of the k-cochains on Ω_h for $k = 0, \dots, 3$, which we denote as $\mathcal{C}^k(\Omega_h)$. As we did for the k-chains, we identify $\mathcal{C}^0(\Omega_h) \equiv \mathcal{V}^h$, $\mathcal{C}^1(\Omega_h) \equiv \mathcal{E}^h$, $\mathcal{C}^2(\Omega_h) \equiv \mathcal{F}^h$ and $\mathcal{C}^3(\Omega_h) \equiv \mathcal{P}^h$.

For the formal construction of the discrete differential operators in the mimetic framework we need two ingredients: *the pairing product between cochains and chains*, which states that a cochain is a linear functional on chains, and the *coboundary operator*, which is the dual of the boundary operator with respect to the duality between cochains and chains. Let φ be a k-cochain and σ be a k-chain on the cell complex Ω_h; the duality pairing $\langle \cdot, \cdot \rangle_k$ between k-cochains and k-chains is expressed by

$$\langle \varphi, \sigma \rangle_k = \varphi(\sigma). \tag{1}$$

Let φ be a $(k-1)$-cochain and σ be a k-chain on the cell complex Ω_h; the coboundary operator $d_h^k : \mathcal{C}^k(\Omega_h) \to \mathcal{C}^{k+1}(\Omega_h)$ is given by:

$$\left\langle d_h^k \varphi, \sigma \right\rangle_k = \langle \varphi, \partial_k \sigma \rangle_{k-1}. \tag{2}$$

Taking the coboundary operator d_h^k as the discrete differential operator acting on the cochains in $\mathcal{C}^k(\Omega_h)$ is a natural choice as relation (2) is a discrete version of the Stokes Theorem. We apply (2) to derive the expression of the *primal mimetic operators* $d_h^0 \equiv \mathcal{GRAD}$, the discrete gradient acting on the 0-cochains, $d_h^1 \equiv \mathcal{CURL}$, the discrete curl acting on the 1-cochains, and $d_h^2 \equiv \mathcal{DIV}$, the discrete divergence acting on the 2-cochains.

- The coboundary of the vertex function $q = (q_{\mathsf{v}})_{\mathsf{v} \in \mathcal{V}}$ is the edge function $d_h^0 q := \mathcal{GRAD}(q)$ such that

$$\left\langle d_h^0(q), \mathsf{e} \right\rangle_1 = \langle q, \partial_0 \mathsf{e} \rangle_0 = \langle q, \mathsf{v}_2 - \mathsf{v}_1 \rangle_0 = q_{\mathsf{v}_2} - q_{\mathsf{v}_1} \quad \forall \mathsf{e} \in \mathcal{E},$$

  where, for $i = 1, 2$, $q_{\mathsf{v}_i} = \langle q, \mathsf{v}_i \rangle_0 = q(\mathsf{v}_i)$ is the value of the 0-cochain q at the vertex v_i. Accordingly, we say that the discrete gradient operator $\mathcal{GRAD} : \mathcal{V}^h \to \mathcal{E}^h$ is given by

$$\big(\mathcal{GRAD}(q)\big)_{\mathsf{e}} = q_{\mathsf{v}_2} - q_{\mathsf{v}_1} \quad \forall q \in \mathcal{V}^h \tag{3}$$

  at every edge e connecting the vertices v_1 and v_2 and oriented from v_1 to v_2.
- The discrete curl of the edge function $\mathbf{u} = (u_{\mathsf{e}})_{\mathsf{e} \in \mathcal{E}}$ is the face function $d_h^1 := \mathcal{CURL}(\mathbf{u})$ such that

$$\left\langle d_h^1(\mathbf{u}), \mathsf{f} \right\rangle_2 = \langle \mathbf{u}, \partial_1 \mathsf{f} \rangle_1 = \left\langle \mathbf{u}, \sum_{i=1}^{N_{\mathsf{f}}^{\mathcal{E}}} s_{\mathsf{f},i} \mathsf{e}_i \right\rangle_1 = \sum_{i=1}^{N_{\mathsf{f}}^{\mathcal{E}}} s_{\mathsf{f},i} \langle \mathbf{u}, \mathsf{e}_i \rangle_1 = \sum_{i=1}^{N_{\mathsf{f}}^{\mathcal{E}}} s_{\mathsf{f},i} u_{\mathsf{e}_i} \quad \forall \mathsf{f} \in \mathcal{F},$$

  where $u_{\mathsf{e}_i} = \langle \mathbf{u}, \mathsf{e}_i \rangle_1 = \mathbf{u}(\mathsf{e}_i)$ for $i = 1, \dots, N_{\mathsf{f}}^{\mathcal{E}}$ is the value of the 1-cochain $\mathbf{u}$ at the i-th edge e_i. Accordingly, we say that the discrete curl operator $\mathcal{CURL} : \mathcal{E}^h \to \mathcal{F}^h$ is given by

$$\big(\mathcal{CURL}(\mathbf{u})\big)_{\mathsf{f}} = \sum_{i=1}^{N_{\mathsf{f}}^{\mathcal{E}}} s_{\mathsf{f},i} u_{\mathsf{e}_i} \quad \forall \mathbf{u} \in \mathcal{E}^h \tag{4}$$

  at every face f enclosed by the sequence of $N_{\mathsf{f}}^{\mathcal{E}}$ edges $\{\mathsf{e}_1, \mathsf{e}_2, \dots, \mathsf{e}_{N_{\mathsf{f}}^{\mathcal{E}}}\}$.

	k			
n_σ	0	1	2	3
0	$\mathcal{V}_{\mathsf{v}}$			
1	$\mathcal{V}_{\mathsf{e}}$	$\mathcal{E}_{\mathsf{e}}$		
2	$\mathcal{V}_{\mathsf{f}}$	$\mathcal{E}_{\mathsf{f}}$	$\mathcal{F}_{\mathsf{f}}$	
3	$\mathcal{V}_{\mathsf{P}}$	$\mathcal{E}_{\mathsf{P}}$	$\mathcal{F}_{\mathsf{P}}$	$\mathcal{P}_{\mathsf{P}}$

duality relation

	k			
n_σ	0	1	2	3
0	$\mathcal{V}_{\mathsf{v}}^h$			
1	$\mathcal{V}_{\mathsf{e}}^h$	$\mathcal{E}_{\mathsf{e}}^h$		
2	$\mathcal{V}_{\mathsf{f}}^h$	$\mathcal{E}_{\mathsf{f}}^h$	$\mathcal{F}_{\mathsf{f}}^h$	
3	$\mathcal{V}_{\mathsf{P}}^h$	$\mathcal{E}_{\mathsf{P}}^h$	$\mathcal{F}_{\mathsf{P}}^h$	$\mathcal{P}_{\mathsf{P}}^h$

Fig. 2. Restriction of the k-chains (left table) and the k-cochains (right table) for $k = 0, \ldots, 3$ to the geometric objects $\sigma = \mathsf{v}, \mathsf{e}, \mathsf{f}, \mathsf{P}$ with dimension n_σ such that $k \leqslant n_\sigma \leqslant 3$, respectively. The "diagonal" entries of the chain table are $\mathcal{V}_{\mathsf{v}} = \mathrm{span}\{\mathsf{v}\}$, $\mathcal{E}_{\mathsf{e}} = \mathrm{span}\{\mathsf{e}\}$, $\mathcal{F}_{\mathsf{f}} = \mathrm{span}\{\mathsf{f}\}$, $\mathcal{P}_{\mathsf{P}} = \mathrm{span}\{\mathsf{P}\}$.

– The discrete divergence of the face function $\mathbf{u} = (u_{\mathsf{f}})_{\mathsf{f}\in\mathcal{F}}$ is the cell function $d_h^2 := \mathcal{DIV}(\mathbf{u})$ such that, for every cell P, it holds:

$$\left\langle d_h^2(\mathbf{u}), \mathsf{P}\right\rangle_3 = \langle \mathbf{u}, \partial_2 \mathsf{P}\rangle_2 = \left\langle \mathbf{u}, \sum_{i=1}^{N_{\mathsf{P}}^{\mathcal{F}}} s_{\mathsf{P},i}\mathsf{f}_i \right\rangle_2 = \sum_{i=1}^{N_{\mathsf{P}}^{\mathcal{F}}} s_{\mathsf{P},i}\langle \mathbf{u}, \mathsf{f}_i\rangle_2 = \sum_{i=1}^{N_{\mathsf{P}}^{\mathcal{F}}} s_{\mathsf{P},i} u_{\mathsf{f}_i},$$

where $u_{\mathsf{f}_i} = \langle \mathbf{u}, \mathsf{f}_i\rangle_2 = \mathbf{u}(\mathsf{f}_i)$ for $i = 1, \ldots, N_{\mathsf{P}}^{\mathcal{F}}$ is the value of the 2-cochain $\mathbf{u}$ at the i-th face f_i. Accordingly, we say that the discrete divergence operator $\mathcal{DIV} : \mathcal{F}^h \to \mathcal{P}^h$ is given by

$$\big(\mathcal{DIV}(\mathbf{u})\big)_{\mathsf{P}} = \sum_{i=1}^{N_{\mathsf{P}}^{\mathcal{F}}} s_{\mathsf{P},i} u_{\mathsf{f}_i} \quad \forall \mathbf{u} \in \mathcal{F}^h \tag{5}$$

at every polyhedral element P enclosed by the set of $N_{\mathsf{P}}^{\mathcal{F}}$ faces $\{\mathsf{f}_1, \mathsf{f}_2, \ldots, \mathsf{f}_{N_{\mathsf{f}}^{\mathcal{E}}}\}$.

A straightforward calculation shows that $\mathcal{CURL} \circ \mathcal{GRAD} = 0$ and $\mathcal{DIV} \circ \mathcal{CURL} = 0$. These relations mimic the relations $\mathbf{curl} \circ \mathbf{grad} = 0$ and $\mathrm{div} \circ \mathbf{curl} = 0$ and follow from the general property that $d_h^{k+1} \circ d_h^k = 0$ for $k \geqslant 0$. Consequently, the following *de Rham complex* can be established:

$$0 \longrightarrow \mathcal{V}^h \xrightarrow{\mathcal{GRAD}} \mathcal{E}^h \xrightarrow{\mathcal{CURL}} \mathcal{F}^h \xrightarrow{\mathcal{DIV}} \mathcal{P}^h \longrightarrow 0$$

2.2. Local restrictions of chains and cochains

Throughout the paper, we will consider the restriction of the k-chains and the k-cochains for $k = 0, \ldots, 3$ to the geometric objects $\sigma = \mathsf{v}, \mathsf{e}, \mathsf{f}, \mathsf{P}$ that have spatial dimension n_σ and such that $k \leqslant n_\sigma \leqslant 3$. The chain restrictions are denoted by $\mathcal{C}_k(\sigma)$ and the cochain restrictions by $\mathcal{C}^k(\sigma)$. We also use the specific notation illustrated in the two tables of Fig. 2. The meaning of the symbols in Fig. 2 is self-explanatory; for example, $\mathcal{V}_{\mathsf{P}}$ is the linear space of the formal linear combinations of the vertices of the polyhedral element P; $\mathcal{V}_{\mathsf{P}}^h$ is the linear space of the vertex functions defined on $\mathcal{V}_{\mathsf{P}}$, etc. Concerning the numerical approximation of the PDEs, the restriction of the cochains can be identified with the local degrees of freedom used to build the mimetic inner products. More precisely,

– for $k = 0$ and $0 \leqslant n_\sigma \leqslant 3$, the linear spaces of the *nodal* degrees of freedom are $\mathcal{V}_{\mathsf{P}}^h$, $\mathcal{V}_{\mathsf{f}}^h$, $\mathcal{V}_{\mathsf{e}}^h$, $\mathcal{V}_{\mathsf{v}}^h$;
– for $k = 1$ and $1 \leqslant n_\sigma \leqslant 3$, the linear spaces of the *edge* degrees of freedom are $\mathcal{E}_{\mathsf{P}}^h$, $\mathcal{E}_{\mathsf{f}}^h$, $\mathcal{E}_{\mathsf{e}}^h$;
– for $k = 2$ and $2 \leqslant n_\sigma \leqslant 3$, the linear spaces of the *face* degrees of freedom are $\mathcal{F}_{\mathsf{P}}^h$, $\mathcal{F}_{\mathsf{f}}^h$;
– for $k = 3$ and $n_\sigma = 3$, the linear space of the *elemental* degrees of freedom is $\mathcal{P}_{\mathsf{P}}^h$.

In particular, the cochains that belong to the diagonal entries of the cochain table, i.e., $\mathcal{V}_{\mathsf{v}}^h$ $\mathcal{E}_{\mathsf{e}}^h$, $\mathcal{F}_{\mathsf{f}}^h$, $\mathcal{P}_{\mathsf{P}}^h$, are formed by single-valued functions since the corresponding entries of the chain table are $\mathcal{V}_{\mathsf{v}} = \mathrm{span}\{\mathsf{v}\}$, $\mathcal{E}_{\mathsf{e}} = \mathrm{span}\{\mathsf{e}\}$, $\mathcal{F}_{\mathsf{f}} = \mathrm{span}\{\mathsf{f}\}$, $\mathcal{P}_{\mathsf{P}} = \mathrm{span}\{\mathsf{P}\}$. For example, the 0-cochain $\varphi \in \mathcal{V}_{\mathsf{v}}^h$ is the grid function $\varphi = (\varphi_{\mathsf{v}})$, which assigns the value $\varphi_{\mathsf{v}} \in \mathbb{R}$ to v, the unique vertex of $\mathcal{V}_{\mathsf{v}}$.

2.3. Projection and reconstruction operators

2.3.1. Projection and trace operators

The *projection operators* (often referred to as *interpolation operators* in the mimetic literature) translate the spaces of smooth scalar or vector-valued functions into the discrete spaces of cochains $\mathcal{V}_\sigma^h$, $\mathcal{E}_\sigma^h$, $\mathcal{F}_\sigma^h$, and $\mathcal{P}_\sigma^h$ where the geometric object σ ranges through the set $\{\mathsf{v}, \mathsf{e}, \mathsf{f}, \mathsf{P}\}$ according to the combinations displayed in Fig. 2. We use the symbol "Π_σ^k" to

denote the projection operator that returns a k-cochain restricted to the geometric object σ and we specialize its definition for $k = 0, \dots, 3$. Let $\mathbf{t}_{\mathsf{e}}$ denote the unit vector parallel to edge e and $\mathbf{n}_{\mathsf{f}}$ the unit vector orthogonal to face f; their orientation is assumed fixed once and for all consistently with orientations of all the geometric objects forming the mesh complex Ω_h. We consider:

- $k = 0$, the projection operator $\Pi^{\mathcal{V}}_{\sigma}(q) \in \mathcal{V}^h_{\sigma}$ applied to the scalar function q is defined as

$$\left(\Pi^{\mathcal{V}}_{\sigma}(q)\right)_{\mathsf{v}} = q(\mathbf{x}_{\mathsf{v}}) \quad \forall \mathsf{v} \in \sigma,$$

  where σ can be any vertex $\mathsf{v} \in \mathcal{V}$, any edge $\mathsf{e} \in \mathcal{E}$, any face $\mathsf{f} \in \mathcal{F}$, and any element $\mathsf{P} \in \mathcal{P}$;
- $k = 1$, the projection operator $\Pi^{\mathcal{E}}_{\sigma}(\mathbf{u}) \in \mathcal{E}^h_{\sigma}$ applied to the vector-valued function $\mathbf{u}$ is defined as

$$\left(\Pi^{\mathcal{E}}_{\sigma}(\mathbf{u})\right)_{\mathsf{e}} = \int_{\mathsf{e}} \mathbf{u} \cdot \mathbf{t}_{\mathsf{e}}\, dL \quad \forall \mathsf{e} \in \sigma,$$

  where σ can be any edge $\mathsf{e} \in \mathcal{E}$, any face $\mathsf{f} \in \mathcal{F}$, and any element $\mathsf{P} \in \mathcal{P}$;
- $k = 2$, the projection operator $\Pi^{\mathcal{F}}_{\sigma}(\mathbf{u}) \in \mathcal{F}^h_{\sigma}$ applied to the vector-valued function $\mathbf{u}$ is defined as

$$\left(\Pi^{\mathcal{F}}_{\sigma}(\mathbf{u})\right)_{\mathsf{f}} = \int_{\mathsf{f}} \mathbf{u} \cdot \mathbf{n}_{\mathsf{f}}\, dS \quad \forall \mathsf{f} \in \sigma,$$

  where σ can be any face $\mathsf{f} \in \mathcal{F}$ and any element $\mathsf{P} \in \mathcal{P}$;
- $k = 3$, the projection operator $\Pi^{\mathcal{P}}_{\sigma}(\mathbf{u}) \in \mathcal{P}^h_{\sigma}$ applied to the scalar function q is defined as

$$\left(\Pi^{\mathcal{P}}_{\sigma}(q)\right)_{\mathsf{P}} = \int_{\mathsf{P}} q\, dV \quad \forall \mathsf{P} \in \sigma,$$

  where σ can be any element $\mathsf{P} \in \mathcal{P}$.

Let us denote the differential operators of the continuum setting as $d^0 = \mathbf{grad}$, $d^1 = \mathbf{curl}$, $d^2 = \mathrm{div}$. The projection operators, the mimetic differential operators d^k_h and the differential operators d^k are characterized by the commuting property:

$$d^k_h \circ \Pi^k_{\sigma} = \Pi^{k+1}_{\sigma} \circ d^k \quad \text{for } k = 0, 1, 2, \tag{6}$$

where again $\sigma \in \{\mathsf{v}, \mathsf{e}, \mathsf{f}, \mathsf{P}\}$ in accordance with the admissible restrictions reported in Fig. 2.

By specializing the definitions of Π^k_{σ}, d^k_h and d^k we obtain the commuting relations:

$$\mathcal{GRAD} \circ \Pi^{\mathcal{V}}_{\sigma} = \Pi^{\mathcal{E}}_{\sigma} \circ \mathbf{grad}, \qquad \mathcal{CURL} \circ \Pi^{\mathcal{E}}_{\sigma} = \Pi^{\mathcal{F}}_{\sigma} \circ \mathbf{curl} \quad \text{and} \quad \mathcal{DIV} \circ \Pi^{\mathcal{F}}_{\sigma} = \Pi^{\mathcal{P}}_{\sigma} \circ \mathrm{div}\,. \tag{7}$$

We define the global projection operators $\Pi^{\mathcal{V}}$, $\Pi^{\mathcal{E}}$, $\Pi^{\mathcal{F}}$, $\Pi^{\mathcal{P}}$, that return the cochains defined on the mesh complex Ω_h by collecting together the local contributions. For example, $\Pi^{\mathcal{V}}$ is such that $\Pi^{\mathcal{V}}(\varphi)_{|\mathsf{P}} = \Pi^{\mathcal{V}}_{\mathsf{P}}(\varphi_{|\mathsf{P}})$ for every $\varphi \in \mathcal{V}^h$. For such global projection operators there hold a set of commuting relations like (7) that prove the following commuting diagram:

$$\begin{array}{ccccccc}
C^\infty(\Omega) & \xrightarrow{\ \mathbf{grad}\ } & (C^\infty(\Omega))^3 & \xrightarrow{\ \mathbf{curl}\ } & (C^\infty(\Omega))^3 & \xrightarrow{\ \mathrm{div}\ } & C^\infty(\Omega) \\
\Big\downarrow{\scriptstyle \Pi^{\mathcal{V}}} & & \Big\downarrow{\scriptstyle \Pi^{\mathcal{E}}} & & \Big\downarrow{\scriptstyle \Pi^{\mathcal{F}}} & & \Big\downarrow{\scriptstyle \Pi^{\mathcal{P}}} \\
\mathcal{V}^h & \xrightarrow{\ \mathcal{GRAD}\ } & \mathcal{E}^h & \xrightarrow{\ \mathcal{CURL}\ } & \mathcal{F}^h & \xrightarrow{\ \mathcal{DIV}\ } & \mathcal{P}^h
\end{array}$$

We also consider the *local* projection operators in accordance with the restriction of the corresponding global operators to σ. Let Π^k_{σ} be the restriction of Π^k to σ for $0 \leqslant k \leqslant n_{\sigma} \leqslant 3$. We assume that $\Pi^k_{\sigma}(\lambda_{|\sigma}) = \Pi^k(\lambda)_{|\sigma}$, where $\lambda_{|\sigma}$ is the restriction of the function λ defined on Ω to the geometric object σ.

Let q be a smooth scalar field. Then, we introduce the following *trace operators*

- $\gamma_{\mathsf{v}}(q) := q(\mathbf{x}_{\mathsf{v}})$ is the value of q at the vertex v;
- $\gamma_{\mathsf{e}}(q)(\mathbf{x}) := q(\mathbf{x})$ for $\mathbf{x} \in \mathsf{e}$ is the value of q along the edge e;
- $\gamma_{\mathsf{f}}(q)(\mathbf{x}) := q(\mathbf{x})$ for $\mathbf{x} \in \mathsf{f}$ is the value of q on the face f.

Let $\mathbf{v}$ be a smooth vector field. Then, we introduce the following *trace operators*

- $\gamma_{t,\mathsf{e}}(\mathbf{v}) := \mathbf{v}\cdot\mathbf{t}_{\mathsf{e}}$ is the trace of the tangential component of $\mathbf{v}$ along the edge e;
- $\gamma_{n,\mathsf{e}}(\mathbf{v}) := \mathbf{v}\cdot\mathbf{n}_{\mathsf{e}}$ is the trace of the normal component of $\mathbf{v}$ along the edge e of the polygonal boundary $\partial\mathsf{f}$ in the plane containing f;
- $\gamma_{n,\mathsf{f}}(\mathbf{v}) := \mathbf{v}\cdot\mathbf{n}_{\mathsf{f}}$ is the normal trace of $\mathbf{v}$ on the face f.

2.3.2. Reconstruction operators

The *reconstruction operators* are designed to remap cochains into scalar and vector-valued functions when they are applied to the grid functions, i.e., the degrees of freedom, associated with vertices, edges, faces and elements. Let R^k_σ denote the reconstruction operator acting on the k-cochains restricted to the geometric object σ. The reconstruction operator R^k_σ is required to satisfy a number of formal properties that involve the projection operators Π^k_σ and the differentiation operators d^k_h and d^k. Among these properties, we have the orthogonality property whose formulation requires the linear polynomial subspaces $\mathcal{O}^k_\sigma$ defined as follows. Let "$\times$" denote the cross product between three-dimensional vectors.

- For $\sigma = \mathsf{P}$ and $k = 0,\dots,3$, we specialize $\mathcal{O}^k_{\mathsf{P}}$ as follows:

$$\mathcal{O}^{\mathcal{V}}_{\mathsf{P}} = \{0\}, \qquad \mathcal{O}^{\mathcal{E}}_{\mathsf{P}} = \big\{c(\mathbf{x}-\mathbf{x}_{\mathsf{P}}),\ \forall c\in\mathbb{R},\ \forall\mathbf{x}\in\mathsf{P}\big\},$$
$$\mathcal{O}^{\mathcal{F}}_{\mathsf{P}} = \big\{\mathbf{c}\times(\mathbf{x}-\mathbf{x}_{\mathsf{P}}),\ \forall\mathbf{c}\in\mathbb{R}^3, \forall\mathbf{x}\in\mathsf{P}\big\}, \qquad \mathcal{O}^{\mathcal{P}}_{\mathsf{P}} = \big\{\mathbf{c}\cdot(\mathbf{x}-\mathbf{x}_{\mathsf{P}}),\ \forall\mathbf{c}\in\mathbb{R}^3,\ \forall\mathbf{x}\in\mathsf{P}\big\},$$

  where $\mathbf{x}_{\mathsf{P}}$ is the barycenter of the cell P;
- for $\sigma = \mathsf{f}$ and $k = 0,\dots,2$, we specialize $\mathcal{O}^k_{\mathsf{P}}$ as follows:

$$\mathcal{O}^{\mathcal{V}}_{\mathsf{f}} = \{0\}, \qquad \mathcal{O}^{\mathcal{E}}_{\mathsf{f}} = \big\{c(\boldsymbol{\xi}-\boldsymbol{\xi}_{\mathsf{f}}),\ \forall c\in\mathbb{R}, \forall\boldsymbol{\xi}\in\mathsf{f}\big\}, \qquad \mathcal{O}^{\mathcal{F}}_{\mathsf{f}} = \big\{\mathbf{c}\cdot(\boldsymbol{\xi}-\boldsymbol{\xi}_{\mathsf{f}}),\ \forall\mathbf{c}\in\mathbb{R}^3,\ \forall\boldsymbol{\xi}\in\mathsf{f}\big\},$$

  where $\boldsymbol{\xi}_{\mathsf{f}}$ is the barycenter of the face f.

We list these properties as follows.

(R1) *The reconstruction operator R^k_σ is a right inverse of the projection operator Π^k_σ:*

$$\Pi^k_\sigma \circ R^k_\sigma = \mathbb{I}, \tag{8}$$

where $\mathbb{I}$ is the identity operator. For $k = 0,\dots,3$ we obtain the relations:

$$\Pi^{\mathcal{V}}_\sigma \circ R^{\mathcal{V}} = \mathbb{I}, \qquad \Pi^{\mathcal{E}}_\sigma \circ R^{\mathcal{E}} = \mathbb{I}, \qquad \Pi^{\mathcal{F}}_\sigma \circ R^{\mathcal{F}} = \mathbb{I}, \qquad \Pi^{\mathcal{P}}_\sigma \circ R^{\mathcal{P}} = \mathbb{I}. \tag{9}$$

(R2) *The reconstruction operator R^k_σ is exact on the projection of polynomial fields of degree $m \geqslant 0$:*

$$R^k_\sigma \circ \Pi^k_\sigma(\lambda) = \lambda \quad \forall\lambda\in\mathcal{C}^k(\Omega_h),\ \text{with}\ \lambda\in\big(\mathbb{P}_m(\sigma)\big)^d \tag{10}$$

where λ stands for a scalar polynomial function q ($d=1$) or a d-sized vector-valued polynomial function $\mathbf{q}$ (with $d>1$). We specialize (10) for $k = 0,\dots,3$ as follows:

$$R^{\mathcal{V}}_\sigma \circ \Pi^{\mathcal{V}}_\sigma(c) = c, \qquad R^{\mathcal{E}}_\sigma \circ \Pi^{\mathcal{E}}_\sigma(\mathbf{c}) = \mathbf{c}, \qquad R^{\mathcal{F}}_\sigma \circ \Pi^{\mathcal{F}}_\sigma(\mathbf{c}) = \mathbf{c}, \qquad R^{\mathcal{P}}_\sigma \circ \Pi^{\mathcal{P}}_\sigma(c) = c. \tag{11}$$

(R3) *The reconstruction operators "commutes" with the differentiation operators*:

$$R^{k+1}_\sigma \circ d^k_h = d^k \circ R^k_\sigma. \tag{12}$$

For $k = 0,1,2$ we specialize (12) through the relations:

$$R^{\mathcal{E}}_\sigma \circ \mathcal{GRAD} = \mathbf{grad} \circ R^{\mathcal{V}}_\sigma, \qquad R^{\mathcal{F}}_\sigma \circ \mathcal{CURL} = \mathbf{curl} \circ R^{\mathcal{E}}_\sigma, \qquad R^{\mathcal{P}}_\sigma \circ \mathcal{DIV} = \mathrm{div} \circ R^{\mathcal{F}}_\sigma. \tag{13}$$

(R4) *The reconstruction operator R^k_σ for $\sigma\in\{\mathsf{f},\mathsf{P}\}$ and $k\in[0,n_\sigma]$ is orthogonal to $\mathcal{O}^k_\sigma$ with respect to the L^2 scalar products on σ:*

$$\int_\sigma R^k_\sigma(\alpha)\cdot\mu_1 = 0 \quad \forall\alpha\in\mathcal{C}^k(\sigma),\ \forall\mu^1\in\mathcal{O}^k_\sigma, \tag{14}$$

where the dot symbol "$\cdot$" in the integral argument obviously depends on the spatial dimension of the reconstructed fields.

(R5) Let γ_σ be one of the trace operators defined at the end of Section 2.3.1. For $0 \leqslant k < n_\sigma \leqslant 3$, it holds:

$$\gamma_\sigma \circ R^k_\sigma(\alpha) = R^k_s(\alpha_{|_\sigma}) \quad \forall \alpha \in \mathcal{C}^k(\sigma),\ \forall s \in \partial\sigma. \tag{15}$$

(R6) When $k = n_\sigma = 0, \dots, 3$ we have the basic choice

$$R^k_\sigma(\varphi) = \begin{cases} \varphi_{|_\sigma} = \varphi_{\mathsf{v}} & \text{if } k = n_\sigma = 0, \text{ i.e., } \sigma = V; \\ \varphi_{|_\sigma}/|\sigma| = \varphi_\sigma/|\sigma| & \text{if } k = n_\sigma > 0. \end{cases}$$

We particularize the basic choice as follows:

$$R^{\mathcal{V}}_{\mathsf{v}}(\alpha) = \alpha_{\mathsf{v}} \quad \forall \alpha = (\alpha_{\mathsf{v}})_{\mathsf{v}\in\mathcal{V}_{\mathsf{v}}} \in \mathcal{V}^h_{\mathsf{v}}, \tag{16}$$

$$R^{\mathcal{E}}_{\mathsf{e}}(\alpha) = \alpha_{\mathsf{e}}/|\mathsf{e}| \quad \forall \alpha = (\alpha_{\mathsf{e}})_{\mathsf{e}\in\mathcal{E}_{\mathsf{e}}} \in \mathcal{E}^h_{\mathsf{e}}, \tag{17}$$

$$R^{\mathcal{F}}_{\mathsf{f}}(\alpha) = \alpha_{\mathsf{f}}/|\mathsf{f}| \quad \forall \alpha = (\alpha_{\mathsf{f}})_{\mathsf{f}\in\mathcal{F}_{\mathsf{f}}} \in \mathcal{F}^h_{\mathsf{f}}, \tag{18}$$

$$R^{\mathcal{P}}_{\mathsf{P}}(\alpha) = \alpha_{\mathsf{P}}/|\mathsf{P}| \quad \forall \alpha = (\alpha_{\mathsf{P}})_{\mathsf{P}\in\mathcal{P}_{\mathsf{P}}} \in \mathcal{P}^h_{\mathsf{P}}. \tag{19}$$

Remark 2.3. The first three properties listed above are also considered in [22], although property (R2) is given in the alternative but equivalent form (20) that we discuss in the following remark. In particular, in [22] property (R1) is referred as the "*consistency property of the reconstruction*", property (R2) as the "*approximation property*", and property (R3) as the "*commuting property CDP2*". According to [22], these three properties allows us to identify the class of "*conforming reconstruction operators*", e.g., the Withney form [47,57,88] on meshes of simplexes. Instead, properties (R4)–(R5) are here considered for the construction of the mimetic inner product of Section 3 through the consistency condition.

Remark 2.4. In [22,57], it is considered the general approximation property that states that

$$R^k_\sigma \circ \Pi^k_\sigma = \mathbb{I} + \mathcal{O}(h^r), \tag{20}$$

for some integer number $r \geqslant 1$, which leads to the development of numerical methods of order r. To characterize the accuracy of our mimetic approximation, we pursue a different approach by introducing a consistency condition that ensures the exactness of the mimetic inner products when applied to k-cochains that are the projection of constant (scalar or vector-valued) functions.

Remark 2.5. Assumptions (R5) express the locality of the reconstructions in the hierarchy of cochains shown by Fig. 2. For example, $R^{\mathcal{V}}_{\mathsf{P}}(\varphi)$ is the scalar field defined on P that is reconstructed from the values of the cochain $\varphi \in \mathcal{V}_{\mathsf{P}}$ at the vertices of P. Its restriction to the face $\mathsf{f} \in \partial\mathsf{P}$, i.e., $\gamma_{\mathsf{f}} \circ R^{\mathcal{V}}_{\mathsf{P}}(\varphi)$, is only determined by the values that φ takes at the vertices of f and is equal to $R^{\mathcal{V}}_{\mathsf{f}}(\alpha_{|_{\mathsf{f}}})$.

We end this subsection with the definition of an *admissible set of reconstruction*.

Definition 1.

- A set of reconstructions $\{R^k_\sigma,\ \text{for } 0 \leqslant k \leqslant 3 \text{ and } \sigma \text{ such that } n_\sigma \geqslant k\}$ defined on the cochain structure $(\mathcal{V}^h, \mathcal{E}^h, \mathcal{F}^h, \mathcal{P}^h)$ is said *admissible* if all the reconstructions satisfy properties (R1)–(R6) for every $0 \leqslant k \leqslant 3$ and every σ of dimension $n_\sigma \geqslant k$.

3. Mimetic inner products for a single element

We endow the linear space $\mathcal{C}^k(\Omega)$ of the k-cochains defined on Ω_h with the inner product

$$(\alpha, \beta)_{\mathcal{C}^k(\Omega)} := \int_\Omega R^k(\alpha) \cdot R^k(\beta) \quad \forall \alpha, \beta \in \mathcal{C}^k(\Omega_h). \tag{21}$$

Similarly, the local inner product on $\sigma \in \{\mathsf{v}, \mathsf{e}, \mathsf{f}, \mathsf{P}\}$ takes the form:

$$(\alpha, \beta)_{\mathcal{C}^k(\sigma)} := \int_\sigma R^k_\sigma(\alpha) \cdot R^k_\sigma(\beta) \quad \forall \alpha, \beta \in \mathcal{C}^k(\sigma). \tag{22}$$

On one hand, the local reconstructions are the restriction of the global ones; on the other hand, the global reconstructions collect together the contributions from the local ones. For example, let us identify σ with the polyhedra P of Ω_h. The reconstruction of the k-cochain α in $\mathcal{C}^k(\Omega_h)$ is defined by

$$R^k(\alpha)_{|\mathsf{P}} = R^k_{\mathsf{P}}(\alpha_{|\mathsf{P}}) \quad \forall \mathsf{P} \in \Omega_h,$$

i.e., by considering all the local reconstructions R^k_{P} acting on the local degrees of freedom $\alpha_{|\mathsf{P}}$.

The locality of the reconstructions implies that the reconstruction of a k-cochain φ on σ with $0 \leqslant n_\sigma \leqslant 3$ only depends on the restricted set of data $\varphi_{|\sigma}$. This property allows us to split the global inner product for the k-cochains defined on Ω in (21) into the sum of the local inner products for the polyhedral elements $\mathsf{P} \in \mathcal{P}$ defined in (22) (take $\sigma = \mathsf{P}$):

$$(\alpha, \beta)_{\mathcal{C}^k(\Omega)} = \sum_{\mathsf{P}\in\Omega_h} (\alpha, \beta)_{\mathcal{C}^k(\mathsf{P})} = \sum_{\mathsf{P}\in\Omega_h} \int_{\mathsf{P}} R^k_{\mathsf{P}}(\alpha) \cdot R^k_{\mathsf{P}}(\beta) \quad \forall \alpha, \beta \in \mathcal{C}^k(\Omega).$$

A similar splitting holds for every local inner product defined on the generic object σ.

Definition (22) is practically useless since to have an explicit representation of the reconstructed fields and, hence, of the corresponding scalar product, is a very difficult task, except for very simple mesh geometries such as decompositions into tetrahedra or regular hexahedra. Nonetheless, we can construct the mimetic scalar product for the cochain space $\mathcal{C}^k(\mathsf{P})$ through a more effective and practical strategy. This strategy is based on the remarkable property that all admissible reconstructions acting on the same cochain space share the same average on the geometric object on which the cochains are defined. As a consequence, when one of the arguments of the inner product is the projection of a constant field, its value does not depend on the explicit form of the reconstruction itself. As we will see in the next subsections, this property is all we need to define a family of mimetic inner products, and, eventually, a family of mimetic discretization methods. The crucial point here is that *we do not need to specify an explicit representation of the reconstruction operators to implement a mimetic inner product, and, thus, a mimetic scheme*, but only to prove that such operators exist and satisfy the set of local conditions (R1)–(R6) of the previous section.

3.1. Average of admissible reconstructions

In this section, we prove that the average of the reconstruction operators that belong to an admissible set can be determined without the explicit knowledge of the form of the reconstruction operators. For each case, we give the final formula for the average; its derivation is mainly based on the integration by parts, which is occasionally applied recursively. Similar reconstruction formulas are also reviewed in [78]. The reconstruction operators $R^{\mathcal{V}}_{\mathsf{v}}$ and $R^{\mathcal{E}}_{\mathsf{e}}$, which correspond to the zero-dimensional case $k = n_\sigma = 0$ and the one-dimensional case $k = n_\sigma = 1$, are uniquely determined by the basic choices (16) and (17), respectively. Therefore, we have $R^{\mathcal{V}}_{\mathsf{v}}(\varphi) = \varphi_{\mathsf{v}}$ for the single-valued 0-cochain $\varphi = (\varphi_{\mathsf{v}}) \in \mathcal{V}^h_{\mathsf{v}}$ and $R^{\mathcal{E}}_{\mathsf{e}}(\varphi) = \varphi_{\mathsf{e}}/|\mathsf{e}|$ for the single-valued 1-cochain $\varphi = (\varphi_{\mathsf{e}}) \in \mathcal{E}^h_{\mathsf{e}}$, and it is obvious that the quantity

$$\int_{\mathsf{e}} R^{\mathcal{E}}_{\mathsf{e}}(\varphi)\, dL = \varphi_{\mathsf{e}}$$

only depends on φ (and not on the specific choice of the reconstruction operator $R^{\mathcal{E}}_{\mathsf{e}}$).

The reconstruction operator $R^{\mathcal{V}}_{\mathsf{e}}$, i.e., the one-dimensional case determined by $n_\sigma = 1$ and $k = 0$, is the first non-trivial case.

Proposition 3.1. *Let* e *be the edge that connects the vertices* v_1 *and* v_2. *For every admissible linear operator* $R^{\mathcal{V}}_{\mathsf{e}}$ *and every* 0*-cochain* $\varphi = (\varphi_{\mathsf{v}})_{\mathsf{v}\in\partial\mathsf{e}} \in \mathcal{V}^h_{\mathsf{e}}$ *it holds*:

$$\int_{\mathsf{e}} R^{\mathcal{V}}_{\mathsf{e}}(\varphi)\, dL = \frac{\varphi_{\mathsf{v}_1} + \varphi_{\mathsf{v}_2}}{2}|\mathsf{e}| \quad \forall \mathsf{e} \in \mathcal{E}, \tag{23}$$

which only depends on φ *and* e.

Proof. Let us consider the identity $1 = d(\xi - \xi_{\mathsf{e}})/d\xi$ for the constant scalar field ξ, where ξ is a local coordinate on the edge e connecting the vertices v_1 and v_2 and ξ_{e} is the midpoint of e. We integrate by parts to obtain:

$$\begin{aligned}\int_{\mathsf{e}} R^{\mathcal{V}}_{\mathsf{e}}(\varphi)\, dL &= \int_{\mathsf{e}} R^{\mathcal{V}}_{\mathsf{e}}(\varphi)\, \frac{d}{d\xi}(\xi - \xi_{\mathsf{e}})\, dL \\ &= -\int_{\mathsf{e}} \frac{d}{d\xi}\big(R^{\mathcal{V}}_{\mathsf{e}}(\varphi)\big)(\xi - \xi_{\mathsf{e}})\, dL + \gamma_{\mathsf{v}_2}\big(R^{\mathcal{V}}_{\mathsf{e}}(\varphi)\big)(\xi_{\mathsf{v}_2} - \xi_{\mathsf{e}}) - \gamma_{\mathsf{v}_1}\big(R^{\mathcal{V}}_{\mathsf{e}}(\varphi)\big)(\xi_{\mathsf{v}_1} - \xi_{\mathsf{e}}),\end{aligned} \tag{24}$$

where, for $i = 1, 2$, ξ_{v_i} is the coordinate vector of vertex v_i and γ_{v_i} is the restriction operator that evaluates a scalar function at v_i. The integral term in the right-hand side of (24) is zero. Indeed, we use (R3) with the discrete gradient definition (3), the fact that $R^{\mathcal{E}}_{\mathsf{e}}$ is constant on e, cf. (17), and we obtain:

$$\int_{\mathsf{e}} \frac{d}{d\xi}\big(R_{\mathsf{e}}^{\mathcal{V}}(\varphi)\big)\,(\xi-\xi_{\mathsf{e}})\,dL = \int_{\mathsf{e}} R_{\mathsf{e}}^{\mathcal{E}}\big(\mathcal{GRAD}(\varphi)_{|_{\mathsf{e}}}\big)\,(\xi-\xi_{\mathsf{e}})\,dL = R_{\mathsf{e}}^{\mathcal{E}}\big(\mathcal{GRAD}(\varphi)_{|_{\mathsf{e}}}\big)\int_{\mathsf{e}} (\xi-\xi_{\mathsf{e}})\,dL = 0.$$

Relation (23) follows from (24) by using (R5) and noting that $\gamma_{\mathsf{v}_i}(R_{\mathsf{e}}^{\mathcal{V}}(\varphi)) = R_{\mathsf{v}}^{\mathcal{V}}(\varphi_{|_{\mathsf{v}_i}}) = \varphi_{\mathsf{v}_i}$ for $i=1,2$, $\xi_{\mathsf{e}} = (\xi_{\mathsf{v}_1}+\xi_{\mathsf{v}_2})/2$ and $|\mathsf{e}| = (\xi_{\mathsf{v}_2}-\xi_{\mathsf{v}_1})$. □

Let us now consider the two-dimensional reconstruction operators $R_{\mathsf{f}}^{\mathcal{F}}$, $R_{\mathsf{f}}^{\mathcal{E}}$ and $R_{\mathsf{f}}^{\mathcal{V}}$ that return scalar or vector-valued fields on f from the cochain spaces defined on such face. On each face f, we set the local two-dimensional coordinate frame $\boldsymbol{\xi} = (\xi_1,\xi_2)$ and we will make use of the differential operators **rot** and *rot*. Such operators, for every vector field $\mathbf{w}(\boldsymbol{\xi}) = (w_1(\boldsymbol{\xi}), w_2(\boldsymbol{\xi}))$ and every scalar field $v(\xi)$ for $\boldsymbol{\xi}\in\mathsf{f}$, satisfy the definitions

$$\mathbf{rot}(v) = \left(-\frac{\partial v}{\partial\xi_2}, \frac{\partial v}{\partial\xi_1}\right) \quad \text{and} \quad rot(\mathbf{w}) = -\frac{\partial w_1}{\partial\xi_2} + \frac{\partial w_2}{\partial\xi_1},$$

and are related to one another by the integration by parts formula:

$$\int_{\mathsf{f}} \mathbf{w}\cdot\mathbf{rot}(v)\,dS = -\int_{\mathsf{f}} rot(\mathbf{w})\,v\,dS + \int_{\partial\mathsf{f}} \gamma_{t,\mathsf{e}}(\mathbf{w})\,v\,dL \quad \text{where } \gamma_{t,\mathsf{e}}(\mathbf{w}) = \mathbf{t}_{\mathsf{f},\mathsf{e}}\cdot\mathbf{w} \text{ and } \mathbf{t}_{\mathsf{f},\mathsf{e}} = \begin{pmatrix} 0 & -1 \\ 1 & 0 \end{pmatrix}\mathbf{n}_{\mathsf{f},\mathsf{e}}.$$

As $R_{\mathsf{f}}^{\mathcal{F}}$ must obey the basic choice (18), the non-trivial cases are only those of $R_{\mathsf{f}}^{\mathcal{E}}$ and $R_{\mathsf{f}}^{\mathcal{V}}$, for which we prove Proposition 3.2 here below.

Proposition 3.2.

(i) *Let $\mathbf{n}_{\mathsf{f},\mathsf{e}}$ denote the unit vector orthogonal to $\mathsf{e}\in\partial\mathsf{P}$ in the plane containing* f. *Then, for every admissible reconstruction operator $R_{\mathsf{f}}^{\mathcal{V}}$ and every* 0*-cochain $\varphi = (\varphi_{\mathsf{v}})_{\mathsf{v}\in\partial\mathsf{f}} \in \mathcal{V}_{\mathsf{f}}^h$ it holds that*

$$\int_{\mathsf{f}} R_{\mathsf{f}}^{\mathcal{V}}(\varphi)\,dS = \frac{1}{2}\sum_{\mathsf{e}\in\partial\mathsf{f}} (\boldsymbol{\xi}_{\mathsf{e}}-\boldsymbol{\xi}_{\mathsf{f}})\cdot\mathbf{n}_{\mathsf{f},\mathsf{e}}\left(\frac{\varphi_{\mathsf{v}_1}+\varphi_{\mathsf{v}_2}}{2}|\mathsf{e}|\right), \tag{25}$$

where we recall that $\boldsymbol{\xi}_{\mathsf{e}}$ is the midpoint of e. *Relation (25) only depends on φ, the face* f *and the edges $\mathsf{e}\in\partial\mathsf{f}$.*

(ii) *Let $\mathbf{e}_i$ for $i=1,2$ be the i-th vector of the canonical basis of $\mathbb{R}^2$, and p_i^1 be a linear polynomial on* e *such that $\mathbf{e}_i = \mathbf{rot}(p_i^1(\xi))$ for $\xi\in\mathsf{e}$. Then, for every admissible reconstruction operator $R_{\mathsf{f}}^{\mathcal{E}}$ and every* 1*-cochain $\varphi = (\varphi_{\mathsf{e}})_{\mathsf{e}\in\partial\mathsf{f}} \in \mathcal{E}_{\mathsf{f}}^h$ it holds that*

$$\int_{\mathsf{f}} R_{\mathsf{f}}^{\mathcal{E}}(\varphi)\cdot\mathbf{e}_i\,dS = -\sum_{\mathsf{e}\in\partial\mathsf{f}} \frac{\varphi_{\mathsf{e}}}{|\mathsf{e}|}\int_{\mathsf{e}} p_i^1(\boldsymbol{\xi})\,dL, \tag{26}$$

which only depends on φ, $\mathbf{e}_i$, the face f *and the edges $\mathsf{e}\in\partial\mathsf{f}$.*

Proof. (i) Let us consider the identity $2 = \mathrm{div}(\boldsymbol{\xi}-\boldsymbol{\xi}_{\mathsf{f}})$, which holds for every $\boldsymbol{\xi}\in\mathsf{f}$. We integrate by parts and we obtain

$$\begin{aligned} 2\int_{\mathsf{f}} R_{\mathsf{f}}^{\mathcal{V}}(\varphi)\,dS &= \int_{\mathsf{f}} R_{\mathsf{f}}^{\mathcal{V}}(\varphi)\ \mathrm{div}(\boldsymbol{\xi}-\boldsymbol{\xi}_{\mathsf{f}})\,dS \\ &= -\int_{\mathsf{f}} \mathbf{grad}\big(R_{\mathsf{f}}^{\mathcal{V}}(\varphi)\big)\cdot(\boldsymbol{\xi}-\boldsymbol{\xi}_{\mathsf{f}})\,dS + \sum_{\mathsf{e}\in\partial\mathsf{f}}\int_{\mathsf{e}} \gamma_{\mathsf{e}}\big(R_{\mathsf{f}}^{\mathcal{V}}(\varphi)\big)\,\mathbf{n}_{\mathsf{f},\mathsf{e}}\cdot(\boldsymbol{\xi}-\boldsymbol{\xi}_{\mathsf{f}})\,dL, \end{aligned} \tag{27}$$

where γ_{e} is the trace operator associated with the edge e and $\mathbf{n}_{\mathsf{f},\mathsf{e}}$ is the two-dimensional unit vector orthogonal to e and pointing out of the two-dimensional planar region enclosed by ∂f. The first integral term in the right-hand side of (27) is zero. Indeed, we use (R3) with the discrete gradient definition (3) and (R4), which implies that $R_{\mathsf{f}}^{\mathcal{E}}$ is orthogonal to $\mathcal{O}_{\mathsf{f}}^{\mathcal{E}}$. We obtain:

$$\int_{\mathsf{f}} \mathbf{grad}\big(R_{\mathsf{f}}^{\mathcal{V}}(\varphi)\big)\cdot(\boldsymbol{\xi}-\boldsymbol{\xi}_{\mathsf{f}})\,dS = \int_{\mathsf{f}} R_{\mathsf{f}}^{\mathcal{E}}\big(\mathcal{GRAD}(\varphi)_{|_{\mathsf{f}}}\big)\cdot(\boldsymbol{\xi}-\boldsymbol{\xi}_{\mathsf{f}})\,dS = 0. \tag{28}$$

We use (28) in (27), we apply (R5), we evaluate $(\boldsymbol{\xi}-\boldsymbol{\xi}_{\mathsf{f}})\cdot\mathbf{n}_{\mathsf{f},\mathsf{e}}$, which is constant along each edge $\mathsf{e}\in\partial\mathsf{f}$, at the edge midpoint $\boldsymbol{\xi}_{\mathsf{e}}$, and we get

$$2\int_{\mathsf{f}} R_{\mathsf{f}}^{\mathcal{V}}(\varphi)\,dS = \sum_{\mathsf{e}\in\partial\mathsf{f}}\int_{\mathsf{e}} R_{\mathsf{e}}^{\mathcal{V}}(\varphi_{|_{\mathsf{e}}})\,\mathbf{n}_{\mathsf{f},\mathsf{e}}\cdot(\boldsymbol{\xi}-\boldsymbol{\xi}_{\mathsf{f}})\,dL = \sum_{\mathsf{e}\in\partial\mathsf{f}}\mathbf{n}_{\mathsf{f},\mathsf{e}}\cdot(\boldsymbol{\xi}_{\mathsf{e}}-\boldsymbol{\xi}_{\mathsf{f}})\int_{\mathsf{e}} R_{\mathsf{e}}^{\mathcal{V}}(\varphi_{|_{\mathsf{e}}})\,dL. \tag{29}$$

Eventually, we evaluate the integrals in the right-hand side of (29) by the result of Proposition 3.1 and we obtain (25).

(ii) Let us consider the constant vector field

$$\mathbf{e}_i = \mathbf{rot}\big(p_i^1\big) \quad \text{where } p_i^1(\boldsymbol{\xi}) := -\begin{pmatrix} 0 & -1 \\ 1 & 0 \end{pmatrix}(\boldsymbol{\xi} - \boldsymbol{\xi}_{\mathsf{f}}). \tag{30}$$

Using (30) and integrating by parts yield

$$\int_{\mathsf{f}} R_{\mathsf{f}}^{\mathcal{E}}(\varphi)\cdot\mathbf{e}_i\,dS = -\int_{\mathsf{f}} \mathbf{rot}\big(R_{\mathsf{f}}^{\mathcal{E}}(\varphi)\big)p_i^1\,dS + \sum_{\mathsf{e}\in\partial\mathsf{f}}\int_{\mathsf{e}} \gamma_{t,\mathsf{e}}\big(R_{\mathsf{f}}^{\mathcal{E}}(\varphi)\big)p_i^1\,dL, \tag{31}$$

where $\gamma_{t,\mathsf{e}}$ is the trace operator that returns the tangential component of a vector on the edge e. The first integral term in the right-hand side of (31) is zero. Indeed, we use (R3) with the discrete curl definition (4), the fact that $R_{\mathsf{f}}^{\mathcal{F}}$ is constant on f, cf. (18), and we obtain:

$$\int_{\mathsf{f}} \mathbf{rot}\big(R_{\mathsf{f}}^{\mathcal{E}}(\varphi)\big)p_i^1\,dS = \int_{\mathsf{f}} R_{\mathsf{f}}^{\mathcal{F}}\big(\mathcal{CURL}(\varphi)_{|\mathsf{f}}\big)p_i^1(\xi)\,dS = R_{\mathsf{f}}^{\mathcal{F}}\big(\mathcal{CURL}(\varphi)_{|\mathsf{f}}\big)\int_{\mathsf{f}} p_i^1\,dS = 0. \tag{32}$$

We use (32) in (31), property (R5) and the basic choice of $R_{\mathsf{e}}^{\mathcal{E}}$ from (R6), cf. (17), to obtain

$$\int_{\mathsf{f}} R_{\mathsf{f}}^{\mathcal{E}}(\varphi)\cdot\mathbf{e}_i\,dS = -\sum_{\mathsf{e}\in\partial\mathsf{f}}\int_{\mathsf{e}} \gamma_{t,\mathsf{e}}\big(R_{\mathsf{f}}^{\mathcal{E}}(\varphi)\big)p_i^1\,dL = -\sum_{\mathsf{e}\in\partial\mathsf{f}}\int_{\mathsf{e}} R_{\mathsf{e}}^{\mathcal{E}}(\varphi_{|\mathsf{e}})\,p_i^1\,dL = -\sum_{\mathsf{e}\in\partial\mathsf{f}}\int_{\mathsf{e}}\frac{\varphi_{\mathsf{e}}}{|\mathsf{e}|}\int_{\mathsf{e}} p_i^1\,dL$$

and we eventually recognize (26). □

Let us now characterize the three-dimensional reconstruction operators $R_{\mathsf{P}}^{\mathcal{P}}$, $R_{\mathsf{P}}^{\mathcal{F}}$, $R_{\mathsf{P}}^{\mathcal{E}}$ and $R_{\mathsf{P}}^{\mathcal{V}}$. Obviously, $R_{\mathsf{P}}^{\mathcal{P}}$ must obey the basic choice (19) and the non-trivial cases are only those of $R_{\mathsf{P}}^{\mathcal{F}}$, $R_{\mathsf{P}}^{\mathcal{E}}$ and $R_{\mathsf{P}}^{\mathcal{V}}$, for which we prove the following proposition.

Proposition 3.3. *Let $\mathbf{e}_i$ be the i-th vector of the canonical basis of $\mathbb{R}^3$, $i = 1, 2, 3$.*

(i) *For every admissible reconstruction operator $R_{\mathsf{P}}^{\mathcal{V}}$ and every 0-cochain $\varphi = (\varphi_{\mathsf{v}})_{\mathsf{v}\in\partial\mathsf{P}} \in \mathcal{V}_{\mathsf{P}}^h$ it holds*:

$$\int_{\mathsf{P}} R^{\mathcal{V}}(\varphi)\,dV = \frac{1}{3}\sum_{\mathsf{f}\in\partial\mathsf{P}}(\mathbf{x}-\mathbf{x}_{\mathsf{P}})\cdot\mathbf{n}_{\mathsf{P},\mathsf{f}}\sum_{\mathsf{e}\in\partial\mathsf{f}}\big((\boldsymbol{\xi}_{\mathsf{e}}-\boldsymbol{\xi}_{\mathsf{f}})\cdot\mathbf{n}_{\mathsf{f},\mathsf{e}}\big)_{|\mathsf{e}}\,\frac{\varphi_{|\mathsf{v}_1}+\varphi_{|\mathsf{v}_2}}{2}|\mathsf{e}|,$$

where $\boldsymbol{\xi}_{\mathsf{e}}$ is the midpoint of edge $\mathsf{e}\in\partial\mathsf{f}$, $\boldsymbol{\xi}_{\mathsf{f}}$ is the barycenter of face f, and $\mathbf{n}_{\mathsf{f},\mathsf{e}}$ is the unit vector orthogonal to $\mathsf{e}\in\partial\mathsf{P}$ in the plane containing f.

(ii) *For every admissible reconstruction operator $R_{\mathsf{P}}^{\mathcal{E}}$ and every 1-cochain $\varphi = (\varphi_{\mathsf{e}})_{\mathsf{e}\in\partial\mathsf{P}} \in \mathcal{E}_{\mathsf{P}}^h$ it holds*:

$$\int_{\mathsf{P}} R_{\mathsf{P}}^{\mathcal{E}}(\varphi)\cdot\mathbf{e}_i\,dV = \frac{1}{2}\sum_{\mathsf{f}\in\partial\mathsf{P}}\int_{\mathsf{f}} R_{\mathsf{f}}^{\mathcal{E}}(\varphi_{|\mathsf{f}})\cdot\boldsymbol{\alpha}_{\mathsf{f},i}\,dS, \tag{33}$$

where $R_{\mathsf{f}}^{\mathcal{E}}$ is any admissible reconstruction operator for $\mathsf{f}\in\partial\mathsf{P}$ and the vector field $\boldsymbol{\alpha}_{\mathsf{f},i}$ is given by

$$\boldsymbol{\alpha}_{\mathsf{f},i} = \mathbf{n}_{\mathsf{P},\mathsf{f}}\cdot(\mathbf{x}_{\mathsf{f}}-\mathbf{x}_{\mathsf{P}})\gamma_{t,\mathsf{f}}(\mathbf{e}_i) + (\mathbf{n}_{\mathsf{P},\mathsf{f}}\cdot\mathbf{e}_i)\big(\gamma_{t,\mathsf{f}}(\mathbf{x}_{\mathsf{P}}) - \boldsymbol{\xi}_{\mathsf{f}}\big), \tag{34}$$

and $\mathbf{x}_{\mathsf{f}}$ and $\mathbf{x}_{\mathsf{P}}$ are the barycenters of f and P, respectively.

(iii) *For every admissible reconstruction operator $R_{\mathsf{P}}^{\mathcal{F}}$ and every 2-cochain $\varphi = (\varphi_{\mathsf{f}})_{\mathsf{f}\in\partial\mathsf{P}} \in \mathcal{F}_{\mathsf{P}}^h$ it holds*:

$$\int_{\mathsf{P}} R_{\mathsf{P}}^{\mathcal{F}}(\varphi)\cdot\mathbf{e}_i\,dV = \sum_{\mathsf{f}\in\partial\mathsf{P}}\frac{\varphi_{|\mathsf{f}}}{|\mathsf{f}|}\mathbf{e}_i\cdot(\mathbf{x}_{\mathsf{f}}-\mathbf{x}_{\mathsf{P}})|\mathsf{f}|. \tag{35}$$

Proof. (i) Let us consider the identity $3 = \mathrm{div}(\mathbf{x}-\mathbf{x}_{\mathsf{P}})$. We integrate by parts and we obtain

$$\begin{aligned} 3\int_{\mathsf{P}} R_{\mathsf{P}}^{\mathcal{V}}(\varphi)\,dV &= \int_{\mathsf{P}} R_{\mathsf{P}}^{\mathcal{V}}(\varphi)\ \mathrm{div}(\mathbf{x}-\mathbf{x}_{\mathsf{P}})\,dV \\ &= -\int_{\mathsf{P}} \mathbf{grad}\big(R_{\mathsf{P}}^{\mathcal{V}}(\varphi)\big)\cdot(\mathbf{x}-\mathbf{x}_{\mathsf{P}})\,dV + \sum_{\mathsf{f}\in\partial\mathsf{P}}\int_{\mathsf{f}}\gamma_{n,\mathsf{f}}\big(R_{\mathsf{f}}^{\mathcal{V}}(\varphi)\big)(\mathbf{x}-\mathbf{x}_{\mathsf{P}})\cdot\mathbf{n}_{\mathsf{P},\mathsf{f}}\,dL, \end{aligned} \tag{36}$$

where $\gamma_{n,\mathsf{f}}$ is the normal trace operator associated with the face f and $\mathbf{n}_{\mathsf{P},\mathsf{f}}$ is the unit vector perpendicular to f and pointing out of P. The first integral term in the right-hand side of (36) is zero. Indeed, we use (R3) with the discrete gradient definition (3) and (R4), which implies that $R^{\mathcal{E}}_{\mathsf{P}}$ is orthogonal to $\mathcal{O}^{\mathcal{E}}_{\mathsf{P}}$. We obtain:

$$\int_{\mathsf{P}} \mathbf{grad}\big(R^{\mathcal{V}}_{\mathsf{P}}(\varphi)\big)\cdot(\mathbf{x}-\mathbf{x}_{\mathsf{P}})\,dV = \int_{\mathsf{P}} R^{\mathcal{E}}_{\mathsf{P}}\big(\mathbf{grad}(\varphi)\big)\cdot(\mathbf{x}-\mathbf{x}_{\mathsf{P}})\,dV = 0. \tag{37}$$

We use (37) in (36) and we get:

$$3\int_{\mathsf{P}} R^{\mathcal{V}}_{\mathsf{P}}(\varphi)\,dV = \sum_{\mathsf{f}\in\partial\mathsf{P}}\int_{\mathsf{f}} R^{\mathcal{V}}_{\mathsf{f}}(\varphi_{|\mathsf{f}})(\mathbf{x}-\mathbf{x}_{\mathsf{P}})\cdot\mathbf{n}_{\mathsf{P},\mathsf{f}}\,dL = 0. \tag{38}$$

Since $(\mathbf{x}-\mathbf{x}_{\mathsf{P}})\cdot\mathbf{n}_{\mathsf{P},\mathsf{f}}$ is constant on each face f and $R^{\mathcal{V}}_{\mathsf{f}}$ is an admissible reconstruction operator the result of the left-hand side of (36) does not depend on the reconstruction operator $R^{\mathcal{V}}_{\mathsf{P}}$ (and nor on $R^{\mathcal{V}}_{\mathsf{f}}$ for each f of $\partial\mathsf{P}$).

(ii) Let us consider the constant vector field

$$2\,\mathbf{e}_i = \mathbf{curl}\big(\mathbf{p}^1(\mathbf{x})\big) \quad \text{with } \mathbf{p}^1_i(\mathbf{x}) = \mathbf{e}_i\times(\mathbf{x}-\mathbf{x}_{\mathsf{P}}) \text{ for } \mathbf{x}\in\mathsf{P}, \tag{39}$$

where "$\times$" denotes the cross product between three-dimensional vectors. We use (39), we integrate by parts and we obtain

$$\begin{aligned} 2\int_{\mathsf{P}} R^{\mathcal{E}}_{\mathsf{P}}(\varphi)\cdot\mathbf{e}_i\,dV &= \int_{\mathsf{P}} R^{\mathcal{E}}_{\mathsf{P}}(\varphi)\cdot\mathbf{curl}\big(\mathbf{p}^1_i\big)\,dV \\ &= \int_{\mathsf{P}} \mathbf{curl}\big(R^{\mathcal{E}}_{\mathsf{P}}(\varphi)\big)\cdot\mathbf{p}^1_i\,dV + \sum_{\mathsf{f}\in\partial\mathsf{P}}\int_{\mathsf{f}} \gamma_{t,\mathsf{f}}\big(R^{\mathcal{E}}_{\mathsf{P}}(\varphi)\big)\cdot\gamma_{t,\mathsf{f}}\big(\mathbf{n}_{\mathsf{P},\mathsf{f}}\times\mathbf{p}^1_i\big)\,dS, \end{aligned} \tag{40}$$

where $\gamma_{t,\mathsf{f}}$ is the trace operator that returns the trace of a three-dimensional vector field over a generic two-dimensional face f of $\partial\mathsf{P}$ and $\mathbf{n}_{\mathsf{P},\mathsf{f}}$ is the unit normal vector pointing out of P. The first integral term in the right-hand side of (40) is zero. Indeed, we use (R3) with the discrete curl definition (4) and (R4), which implies that $R^{\mathcal{F}}_{\mathsf{P}}$ is orthogonal to $\mathcal{O}^{\mathcal{F}}_{\mathsf{P}}$. We obtain:

$$\int_{\mathsf{P}} \mathbf{curl}\big(R^{\mathcal{E}}_{\mathsf{P}}(\varphi)\big)\cdot\mathbf{p}^1_i\,dV = \int_{\mathsf{P}} R^{\mathcal{F}}_{\mathsf{P}}\big(\mathcal{CURL}(\varphi)\big)\cdot\mathbf{p}^1_i\,dV = 0. \tag{41}$$

We use (41) in (40) and assumption (R5) to get

$$\begin{aligned} 2\int_{\mathsf{P}} R^{\mathcal{E}}_{\mathsf{P}}(\varphi)\cdot\mathbf{e}_i\,dV &= \sum_{\mathsf{f}\in\partial\mathsf{P}}\int_{\mathsf{f}} \gamma_{t,\mathsf{f}}\big(R^{\mathcal{E}}_{\mathsf{P}}(\varphi)\big)\cdot\gamma_{t,\mathsf{f}}\big(\mathbf{n}_{\mathsf{P},\mathsf{f}}\times\mathbf{p}^1\big)\,dS \\ &= \sum_{\mathsf{f}\in\partial\mathsf{P}}\int_{\mathsf{f}} R^{\mathcal{E}}_{\mathsf{f}}(\varphi)\cdot\gamma_{t,\mathsf{f}}\big(\mathbf{n}_{\mathsf{P},\mathsf{f}}\times\mathbf{p}^1\big)\,dS. \end{aligned} \tag{42}$$

We apply some vector calculus to check that

$$\mathbf{n}_{\mathsf{P},\mathsf{f}}\times\mathbf{p}^1_i = \mathbf{n}_{\mathsf{P},\mathsf{f}}\cdot(\mathbf{x}-\mathbf{x}_{\mathsf{P}})\mathbf{e}_i - (\mathbf{n}_{\mathsf{P},\mathsf{f}}\cdot\mathbf{e}_i)(\mathbf{x}-\mathbf{x}_{\mathsf{P}}). \tag{43}$$

Using the linearity of the traces (and noting that $\mathbf{n}_{\mathsf{P},\mathsf{f}}\cdot(\mathbf{x}-\mathbf{x}_{\mathsf{P}})$ is a constant quantity on f) yields

$$\gamma_{t,\mathsf{f}}\big(\mathbf{n}_{\mathsf{P},\mathsf{f}}\times\mathbf{p}^1\big) = \mathbf{n}_{\mathsf{P},\mathsf{f}}\cdot(\mathbf{x}-\mathbf{x}_{\mathsf{P}})\gamma_{t,\mathsf{f}}(\mathbf{e}_i) - (\mathbf{n}_{\mathsf{P},\mathsf{f}}\cdot\mathbf{e}_i)\gamma_{t,\mathsf{f}}(\mathbf{x}-\mathbf{x}_{\mathsf{P}}). \tag{44}$$

We set $\boldsymbol{\xi}=\gamma_t(\mathbf{x})$ and recall that $\boldsymbol{\xi}_{\mathsf{f}}$ stands for the barycenter of face f. Adding and subtracting $(\mathbf{n}_{\mathsf{P},\mathsf{f}}\cdot\mathbf{e}_i)\cdot\boldsymbol{\xi}_{\mathsf{f}}$ and rearranging the terms in (44) yields

$$\gamma_{t,\mathsf{f}}\big(\mathbf{n}_{\mathsf{P},\mathsf{f}}\times\mathbf{p}^1_i\big) = \mathbf{n}_{\mathsf{P},\mathsf{f}}\cdot(\mathbf{x}-\mathbf{x}_{\mathsf{P}})\gamma_{t,\mathsf{f}}(\mathbf{e}_i) + (\mathbf{n}_{\mathsf{P},\mathsf{f}}\cdot\mathbf{e}_i)\big(\gamma_{t,\mathsf{f}}(\mathbf{x}_{\mathsf{P}})-\boldsymbol{\xi}_{\mathsf{f}}\big) - (\mathbf{n}_{\mathsf{P},\mathsf{f}}\cdot\mathbf{e}_i)(\boldsymbol{\xi}-\boldsymbol{\xi}_{\mathsf{f}}). \tag{45}$$

We shorten the notation by introducing the constant vector $\boldsymbol{\alpha}_{\mathsf{f},i}$ that collects the first two terms in the right-hand side of (45) as in (34). We also evaluate $\mathbf{n}_{\mathsf{P},\mathsf{f}}\cdot(\mathbf{x}-\mathbf{x}_{\mathsf{P}})$ at the face center $\mathbf{x}_{\mathsf{f}}$ since, as we have already noted, this quantity is constant on f. Then, by going back to (42) and using (R5) we obtain the following relation:

$$2\int_{\mathsf{P}} R^{\mathcal{E}}_{\mathsf{P}}(\varphi)\cdot\mathbf{e}_i\,dV = \sum_{\mathsf{f}\in\partial\mathsf{P}}\int_{\mathsf{f}} R^{\mathcal{E}}_{\mathsf{f}}(\varphi_{|\mathsf{f}})\cdot\boldsymbol{\alpha}_{\mathsf{f},i}\,dS - \sum_{\mathsf{f}\in\partial\mathsf{P}}(\mathbf{n}_{\mathsf{P},\mathsf{f}}\cdot\mathbf{e}_i)\int_{\mathsf{f}} R^{\mathcal{E}}_{\mathsf{f}}(\varphi_{|\mathsf{f}})\cdot(\boldsymbol{\xi}-\boldsymbol{\xi}_{\mathsf{f}})\,dS. \tag{46}$$

Since $R_{\mathsf{f}}^{\mathcal{E}}$ is an admissible reconstruction operator, the first term in the right-hand side of (46) does not depend on the choice of the reconstruction operator $R_{\mathsf{P}}^{\mathcal{E}}$. Moreover, the second term in the right-hand side of (46) is zero. In fact, (R4) implies that $R_{\mathsf{f}}^{\mathcal{E}}$ is orthogonal to $\mathcal{O}_{\mathsf{f}}^{\mathcal{E}}$, and using (R5) yields

$$\int_{\mathsf{f}} \gamma_t\big(R_{\mathsf{P}}^{\mathcal{E}}(\varphi)\big)\cdot(\boldsymbol{\xi}-\boldsymbol{\xi}_{\mathsf{f}})\,dS = \int_{\mathsf{f}} R_{\mathsf{f}}^{\mathcal{E}}(\varphi_{|\mathsf{f}})\cdot(\boldsymbol{\xi}-\boldsymbol{\xi}_{\mathsf{f}})\,dS = 0.$$

Using this fact in (46) proves (34).

(iii) Let us consider the constant vector field

$$\mathbf{e}_i = \mathbf{grad}\big(p_i^1\big) \quad \text{where } p_i^1(\mathbf{x}) := \mathbf{e}_i\cdot(\mathbf{x}-\mathbf{x}_{\mathsf{P}}) \text{ for } \mathbf{x}\in\mathsf{P}. \tag{47}$$

We use (47), we integrate by parts and we obtain

$$\begin{aligned}\int_{\mathsf{P}} R_{\mathsf{P}}^{\mathcal{F}}(\varphi)\cdot\mathbf{e}_i\,dV &= \int_{\mathsf{P}} R_{\mathsf{P}}^{\mathcal{F}}(\varphi)\cdot\mathbf{grad}\big(p_i^1\big)\,dV\\ &= -\int_{\mathsf{P}} \mathrm{div}\big(R_{\mathsf{P}}^{\mathcal{F}}(\varphi)\big)\,p_i^1\,dV + \sum_{\mathsf{f}\in\partial\mathsf{P}}\int_{\mathsf{f}} \gamma_{n,\mathsf{f}}\big(R_{\mathsf{P}}^{\mathcal{F}}(\varphi)\big)\,p_i^1\,dV,\end{aligned} \tag{48}$$

where $\gamma_{n,\mathsf{f}}$ is the trace operator that returns the normal component of a vector field on face f. Once more, the first integral term in the right-hand side of (48) is zero. Indeed, we use (R3) with the discrete divergence definition (5), the fact that $R_{\mathsf{P}}^{\mathcal{P}}$ is constant on P, cf. (19), and we obtain:

$$\int_{\mathsf{P}} \mathrm{div}\big(R_{\mathsf{P}}^{\mathcal{F}}(\varphi)\big)\,p_i^1\,dV = \int_{\mathsf{P}} R_{\mathsf{P}}^{\mathcal{P}}\big(\mathcal{DIV}(\varphi)_{|\mathsf{P}}\big)\,p_i^1\,dV = R_{\mathsf{P}}^{\mathcal{P}}\big(\mathcal{DIV}(\varphi)_{|\mathsf{P}}\big)\int_{\mathsf{P}} p_i^1\,dV = 0. \tag{49}$$

We use (49) in (48), we apply property (R5), the basic choice (19), and the midpoint integration rule, which is exact for linear polynomials, to obtain (35):

$$\int_{\mathsf{P}} R_{\mathsf{P}}^{\mathcal{F}}(\varphi)\cdot\mathbf{e}_i\,dV = \sum_{\mathsf{f}\in\partial\mathsf{P}}\int_{\mathsf{f}} \gamma_{\mathsf{f}}\big(R_{\mathsf{P}}^{\mathcal{F}}(\varphi)\big)p_i^1(\mathbf{x})\,dV = \sum_{\mathsf{f}\in\partial\mathsf{P}}\frac{\varphi_{|\mathsf{f}}}{|\mathsf{f}|}\int_{\mathsf{f}} p_i^1(\mathbf{x})\,dV = \sum_{\mathsf{f}\in\partial\mathsf{P}}\frac{\varphi_{|\mathsf{f}}}{|\mathsf{f}|}\mathbf{e}_i\cdot(\mathbf{x}_{\mathsf{f}}-\mathbf{x}_{\mathsf{P}}). \qquad \square \tag{50}$$

3.2. Construction of the mimetic inner products

Based on the above results, we can now construct a family of mimetic inner products that are exact when one of the arguments is the projection of a constant field on each polygonal or polyhedral cell, i.e., the local projection of a piecewise constant (scalar or vector) field on the computational mesh. This property does not determine uniquely an inner product in $\mathcal{V}_{\mathsf{P}}^h$, $\mathcal{E}_{\mathsf{P}}^h$, $\mathcal{F}_{\mathsf{P}}^h$ (or in $\mathcal{V}_{\mathsf{f}}^h$ and $\mathcal{E}_{\mathsf{f}}^h$), and, hence, we need to introduce a systematic way to "complete" each inner product. To apply this strategy in all the cases of interest, we need to assume that any face f and edge e in $\partial\mathsf{P}$ scale consistently with P; formally, we require that

$$|\mathsf{P}| \sim \mathrm{diam}(\mathsf{P})^3 \sim |\mathsf{f}|^{3/2} \sim \mathrm{diam}(\mathsf{f})^3 \sim |\mathsf{e}|^3; \tag{51}$$

where $a\sim b$ stands for: "there exist two constants c and C such that $ca\leqslant b\leqslant Ca$". In particular, Eq. (51) implies that the size of all the geometric objects like faces and edges in an element are comparable. We express this concept through two positive numbers $|\mathsf{f}|_m$ and $|\mathsf{e}|_m$ that are such that:

$$|\mathsf{f}| \sim |\mathsf{f}|_m \quad \forall \mathsf{e}\in\partial\mathsf{P} \quad \text{and} \quad |\mathsf{e}| \sim |\mathsf{e}|_m \quad \forall \mathsf{f}\in\partial\mathsf{P}.$$

Since all the cochain spaces are finite-dimensional linear spaces, the action of any inner product can be represented by a symmetric and positive definite matrix, which is defined with respect to a suitable basis. The canonical basis is not well suited for the construction of the scalar product matrix even if such matrix offers the advantage of acting directly on the degrees of freedom of the discrete differential operators defined in Section 2.1.3. A better alternative basis at the cost of a basis transformation is provided by first choosing the projection of constant (scalar or vector) fields as the first elements of the basis set, and, then, completing the basis set in accordance with an orthogonality relation. We illustrate the process by discussing in details the construction of the scalar product $(\cdot,\cdot)_{\mathcal{F}_{\mathsf{P}}^h}$ for the 2-cochain space $\mathcal{F}_{\mathsf{P}}^h$, which is also the case treated in [31]. According to the definition given in (35), we set

$$\big(\varphi, \Pi^{\mathcal{F}}(\mathbf{c})\big)_{\mathcal{F}_{\mathsf{P}}^h} = \sum_{\mathsf{f}\in\partial\mathsf{P}}\frac{\varphi_{|\mathsf{f}}}{|\mathsf{f}|}\mathbf{c}\cdot(\mathbf{x}_{\mathsf{f}}-\mathbf{x}_{\mathsf{P}})|\mathsf{f}|. \tag{52}$$

Since $(\cdot,\cdot)_{\mathcal{F}_\mathsf{P}^h}$ mimics an L^2-inner product on P, relation (52) implies that the cochain φ must scale as $|\mathsf{f}|_m$. Let $\mathbf{e}_1$, $\mathbf{e}_2$, and $\mathbf{e}_3$ be the canonical basis of the three-dimensional space $\mathbb{R}^3$. First, we set

$$\widetilde{\varphi}_i = \Pi_\mathsf{P}^\mathcal{F}\mathbf{e}_i, \quad i=1,2,3.$$

These three 2-cochains properly scale like $|\mathsf{f}|_m$, cf. the definition of the operator $\Pi_\sigma^\mathcal{F}(\mathbf{u}) \in \mathcal{F}_\sigma^h$ for $\sigma=\mathsf{P}$ (and $k=2$) given in Section 2.3.1. Then, we complete the basis set by adding $(N_\mathsf{P}^\mathcal{F}-3)$ linearly independent cochains that are consistently required to scale like $|\mathsf{f}|_m$ and verify the orthogonality condition

$$(\widetilde{\varphi}_i,\widetilde{\varphi}_j)_{\mathcal{F}_\mathsf{P}^h}=0, \quad i=1,2,3 \text{ and } j=4,\dots N_\mathsf{P}^\mathcal{F}. \tag{53}$$

Thanks to Proposition 3.3, (iii), the scalar product in (53) is uniquely defined as the cochains $\widetilde{\varphi}_i$ are the projection of the constant fields $\mathbf{e}_i$, $i=1,2,3$. Thus, relations (35) and (53) determine the first three lines and three columns of the matrix that represents the scalar product. In fact, we apply the inner product definition (22), we use property (R2) and the result of Proposition 3.3, (iii), and we obtain

$$\big(\varphi,\Pi_\mathsf{P}^\mathcal{F}(\mathbf{e}_i)\big)_{\mathcal{F}_\mathsf{P}^h}=\int_\mathsf{P} R_\mathsf{P}^\mathcal{F}(\varphi)\cdot R_\mathsf{P}^\mathcal{F}\big(\Pi_\mathsf{P}^\mathcal{F}(\mathbf{e}_i)\big)\,dV=\sum_{\mathsf{f}\in\partial\mathsf{P}}\frac{\varphi_{|\mathsf{f}}}{|\mathsf{f}|}\mathbf{e}_i\cdot(\mathbf{x}_\mathsf{f}-\mathbf{x}_\mathsf{P})|\mathsf{f}|, \tag{54}$$

which holds for every 2-cochain $\varphi\in\mathcal{F}_\mathsf{P}^h$ and returns the same value for all the possible admissible reconstructions. Now, we are left to set the $(N_\mathsf{P}^\mathcal{F}-3)\times(N_\mathsf{P}^\mathcal{F}-3)$-sized lower diagonal block, but here any symmetric positive definite matrix that properly scales can be used. The scaling of the lower diagonal block must be the same of the upper diagonal block, and, in view of our choice of the degrees of freedom, the simplest choice for this block is given by:

$$|\mathsf{P}|I_{(N_\mathsf{P}^\mathcal{F}-3)\times(N_\mathsf{P}^\mathcal{F}-3)}.$$

The identity matrix $I_{(N^\mathcal{F}-3)\times(N^\mathcal{F}-3)}$ can be replaced by any symmetric positive definite matrix whose eigenvalues are uniformly bounded away from 0 and $+\infty$. These bounds will guarantee that there exists two constants c and C such that

$$\varphi\in\mathcal{F}_\mathsf{P}^h:\quad c|\mathsf{P}|\sum_{\mathsf{f}\in\partial\mathsf{P}}|\varphi_{|\mathsf{f}}|^2\leqslant(\varphi,\varphi)_{\mathcal{F}_\mathsf{P}^h}\leqslant C|\mathsf{P}|\sum_{\mathsf{f}\in\partial\mathsf{P}}|\varphi_{|\mathsf{f}}|^2.$$

In the rest of the subsection we discuss how to construct a mimetic inner product for the two- and three-dimensional cases considered in this paper by using the results of Section 3.1. In each case, we need two ingredients: (i) the result when one of the elements is the projection of a constant, (ii) the choice of the scaling for the canonical basis, which must be equal to the scaling used for the rest.

3.2.1. Two-dimensional case

We start from the scalar product in $\mathcal{V}_\mathsf{f}^h$ that we denote by $(\cdot,\cdot)_{\mathcal{V}_\mathsf{f}^h}$. For every constant scalar field c on the mesh face f, we apply the inner product definition (22), we use property (R2) and the result of Proposition 3.2, (i), and we obtain

$$\big(\varphi,\Pi_\mathsf{f}^\mathcal{V}(c)\big)_{\mathcal{V}_\mathsf{f}^h}=\int_\mathsf{f} R_\mathsf{f}^\mathcal{V}(\varphi)\cdot R_\mathsf{f}^\mathcal{V}\big(\Pi_\mathsf{f}^\mathcal{V}(c)\big)\,dS=\int_\mathsf{f} R_\mathsf{f}^\mathcal{V}(\varphi)c\,dS=c\sum_{\mathsf{e}\in\partial\mathsf{f}}(\boldsymbol{\xi}_\mathsf{e}-\boldsymbol{\xi}_\mathsf{f})\cdot\mathbf{n}_{\mathsf{f},\mathsf{e}}\frac{\varphi_{\mathsf{v}_1}+\varphi_{\mathsf{v}_2}}{2}|\mathsf{e}|, \tag{55}$$

which holds for every 0-cochain $\varphi\in\mathcal{V}_\mathsf{f}^h$. We take $\Pi_\mathsf{f}^\mathcal{V}(1)$ as the first element of the basis set and we complete the set by choosing $(N_\mathsf{f}^\mathcal{V}-1)$ elements in $\mathcal{V}_\mathsf{f}^h$ that scale as 1 (as $\Pi_\mathsf{f}^\mathcal{V}(1)$ does) and are orthogonal to $\Pi_\mathsf{f}^\mathcal{V}(1)$ with respect to the inner product given by (55). Formula (55) determines the first line and column of the scalar product matrix with respect to this basis. The matrix for the scalar product is eventually constructed by knowing that the scaling to be used is $|\mathsf{f}|_m$.

Then, we consider the scalar product in $\mathcal{E}_\mathsf{f}^h$ that we denote by $(\cdot,\cdot)_{\mathcal{E}_\mathsf{f}^h}$. For every constant vector field $\mathbf{c}=\sum_{i=1}^2 c_i\mathbf{e}_i$ on the mesh face f, we apply the inner product definition (22), we use property (R2) and the result of Proposition 3.2, (ii), and we obtain

$$\begin{aligned}\big(\varphi,\Pi_\mathsf{f}^\mathcal{E}(\mathbf{c})\big)_{\mathcal{E}_\mathsf{f}^h}&=\int_\mathsf{f} R_\mathsf{f}^\mathcal{E}(\varphi)\cdot R_\mathsf{f}^\mathcal{E}\big(\Pi_\mathsf{f}^\mathcal{V}(\mathbf{c})\big)\,dS=\int_\mathsf{f} R_\mathsf{f}^\mathcal{E}(\varphi)\mathbf{c}\,dS=\sum_{i=1}^2 c_i\int_\mathsf{f} R_\mathsf{f}^\mathcal{E}(\varphi)\cdot\mathbf{e}_i\,dS\\&=-\sum_{i=1}^2 c_i\sum_{\mathsf{e}\in\partial\mathsf{f}}\frac{\varphi_\mathsf{e}}{|\mathsf{e}|}\int_\mathsf{e} p_i^1(\boldsymbol{\xi})\,dL,\end{aligned} \tag{56}$$

where p_i^1 is the linear polynomial associated with $\mathbf{e}_i$ through Proposition 3.2, (i), and which holds for every 1-cochain $\varphi\in\mathcal{E}_\mathsf{f}^h$. We take $\Pi_\mathsf{f}^\mathcal{E}(\mathbf{e}_i)$, $i=1,2$, as the first two elements of the basis set and we complete the set by choosing $(N_\mathsf{f}^\mathcal{E}-2)$

elements in $\mathcal{E}_{\mathsf{f}}^h$ that scale as $|\mathsf{e}|$ (as both $\Pi_{\mathsf{f}}^{\mathcal{E}}(\mathbf{e}_1)$ and $\Pi_{\mathsf{f}}^{\mathcal{E}}(\mathbf{e}_2)$ do) and are orthogonal to the first two elements with respect to the inner product given by (56). Formula (56) determines the first two lines and columns of the scalar product matrix with respect to this basis. The matrix for the scalar product is eventually constructed by knowing that the scaling to be used is 1.

3.2.2. Three-dimensional case

In this section, we detail the construction of the mimetic inner product for $\mathcal{V}_{\mathsf{P}}^h$ and $\mathcal{E}_{\mathsf{P}}^h$, respectively denoted by $(\cdot,\cdot)_{\mathcal{V}_{\mathsf{P}}^h}$ and $(\cdot,\cdot)_{\mathcal{E}_{\mathsf{P}}^h}$. The scalar product for $\mathcal{F}_{\mathsf{P}}^h$ has been discussed as the initial example and we will not repeat its derivation here.

To construct the scalar product in $\mathcal{V}_{\mathsf{P}}^h$ we proceed as follows. For every constant scalar field c on the mesh polyhedron P, we apply the inner product definition (22), we use property (R2) and the result of Proposition 3.3, (i), and we obtain

$$\begin{aligned}\left(\varphi, \Pi_{\mathsf{P}}^{\mathcal{V}}(c)\right)_{\mathcal{V}_{\mathsf{P}}^h} &= \int_{\mathsf{P}} R_{\mathsf{P}}^{\mathcal{V}}(\varphi)\cdot R_{\mathsf{P}}^{\mathcal{V}}\left(\Pi_{\mathsf{P}}^{\mathcal{V}}(c)\right) dV = \int_{\mathsf{P}} R_{\mathsf{P}}^{\mathcal{V}}(\varphi) c\, dV \\ &= \frac{c}{3}\sum_{\mathsf{f}\in\partial\mathsf{P}}(\mathbf{x}_{\mathsf{f}}-\mathbf{x}_{\mathsf{P}})\cdot\mathbf{n}_{\mathsf{P},\mathsf{f}}\sum_{\mathsf{e}\in\partial\mathsf{f}}\left((\boldsymbol{\xi}_{\mathsf{e}}-\boldsymbol{\xi}_{\mathsf{f}})\cdot\mathbf{n}_{\mathsf{f},\mathsf{e}}\right)_{|\mathsf{e}}\frac{\varphi_{|\mathsf{v}_1}+\varphi_{|\mathsf{v}_2}}{2}|\mathsf{e}|,\end{aligned} \tag{57}$$

which holds for every 0-cochain $\varphi\in\mathcal{V}_{\mathsf{P}}^h$. We take $\Pi_{\mathsf{P}}^{\mathcal{V}}(1)$ as the first element of the basis set and we complete the set by choosing $(N_{\mathsf{P}}^{\mathcal{F}}-1)$ elements in $\mathcal{V}_{\mathsf{P}}^h$ that scale as $|\mathsf{P}|$ (as $\Pi^{\mathcal{V}}(1)$ does) and are orthogonal to the first basis element with respect to the inner product given by (57).

Then, we deal with the scalar product in $\mathcal{E}_{\mathsf{P}}^h$. For every constant vector field $\mathbf{c}=\sum_{i=1}^3 c_i\mathbf{e}_i$ on the mesh polyhedron P, we apply the inner product definition (22), we use property (R2) and the result of Proposition 3.3, (i), and we obtain

$$\begin{aligned}\left(\varphi, \Pi_{\mathsf{P}}^{\mathcal{E}}(\mathbf{c})\right)_{\mathcal{E}_{\mathsf{P}}^h} &= \int_{\mathsf{P}} R_{\mathsf{P}}^{\mathcal{E}}(\varphi)\cdot R_{\mathsf{P}}^{\mathcal{E}}\left(\Pi_{\mathsf{P}}^{\mathcal{E}}(\mathbf{c})\right) dV = \int_{\mathsf{P}} R_{\mathsf{P}}^{\mathcal{E}}(\varphi)\mathbf{c}\, dV = \sum_{i=1}^3 c_i\int_{\mathsf{P}} R_{\mathsf{P}}^{\mathcal{E}}(\varphi)\cdot\mathbf{e}_i\, dV \\ &= \sum_{i=1}^3\frac{c_i}{2}\sum_{\mathsf{f}\in\partial\mathsf{P}}\int_{\mathsf{f}} R_{\mathsf{f}}^{\mathcal{E}}(\varphi_{|\mathsf{f}})\cdot\boldsymbol{\alpha}_{\mathsf{f},i}\, dS,\end{aligned} \tag{58}$$

where the vector field $\boldsymbol{\alpha}_{\mathsf{f},i}$ is given by (34), and which holds for every 1-cochain $\varphi\in\mathcal{E}_{\mathsf{P}}^h$. We take $\Pi_{\mathsf{P}}^{\mathcal{E}}(\mathbf{e}_i)$ for $i=1,2,3$ as the first three vectors of the basis set, and we complete the set by choosing $(N_{\mathsf{P}}^{\mathcal{E}}-3)$ elements in $\mathcal{E}_{\mathsf{P}}^h$ that scale as $|\mathsf{P}|$ (as the three discrete field $\Pi_{\mathsf{P}}^{\mathcal{E}}(\mathbf{e}_i)$ do) and are orthogonal to the first three elements with respect to the inner product given by (58).

4. Numerical examples

We present a set of numerical experiments to confirm the effectiveness of the mimetic inner products developed in the previous sections to the discretization of partial differential equations. In Sections 4.1 and 4.2 we consider the Maxwell equations related to the *curl–curl* and *div–curl* problems. In Section 4.3 we consider the Maxwell eigenvalue problem. We focus here on the eigenvalue computation because it is well known that such problem is a delicate step in the context of Maxwell equations [23].

In the next subsections we will make use of the functional space

$$H(\mathrm{curl},\Omega)=\left\{\mathbf{v}\in\left(L^2(\Omega)\right)^2 \text{ such that } \mathbf{curl}(\mathbf{v})\in\left(L^2(\Omega)\right)^2\right\} \tag{59}$$

and its affine subspace

$$H_{\mathbf{g}}(\mathrm{curl},\Omega)=\left\{\mathbf{v}\in H(\mathrm{curl},\Omega) \text{ such that } \mathbf{v}\times\mathbf{n}=\mathbf{g} \text{ on } \Gamma\right\}. \tag{60}$$

We shall also consider the functional space $H_0(\mathrm{curl},\Omega)$ that is defined by setting $\mathbf{g}=0$ in (60). We do not explicitly require that the vector fields in $H_{\mathbf{g}}(\mathrm{curl},\Omega)$ be divergence-free. We shall consider the functional space $H^1(\Omega)$ of the scalar fields in $L^2(\Omega)$ with first derivatives in $L^2(\Omega)$ and its linear subspace

$$H_0^1(\Omega)=\left\{q\in L^2(\Omega),\ \mathbf{grad}(q)\in\left(L^2(\Omega)\right)^2,\ \text{with } q=0 \text{ on } \Gamma\right\}. \tag{61}$$

The convergence results presented in this section are reported with respect to the mesh size parameter h, which is defined as usual by $h=\max_{\mathsf{P}\in\Omega_h} h_{\mathsf{P}}$, where the local factor h_{P} is the maximum distance between any two points of the polygonal or polyhedral cell P. The mesh regularity assumptions introduced in Section 2.1 (see also the discussion at the beginning of Section 3.2) imply that h_{P} varies uniformly throughout the mesh elements.

4.1. Magnetostatics: the curl–curl model

Let us consider the magnetostatic model in *curl–curl* form for the vector potential $\mathbf{u}$:

$$\mathbf{curl}\big(\mu^{-1}\mathbf{curl}(\mathbf{u})\big) + c\mathbf{u} = \mathbf{J} \quad \text{in } \Omega, \tag{62}$$

$$\mathbf{u} \times \mathbf{n} = \mathbf{g} \quad \text{on } \partial\Omega, \tag{63}$$

with right-hand side $\mathbf{J} \in (L^2(\Omega))^3$, μ the magnetic permeability, and with the scalar positive coefficient c.

The variational formulation of problem (62)–(63) reads as:

Find $\mathbf{u} \in H_{\mathbf{g}}(\mathrm{curl}, \Omega)$ *such that*:

$$\int_\Omega \mu^{-1}\mathbf{curl}(\mathbf{u}) \cdot \mathbf{curl}(\mathbf{v})\, dV + c\int_\Omega \mathbf{u}\cdot\mathbf{v}\, dV = \int_\Omega \mathbf{J}\cdot\mathbf{v}\, dV \quad \forall \mathbf{v} \in H_0(\mathrm{curl}, \Omega). \tag{64}$$

Under our assumptions on the data, the left-hand side of (64) is a continuous and coercive bilinear form on $H_0(\mathrm{curl}, \Omega) \times H_0(\mathrm{curl}, \Omega)$; the right-hand side of (64) is a continuous functional on $H_0(\mathrm{curl}, \Omega)$. Existence and uniqueness of the solution $\mathbf{u} \in H_{\mathbf{g}}(\mathrm{curl}, \Omega)$ follows from the Lax–Milgram lemma.

To design a mimetic discretization of problem (64), we first define the degrees of freedom, which represent the scalar and vector fields in the discrete setting. To this end, we consider the edge-based discrete field $\mathbf{u}_h \in \mathcal{E}^h$, whose components u_{e} approximate the value of the edge average of the tangential component of the vector field $\mathbf{u}$ along the mesh edge e. The affine subspace $\mathcal{E}^h_g$ of $\mathcal{E}^h$ is formed by the edge functions $\mathbf{v}_h = \{v_{\mathsf{e}}\} \in \mathcal{E}^h$ that are such that each edge value v_{e} equals the average on the edge e of the tangential component of the vector $\mathbf{g}$. The linear subspace $\mathcal{E}^h_0$ is immediately derived by setting $\mathbf{g} = 0$ in the previous definition. We characterize the action of the curl operator on the grid functions in $\mathcal{E}^h$ through the mimetic curl operator $\mathcal{CURL}$ defined in (4). Moreover, to take into account the media properties the mimetic inner product in $\mathcal{F}^h$ is weighted by μ^{-1}.

We approximate the integrals in (64) by the mimetic inner products $(\cdot,\cdot)_{\mathcal{E}^h}$ and $(\cdot,\cdot)_{\mathcal{F}^h}$ for edge and face functions as follows:

$$\int_\Omega \mu^{-1}\mathbf{curl}(\mathbf{u}) \cdot \mathbf{curl}(\mathbf{v})\, dV \approx \big(\mathcal{CURL}(\mathbf{u}_h), \mathcal{CURL}(\mathbf{v}_h)\big)_{\mathcal{F}^h}, \tag{65}$$

$$\int_\Omega \mathbf{u}\cdot\mathbf{v}\, dV \approx (\mathbf{v}_h, q_h)_{\mathcal{E}^h}. \tag{66}$$

The mimetic discretization of (64) reads as:

Find $\mathbf{u}_h \in \mathcal{E}^h_g$ *such that*:

$$\big(\mathcal{CURL}(\mathbf{u}_h), \mathcal{CURL}(\mathbf{v}_h)\big)_{\mathcal{F}^h} + (\mathbf{v}_h, \mathbf{u}_h)_{\mathcal{E}^h} = (\mathbf{J}_h, \mathbf{v}_h)_{\mathcal{E}^h} \quad \forall \mathbf{v}_h \in \mathcal{E}^h_g. \tag{67}$$

We consider the relative errors:

$$\mathsf{E}_{rel}(\mathbf{u}) = \frac{|||\mathbf{u}_h - \Pi^{\mathcal{E}}(\mathbf{u})|||_{\mathcal{E}^h}}{|||\Pi^{\mathcal{E}}(\mathbf{u})|||_{\mathcal{E}^h}}, \qquad \mathsf{E}_{rel}\big(\mathbf{curl}(\mathbf{u})\big) = \frac{|||\mathcal{CURL}(\mathbf{u}_h - \Pi^{\mathcal{E}}(\mathbf{u}))|||_{\mathcal{F}^h}}{|||\mathcal{CURL}(\Pi^{\mathcal{E}}(\mathbf{u}))|||_{\mathcal{F}^h}}, \tag{68}$$

where $|||\cdot|||_{\mathcal{E}^h}$ and $|||\cdot|||_{\mathcal{F}^h}$ are the (mesh-dependent) norms induced by the mimetic inner product defined in $\mathcal{E}^h$ and $\mathcal{F}^h$, respectively.

In Tables 1 and 2, we show the result for the approximation of $\mathbf{u}$ and $\mathbf{curl}(\mathbf{u})$ when we solve (64) on the cubic domain $\Omega =]0,1[\times]0,1[\times]0,1[$ using the mesh sequences "Mesh-A" (regular hexahedra) and "Mesh-F" (prismatic cells) of the FVCA-6 benchmark [49]. Fig. 3 shows the first mesh of the sequence. A portion of the mesh around the vertex $(1,1,1)$ has been removed to show the internal mesh structure.

The current vector $\mathbf{J}$ and the boundary conditions are determined by imposing the exact solution:

$$\mathbf{u}(x,y,z) = \begin{pmatrix} x(1-x)y(1-y)z(1-z) + \sin(2\pi x)y\sin(2\pi z) \\ xy + xz + yz + 1 + \sin(2\pi x)y\cos(2\pi z) \\ \sin(2\pi x)\sin(2\pi y)\sin(2\pi z) \end{pmatrix}.$$

Table 1
Curl–curl magnetostatic problems for constant μ; relative approximation errors and convergence rates with respect to h for $\mathbf{u}$ and $\mathbf{curl}(\mathbf{u})$ using the mesh family "Mesh-A" (regular hexahedra) from the FVCA-6 benchmark [49].

h	$E_{rel}(\mathbf{u})$	Rate	$E_{rel}(\mathbf{curl}(\mathbf{u}))$	Rate
$4.330\,10^{-1}$	$5.148\,10^{-2}$	–	$5.929\,10^{-2}$	–
$2.165\,10^{-1}$	$1.419\,10^{-2}$	1.859	$1.290\,10^{-2}$	2.200
$1.083\,10^{-1}$	$3.587\,10^{-3}$	1.983	$2.610\,10^{-3}$	2.305
$5.413\,10^{-2}$	$8.944\,10^{-4}$	2.003	$5.018\,10^{-4}$	2.378

Table 2
Curl–curl magnetostatic problems for constant μ; relative approximation errors and convergence rates with respect to h for $\mathbf{u}$ and $\mathbf{curl}(\mathbf{u})$ using the mesh family "Mesh-F" (prismatic cells) from the FVCA-6 benchmark [49].

h	$E_{rel}(\mathbf{u})$	Rate	$E_{rel}(\mathbf{curl}(\mathbf{u}))$	Rate
$2.243\,10^{-1}$	$3.404\,10^{-1}$	–	$2.709\,10^{-2}$	–
$1.182\,10^{-1}$	$1.301\,10^{-1}$	1.500	$7.792\,10^{-3}$	1.944
$7.924\,10^{-2}$	$6.589\,10^{-2}$	1.702	$3.300\,10^{-3}$	2.149

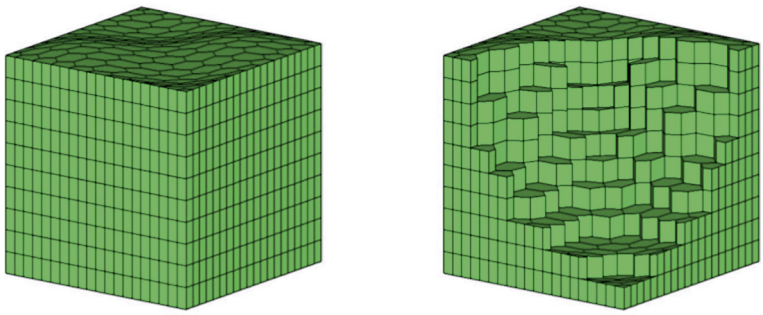

Fig. 3. Test on curl–curl model. Left plot: subdivision of $\Omega =]0,1[\times]0,1[\times]0,1[$ in a prismatic fashion with polygonal basis; right plot: a portion around the vertex $(1,1,1)$ has been removed to show the interior structure. First mesh of the mesh sequence "Mesh-F" of the FVCA-6 benchmark [49].

4.2. Magnetostatics: the div–curl model

Let us consider the magnetostatic model in *div–curl* form for the vector potential $\mathbf{u}$ and a suitable Lagrange multiplier field p to take into account the solenoidal constraint:

$$\mathbf{curl}\big(\mu^{-1}\mathbf{curl}(\mathbf{u})\big) + \mathbf{grad}(p) = \mathbf{J} \quad \text{in } \Omega, \tag{69}$$

$$\mathrm{div}(\mathbf{u}) = 0 \quad \text{in } \Omega, \tag{70}$$

$$\mathbf{u} \times \mathbf{n} = \mathbf{g} \quad \text{on } \partial\Omega, \tag{71}$$

where $\mathbf{J}$ is the current vector and μ the magnetic permeability.

The variational formulation of problem (69)–(71) reads:

Find $(\mathbf{u}, p) \in H_{\mathbf{g}}(\mathrm{curl}, \Omega) \times H_0^1(\Omega)$ *such that*:

$$\int_\Omega \mu^{-1}\mathbf{curl}(\mathbf{u}) \cdot \mathbf{curl}(\mathbf{v})\, dV + \int_\Omega \mathbf{v} \cdot \mathbf{grad}(p)\, dV = \int_\Omega \mathbf{J} \cdot \mathbf{v}\, dV \quad \forall \mathbf{v} \in H_0(\mathrm{curl}, \Omega), \tag{72}$$

$$\int_\Omega \mathbf{u} \cdot \mathbf{grad}(q)\, dV = 0 \quad \forall q \in H_0^1(\Omega). \tag{73}$$

Under suitable assumptions on the regularity of μ, the well-posedness of (72)–(73) can be proved in the framework of Brezzi–Babuska theory for saddle-point problems [30].

To design a mimetic discretization of problem (72)–(73), we first define the degrees of freedom, which represent the scalar and vector fields in the discrete setting:

(i) the node-based discrete field $p_h \in \mathcal{V}^h$, whose components p_v approximate the value of the scalar field p at the vertices of the mesh. The linear subspace $\mathcal{V}_0^h \subset \mathcal{V}^h$ is formed by all the node functions whose value is zero at the boundary nodes;

Table 3
Div–curl magnetostatic problems for constant μ: relative approximation errors and convergence rates with respect to h for $\mathbf{u}$ and $\mathbf{curl}(\mathbf{u})$ using mesh family "Mesh-A" (regular hexahedra) from the FVCA-6 benchmark [49].

h	$E_{rel}(\mathbf{u})$	Rate	$E_{rel}(\mathbf{curl}(\mathbf{u}))$	Rate
$2.500\,10^{-1}$	$2.314\,10^{-1}$	–	$2.335\,10^{-1}$	–
$1.250\,10^{-1}$	$5.559\,10^{-2}$	2.057	$5.896\,10^{-2}$	1.985
$6.250\,10^{-2}$	$1.385\,10^{-2}$	2.004	$1.477\,10^{-2}$	1.996
$3.125\,10^{-2}$	$3.461\,10^{-3}$	2	$3.696\,10^{-3}$	1.999

Table 4
Div–curl magnetostatic problems for variable μ; relative approximation errors and convergence rates with respect to h for $\mathbf{u}$ and $\mathbf{curl}(\mathbf{u})$ using mesh family "Mesh-A" (regular hexahedra) from the FVCA-6 benchmark [49].

h	$E_{rel}(\mathbf{u})$	Rate	$E_{rel}(\mathbf{curl}(\mathbf{u}))$	Rate
$2.500\,10^{-1}$	$2.200\,10^{-1}$	–	$2.290\,10^{-1}$	–
$1.250\,10^{-1}$	$5.588\,10^{-2}$	1.977	$6.183\,10^{-2}$	1.889
$6.250\,10^{-2}$	$1.419\,10^{-2}$	1.977	$1.578\,10^{-2}$	1.970
$3.125\,10^{-2}$	$3.563\,10^{-3}$	1.993	$3.965\,10^{-3}$	1.992

(ii) the edge-based discrete field $\mathbf{u}_h \in \mathcal{E}^h$, whose components $u_{\mathtt{e}}$ approximate the value of the edge average of the tangential component of the vector field $\mathbf{u}$ along the mesh edge $\mathtt{e}$. The affine subspace $\mathcal{E}^h_g$ and the linear subspace $\mathcal{E}^h_0$ are the same defined as in Section 4.1.

We characterize the gradient operator on the grid functions of $\mathcal{V}^h$ through the mimetic operator $\mathcal{GRAD}$ defined in (3). We characterize the curl operator on the grid functions of $\mathcal{E}^h$ through the mimetic operator $\mathcal{CURL}$ defined in (4). Moreover, to take into account the media properties the mimetic inner product in $\mathcal{F}^h$ is weighted by μ^{-1}.

We approximate the integrals in (72)–(73) by the mimetic inner products $(\cdot,\cdot)_{\mathcal{E}^h}$ and $(\cdot,\cdot)_{\mathcal{F}^h}$ for edge and face functions as follows:

$$\int_\Omega \mu^{-1}\mathbf{curl}(\mathbf{u})\cdot\mathbf{curl}(\mathbf{v})\,dV \approx \big(\mathcal{CURL}(\mathbf{u}_h),\mathcal{CURL}(\mathbf{v}_h)\big)_{\mathcal{F}^h}, \tag{74}$$

$$\int_\Omega \mathbf{v}\cdot\mathbf{grad}(q)\,dV \approx \big(\mathbf{v}_h,\mathcal{GRAD}(q_h)\big)_{\mathcal{E}^h}. \tag{75}$$

The mimetic discretization of (72)–(73) reads as:

Find $(\mathbf{u}_h, p_h) \in \mathcal{E}^h_g \times \mathcal{V}^h_0$ *such that*:

$$\big(\mathcal{CURL}(\mathbf{u}_h),\mathcal{CURL}(\mathbf{v}_h)\big)_{\mathcal{F}^h} + \big(\mathbf{v}_h,\mathcal{GRAD}(p_h)\big)_{\mathcal{E}^h} = (\mathbf{J}_h,\mathbf{v}_h)_{\mathcal{E}^h} \quad \forall \mathbf{v}_h \in \mathcal{E}^h_0, \tag{76}$$

$$\big(\mathbf{u}_h,\mathcal{GRAD}(q_h)\big)_{\mathcal{E}^h} = 0 \quad \forall q_h \in \mathcal{V}^h_0. \tag{77}$$

This mimetic discretization is similar to the ones considered in [29,63].

In Tables 3–4 we show the result for the approximation of $\mathbf{u}$ and $\mathbf{curl}(\mathbf{u})$ when we solve (72)–(73) with the variable magnetic permeability

$$\mu^{-1}(x,y,z) = \begin{pmatrix} 1+y^2+z^2 & -xy & -xz \\ -xy & 1+x^2+z^2 & -yz \\ -xz & -yz & 1+x^2+y^2 \end{pmatrix}$$

using the mesh sequences "Mesh-A" (regular hexahedra) of the FVCA-6 benchmark [49]. The relative errors are measured using the two norms defined in (68).

The current vector $\mathbf{J}$ and the boundary conditions are determined by imposing the exact solutions:

$$\mathbf{u}(x,y,z) = \begin{pmatrix} 2\pi\, r(x)\sin(2\pi y)\cos(2\pi z) \\ -r'(x)\cos(2\pi y)\cos(2\pi z) \\ -2r'(x)\sin(2\pi y)\sin(2\pi z) \end{pmatrix}$$

with $r(x) = x^4$ and $p(x,y,z) = 64x(1-x)y(1-y)z(1-z)$.

4.3. Maxwell eigenvalue problem

We build new mimetic approximation schemes for the cavity resonator problem with perfectly conducting boundary conditions. Throughout this section, we will refer to this problem as the "*Maxwell eigenvalue problem*". Let Ω be a polygonal domain in 2-D or a polyhedral domain in 3-D with a Lipschitz boundary Γ. The Maxwell eigenvalue problem on the computational domain Ω involves the electric field $\mathbf{E}$, the magnetic induction field $\mathbf{H}$, the magnetic permeability μ, the electric permittivity ε. It reads as:

Find the real eigenvalues $\lambda = \omega^2$ corresponding to the frequencies $\omega > 0$ and the real eigenfield $\mathbf{E}$ and $\mathbf{H}$ such that

$$\begin{array}{lll} \mathbf{curl}(\mathbf{E}) - i\omega\mu\mathbf{H} = 0 & \text{in } \Omega & \text{(Faraday law)}, \\ \mathbf{curl}(\mathbf{H}) + i\omega\varepsilon\mathbf{E} = 0 & \text{in } \Omega & \text{(Ampère law)}, \\ \mathbf{E}\times\mathbf{n} = 0 \quad \text{and} \quad \mathbf{H}\cdot\mathbf{n} = 0 & \text{on } \Gamma & \text{(perfect conductor b.c.)}, \\ \operatorname{div}(\varepsilon\mathbf{E}) = 0 \quad \text{and} \quad \operatorname{div}(\mu\mathbf{H}) = 0 & \text{in } \Omega & \text{(gauge condition)}, \end{array} \tag{78}$$

where $\mathbf{n}$ denotes the outward normal to Γ. The quantities μ and ε are scalar real-valued functions defined on Ω and describe the material properties that are usually determined through experimental measures. Typical assumptions on μ and ε are that they are piecewise smooth functions with jumps at the material interfaces and that are bounded from below and from above. In the test cases considered in this subsection, μ and ε are either constant fields on the whole domain Ω or constant fields within subdomains of Ω. We recall that the functional space $H(\mathrm{curl}, \Omega)$ is the space of $L^2(\Omega)$ fields with curl in $L^2(\Omega)$; the functional space $H_0(\mathrm{curl}, \Omega)$ is the subspace of $H(\mathrm{curl}, \Omega)$ with perfectly conducting electric boundary conditions; the functional space $H(\mathrm{div}, \Omega)$ is the space of $L^2(\Omega)$ fields with divergence in $L^2(\Omega)$.

The *electric variational formulation* of the Maxwell eigenvalue problem reads as:

Find the frequencies $\omega > 0$ and the electric field $\mathbf{E} \in H_0(\mathrm{curl}, \Omega) \cap H(\mathrm{div}, \Omega)\backslash\{0\}$ such that $\operatorname{div}(\epsilon\mathbf{E}) = 0$ and

$$\int_\Omega \mu^{-1}\mathbf{curl}(\mathbf{E})\cdot\mathbf{curl}(\mathbf{E}')\,dV = \omega^2 \int_\Omega \epsilon\mathbf{E}\cdot\mathbf{E}'\,dV \quad \forall\mathbf{E}' \in H_0(\mathrm{curl}, \Omega)\cap H(\mathrm{div}, \Omega). \tag{79}$$

The triplet $(\omega, \mathbf{E}, \mathbf{H})$ with $\mathbf{H} = \mathbf{curl}(\mathbf{E})/i\omega\mu$ as provided by the Faraday law in (78) is called *the Maxwell eigenmode*. In two dimensions, the domain Ω becomes the section of an infinitely long cylinder, and, under suitable symmetries, the electric field verifies an equation like (79), where "**curl**" denotes the scalar curl operator for a two-component vector. Instead, the magnetic field verifies a Poisson-like equation such as

Find the frequencies $\omega > 0$ such that there exists a scalar field $\varphi \in H_0^1(\Omega)\backslash\{0\}$ such that

$$\int_\Omega \varepsilon^{-1}\mathbf{grad}(\varphi)\cdot\mathbf{grad}(\varphi')\,dV = \omega^2 \int_\Omega \mu\varphi\varphi'\,dV \quad \forall\varphi' \in H_0^1(\Omega). \tag{80}$$

We will refer to (80) as the *2-D scalar magnetic formulation*.

To deal with such problems numerically, we propose a new mimetic approximation of the two-dimensional electric and magnetic variational formulations, and a new mimetic approximation of the three-dimensional electric variational formulation. All these numerical approximations are readily built by specifying the degrees of freedom, the discretizations of the curl and gradient operators, and the mimetic inner products. Most of the test cases that we present in this subsection are taken from the benchmark webpage [46]. We also refer the interested reader to [44] for a thorough description of the Maxwell eigenmodes in three-dimensional tensor product domains.

We approximate the electric variational formulation (79) in two and three dimensions through these three steps:

(i) we represent the electric fields $\mathbf{E}$ and $\mathbf{E}'$ in the mimetic setting through the degrees of freedom of the *edge functions* $\mathbf{E}_h$ and $\mathbf{E}'_h$;
(ii) we characterize the action of the curl operator on such discrete functions through the mimetic curl operator $\mathcal{CURL}$ defined in (4);
(iii) we approximate the integrals in (79) by the mimetic inner products $(\cdot,\cdot)_{\mathcal{E}^h}$ and $(\cdot,\cdot)_{\mathcal{F}^h}$ for edge and face functions as follows:

$$\int_\Omega \mu^{-1}\mathbf{curl}(\mathbf{E})\cdot\mathbf{curl}(\mathbf{E}')\,dS \approx \left(\mathcal{CURL}(\mathbf{E}_h), \mathcal{CURL}(\mathbf{E}'_h)\right)_{\mathcal{F}^h}, \tag{81}$$

$$\int_\Omega \epsilon\mathbf{E}\cdot\mathbf{E}'\,dS \approx \left(\mathbf{E}_h, \mathbf{E}'_h\right)_{\mathcal{E}^h}. \tag{82}$$

To take into account the media properties the mimetic inner product in $\mathcal{F}^h$ is weighted by μ^{-1} and the mimetic inner product in $\mathcal{E}^h$ is weighted by ε. The mimetic approximation of (79) reads as:

Find the frequencies $\omega > 0$ and the edge function $\mathbf{E}_h \in \mathcal{E}^h$ such that

$$\big(\mathcal{CURL}(\mathbf{E}_h), \mathcal{CURL}(\mathbf{E}'_h)\big)_{\mathcal{F}^h} = \omega^2 \big(\mathbf{E}_h, \mathbf{E}'_h\big)_{\mathcal{E}^h} \quad \forall \mathbf{E}'_h \in \mathcal{E}^h. \tag{83}$$

Let us derive the corresponding generalized matrix eigenvalue problem. To this purpose, we consider the matrix operator C that returns the discrete curl of an edge function. On a mesh formed by $N^{\mathcal{F}}$ polygonal cells in 2-D or faces in 3-D and $N^{\mathcal{E}}$ edges, matrix C has $N^{\mathcal{F}}$ rows and $N^{\mathcal{E}}$ columns, its components are given according to (4) and form the face-edge incidence matrix of the mesh. Let $\mathsf{M}^{\mathcal{E}^h}$ and $\mathsf{M}^{\mathcal{F}^h}$ denote the symmetric and positive definite matrices that represent the mimetic inner products $(\cdot,\cdot)_{\mathcal{E}^h}$ and $(\cdot,\cdot)_{\mathcal{F}^h}$. We have:

$$\big(\mathcal{CURL}(\mathbf{E}_h), \mathcal{CURL}(\mathbf{E}'_h)\big)_{\mathcal{F}^h} = \big(\mathbf{E}'_h\big)^T \big(\mathsf{C}^T \mathsf{M}^{\mathcal{F}^h} \mathsf{C}\big)\mathbf{E}_h; \tag{84}$$

$$\big(\mathbf{E}_h, \mathbf{E}'_h\big)_{\mathcal{E}^h} = \big(\mathbf{E}'_h\big)^T \mathsf{M}^{\mathcal{E}^h} \mathbf{E}_h. \tag{85}$$

Using (84) and (85) yields the generalized matrix eigenvalue problem $\mathsf{A}\mathbf{E}_h = \lambda \mathsf{B}\mathbf{E}_h$, for the couple of matrices $\mathsf{A} = \mathsf{C}^T \mathsf{M}^{\mathcal{F}^h} \mathsf{C}$ and $\mathsf{B} = \mathsf{M}^{\mathcal{E}^h}$.

We approximate the magnetic variational formulation (80) in two dimensions through these three steps:

(i) we represent the scalar fields φ and φ' in the mimetic setting through the degrees of freedom of the *vertex functions* φ_h and φ'_h;
(ii) we characterize the action of the gradient operator on such discrete functions through the mimetic gradient operator $\mathcal{GRAD}$ defined in (3);
(iii) we approximate the integrals in (80) by the mimetic inner products $(\cdot,\cdot)_{\mathcal{V}^h}$ and $(\cdot,\cdot)_{\mathcal{E}^h}$ for vertex and edge functions as follows:

$$\int_\Omega \epsilon^{-1} \mathbf{grad}(\varphi) \cdot \mathbf{grad}(\varphi')\, dS \approx \big(\mathcal{GRAD}(\varphi_h), \mathcal{GRAD}(\varphi'_h)\big)_{\mathcal{E}^h}, \tag{86}$$

$$\int_\Omega \epsilon \varphi_h \varphi'_h\, dS \approx \big(\varphi_h, \varphi'_h\big)_{\mathcal{V}^h}. \tag{87}$$

To take into account the media properties the mimetic inner product in $\mathcal{E}^h$ is weighted by ε^{-1} and the mimetic inner product in $\mathcal{V}^h$ is weighted by ε.

The mimetic approximation of (80) reads as:

Find the frequencies $\omega > 0$ and the discrete vertex field $\varphi_h \in \mathcal{V}^h \backslash \{0\}$ such that

$$\big(\mathcal{GRAD}(\varphi_h), \mathcal{GRAD}(\varphi'_h)\big)_{\mathcal{E}^h} = \omega^2 \big(\varphi_h, \varphi'_h\big)_{\mathcal{V}^h} \quad \forall \varphi'_h \in \mathcal{V}^h. \tag{88}$$

To derive the corresponding generalized matrix eigenvalue problem, we consider the matrix operator G that returns the discrete gradient of a vertex function. On a mesh formed by $N^{\mathcal{V}}$ vertices and $N^{\mathcal{E}}$ edges, matrix G has $N^{\mathcal{E}}$ rows and $N^{\mathcal{V}}$ columns, its components are given according to (3) and form the edge–vertex incidence matrix of the mesh. Let $\mathsf{M}^{\mathcal{V}^h}$ and $\mathsf{M}^{\mathcal{E}^h}$ denote the symmetric and positive definite matrices that represent the mimetic inner products $(\cdot,\cdot)_{\mathcal{V}^h}$ and $(\cdot,\cdot)_{\mathcal{E}^h}$. We have:

$$\big(\mathcal{GRAD}(\varphi_h), \mathcal{GRAD}(\varphi'_h)\big)_{\mathcal{E}^h} = \big(\varphi'_h\big)^T \big(\mathsf{G}^T \mathsf{M}^{\mathcal{E}^h} \mathsf{G}\big)\varphi_h, \tag{89}$$

$$\big(\varphi_h, \varphi'_h\big)_{\mathcal{V}^h} = \big(\varphi'_h\big)^T \mathsf{M}^{\mathcal{V}^h} \varphi_h. \tag{90}$$

Using (89) and (90) yields the generalized matrix eigenvalue problem $\mathsf{A}\varphi_h = \lambda \mathsf{B}\varphi_h$, for the couple of matrices $\mathsf{A} = \mathsf{G}^T \mathsf{M}^{\mathcal{E}^h} \mathsf{G}$ and $\mathsf{B} = \mathsf{M}^{\mathcal{V}^h}$.

4.3.1. Related work

In [36], it is considered a mimetic approximation for the Maxwell eigenvalue problem in the mixed "div–grad" form for the scalar field p and the vector field $\mathbf{F}$:

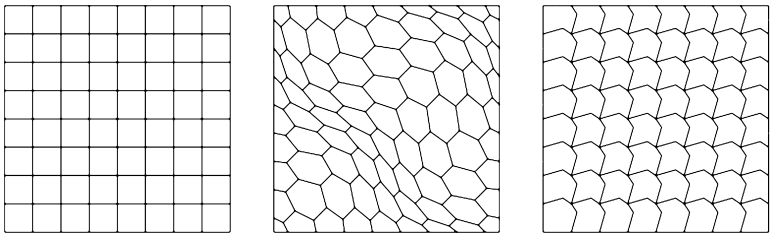

Fig. 4. Maxwell eigenvalue calculation on the square domain $[0,\pi]\times[0,\pi]$; from left to right: the square mesh, the mainly-hexagonal mesh and the non-convex mesh corresponding to refinement parameter $n=8$.

Find λ such that there exist p and $\mathbf{F}$, with $p\neq 0$, satisfying

$$\begin{aligned}&\mathbf{F}=-\mathsf{K}\,\mathbf{grad}(p)\quad \text{in } \Omega,\\ &\operatorname{div}(\mathbf{F})=\lambda p\quad \text{in } \Omega,\end{aligned}\tag{91}$$

where K is a full symmetric and uniformly strongly elliptic tensor. The mixed variational formulation is

$$\begin{aligned}&\int \mathbf{G}\cdot\mathsf{K}^{-1}\mathbf{F}\,dV-\int \operatorname{div}(\mathbf{G})\,p\,dV=0\quad \forall\mathbf{G}\in H(\operatorname{div},\Omega),\\ &\int \operatorname{div}(\mathbf{F})\,q\,dV=\lambda\int p\,q\,dV\quad \forall q\in L^2(\Omega).\end{aligned}\tag{92}$$

The mimetic variational formulation proposed in [36] approximates the scalar field p by the cell function $p_h\in\mathcal{P}^h$, the vector field $\mathbf{F}$ by the face function $\mathbf{F}_h\in\mathcal{F}^h$, and the divergence operator div by the discrete divergence operator $\mathcal{DIV}$ defined in (5). The inner product for the cell functions, e.g., $(\cdot,\cdot)_{\mathcal{P}^h}$, and for the face functions, e.g., $(\cdot,\cdot)_{\mathcal{F}^h}$, coincide with the mimetic inner products obtained by assembling the local ones discussed in Section 3.2.1 and in Section 3.2.2. The mimetic approximation of problem (92) reads as:

Find λ such that there exist a cell function $p_h\in\mathcal{P}^h$ and a face function $\mathbf{F}_h\in\mathcal{F}^h$ such that

$$\begin{aligned}&(\mathbf{F}_h,\mathbf{G}_h)_{\mathcal{F}^h}-\big(p_h,\mathcal{DIV}(\mathbf{F}_h)\big)_{\mathcal{P}^h}=0\quad \text{in } \mathbf{G}_h\in\mathcal{F}^h,\\ &\big(\mathcal{DIV}(\mathbf{F}),\mathbf{G}\big)_{\mathcal{P}^h}=\lambda(p_h,q_h)_{\mathcal{P}^h}\quad \text{in } q_h\in\mathcal{P}^h.\end{aligned}\tag{93}$$

The a priori error analysis that is carried out in [36] proves the optimal convergence rate for the numerical approximation of the eigenvalues and the associated eigenspaces provided by (93). The numerical experiments therein conducted, which are a subset of the test cases considered in this work, confirm such behavior.

4.3.2. Two-dimensional Maxwell eigenvalue problem

Test 1: *Square domain, Dirichlet boundary, constant magnetic permeability*.

Let $\Omega\subset\mathbb{R}^2$ be the square domain $(0,\pi)\times(0,\pi)$. We consider the numerical approximation of the Maxwell eigenvalue problem with Dirichlet boundary conditions. The eigenvalues of both the electric and magnetic formulations are given by $\lambda=m_x^2+m_y^2$ where m_x and m_y are positive integer numbers and correspond to the eigenfunctions $u=\sin(m_x x)\sin(m_y y)$.

We solve this problem on three sequences of meshes that we refer as *square meshes*, *mainly-hexagonal meshes* and *non-convex meshes* as they are formed by square cells, mainly-hexagonal cells, and non-convex cells. These families allows us to test the behavior of the mimetic discretizations on non-structured polygonal meshes. All such mesh families are obtained from a sequence of structured meshes that are parametrized by $n=4,8,16,32$, which is the number of subdivisions in each coordinate direction. In Fig. 4 we plot the meshes for $n=8$. As shown in these plots, a non-convex mesh is made of a regular pattern of octagonal cells, which are built by adding a mesh vertex at each edge midpoint of an underlying square mesh. This additional vertex is then translated by a fixed displacement vector when the original position lies inside the computational domain. The mainly-hexagonal meshes are obtained by a dualization procedure applied to a sequence of nested triangular meshes. The starting, coarser, triangular mesh is a Delaunay triangulation generated by Triangle [82,83]. More details about such mesh constructions can be found in [36].

The results for the first few eigenvalues are shown in Tables 5 and 6 for the mimetic discretizations of the electric and magnetic formulation, respectively. A comparison of the numbers reported in these tables reveals that the eigenvalue calculation on the polygonal meshes give slightly less accurate results than the regular square meshes. Indeed, although the asymptotic rate of convergence with respect to the number of degrees of freedom is the same, the exact eigenvalues are approached more slowly when sequences of polygonal meshes are used. Nonetheless, these numerical results confirm the optimal convergence rate on general polygonal partitions and that the performance of the mimetic discretizations on regular quadrilateral meshes and on general polygonal meshes are qualitatively the same.

Table 5
Maxwell eigenvalues calculated on the square domain $[0,\pi]\times[0,\pi]$ by the mimetic discretization (83) that approximates the electric formulation (79). Column "Slope" refers to the last refinement and the results are computed with respect to the number of degrees of freedom reported in each row labeled by "D.o.f.".

Exact	Computed				Slope
	n = 4	8	16	32	
Square mesh					
2	2.21754	2.05093	2.01253	2.00312	2.05
5	7.46618	5.46054	5.10812	5.02662	2.07
5	7.46618	5.46054	5.10812	5.02662	2.07
8	12.71480	8.87015	8.20371	8.05012	2.07
10	34.95780	12.50340	10.53600	10.12930	2.10
10	34.95780	12.50340	10.53600	10.12930	2.10
13	40.20640	15.91300	13.63160	13.15280	2.09
13	40.20640	15.91300	13.63160	13.15280	2.09
D.o.f.	40	144	544	2112	
Mainly-hexagonal mesh					
2	2.49811	2.12798	2.02916	2.00694	2.21
5	7.48037	5.65446	5.15630	5.03760	2.20
5	11.22230	6.05487	5.21212	5.04852	2.28
8	17.39960	10.38730	8.51853	8.11492	2.33
10	35.36670	13.75470	10.75010	10.17150	2.28
10	39.30300	14.01810	10.75770	10.17320	2.28
13	44.69100	18.23060	14.15180	13.25940	2.30
13	91.49350	23.78100	14.80780	13.36160	2.48
D.o.f.	88	272	928	3392	
Non-convex mesh					
2	5.44954	2.83870	2.20736	2.05155	2.05
5	21.80970	8.66032	5.88914	5.22033	2.06
5	22.05330	8.68731	5.89081	5.22034	2.06
8	68.43580	20.00150	11.34510	8.82647	2.06
10	79.73220	20.16770	12.30020	10.56460	2.07
10	81.47720	21.86630	12.31180	10.56530	2.08
13	169.34100	41.24480	20.74330	14.90180	2.07
13	172.08800	41.35570	20.75190	14.90200	2.07
D.o.f.	80	288	1088	4224	

Test 2: *L-shaped domain, Neumann boundary, constant magnetic permeability*.

This test problem is taken from the benchmark singular solution set [46]. We solve the eigenvalue problem (78) with Neumann boundary conditions on the non-convex L-shaped domain $\Omega = (\Omega_0\backslash\Omega_1)^\circ$, where Ω_0 is the square $(-1,1)\times(-1,1)$ and Ω_1 is the square $(0,1)\times(-1,0)$. The domain presents a reentrant corner of $3\pi/2$ radians and the solution belongs to $H^{1+\sigma}(\Omega)$ with $0\leqslant\sigma<2/3$; thus, eigensolutions with singularities are expected. As for Test 1, we solve this problem on a sequence of regular square meshes, of mainly-hexagonal unstructured meshes, and of non-convex meshes. Each mesh is built by rescaling a mesh of Test 1 to the unit square $(0,1)\times(0,1)$ and by regularly duplicating the resulting mesh to cover the domain Ω entirely. A regular duplication through axial reflection guarantees the conformity of the full mesh as can be seen in Fig. 5, where we show the first two mainly-hexagonal meshes and the first two non-convex meshes.

The results for the calculation of the eigenvalues reported on the benchmark webpage [46] are shown in Tables 7 and 8 for the mimetic discretizations of the electric and magnetic formulation, respectively. As for the results of Test 1, the exact eigenvalues are approached more slowly when sequences of polygonal meshes are used. However, the asymptotic rate of convergence with respect to the number of degrees of freedom is 2 as expected for all eigenvalues except for the first one, which should be 4/3 in accordance with the singularity of the first eigenfunction. The observed rate of the first eigenvalue reveals that we are likely to be again in the pre-asymptotic regime, while the optimality of the mimetic approximation of the other eigenvalues seems confirmed on regular quadrilateral meshes and on general polygonal meshes.

Test 3: *Square domain, Neumann boundary, discontinuous magnetic permeability*.

This test problem is taken from the benchmark singular solution set [46]. We set $\Omega=(-1,1)\times(-1,1)$ and subdivide this domain in a checkerboard fashion into two subdomains Ω_ε and Ω_1 with different material properties; cf. Fig. 6 (left). We assume that the electric permittivity is $\varepsilon=1$ in Ω_1 and $\varepsilon=0.50, 0.10, 0.01$ in Ω_ε. The boundary conditions are of Neumann type.

We apply the MFD method on a sequence of locally unstructured quadrilateral meshes of the type depicted in Fig. 6 (right) by fixing $n=4, 8, 16$, and 32. In Figs. 7 and 8 we show the convergence plots with respect of the number of degrees of freedom for the first eigenvalues considered in [46]. Each error curve in these plots shows the relative errors for the calculation of a given eigenvalue according to the legend displayed in the bottom-left corner. In every plot, the quadratic convergence rate is also explicitly shown. Both the mimetic discretization for the electric formulation and that for the magnetic formulation provide good results for almost all the eigenvalues and an asymptotical convergence rate close to 2 is clearly visible for almost all these error curves. In particular, we see a quadratic convergence rate for all the eigenvalues

Table 6
Maxwell eigenvalues calculated on the square domain $[0,\pi]\times[0,\pi]$ by the mimetic discretization (88) that approximates the magnetic formulation (80). Column "Slope" refers to the last refinement and the results are computed with respect to the number of degrees of freedom reported in each row labeled by "D.o.f.".

Exact	Computed				Slope
	n = 4	8	16	32	
Square mesh					
2	2.22450	2.05252	2.01292	2.00322	2.10
5	7.54035	5.47169	5.11062	5.02723	2.11
5	7.54035	5.47169	5.11062	5.02723	2.11
8	12.84320	8.89798	8.21007	8.05168	2.11
10	36.60440	12.56180	10.54660	10.13170	2.15
10	36.60440	12.56180	10.54660	10.13170	2.15
13	40.64650	15.99910	13.6490	13.15690	2.14
13	40.64650	15.99910	13.6490	13.15690	2.14
D.o.f.	25	81	289	1089	
Mainly-hexagonal mesh					
2	2.20000	2.06120	2.01678	2.00443	2.08
5	5.48585	5.24371	5.08588	5.02398	1.99
5	6.68494	5.43494	5.11737	5.03093	2.08
8	9.21714	8.84384	8.26241	8.07087	2.04
10	11.93550	11.00370	10.37430	10.10690	1.96
10	12.56620	11.00640	10.38280	10.10900	1.96
13	13.31060	14.12870	13.52600	13.15520	1.91
13	14.65280	16.13270	13.82010	13.21590	2.08
D.o.f.	64	192	640	2304	
Non-convex mesh					
2	2.23669	2.05797	2.01458	2.00366	2.05
5	4.49264	4.43190	4.75180	4.92575	1.79
5	4.49290	4.44858	4.75729	4.92723	1.79
8	5.87537	6.66972	8.23130	8.05853	2.04
10	5.87630	6.66994	8.30859	9.43824	1.64
10	6.47492	8.49563	8.31028	9.43825	1.64
13	6.49775	8.49985	11.97530	12.89990	3.46
13	12.39660	8.93935	11.97740	12.91210	3.65
D.o.f.	65	225	833	3201	

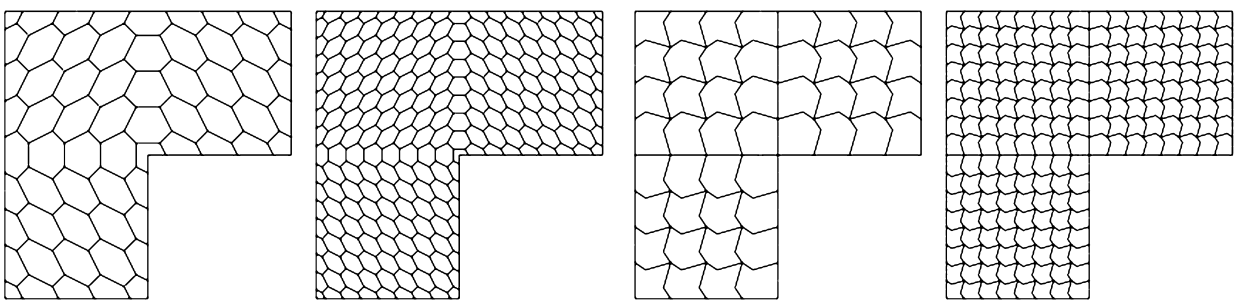

Fig. 5. Test 2. The first two meshes of the unstructured mainly-hexagonal mesh sequence (plots (a) and (b)) and the first two meshes of the unstructured non-convex mesh sequence (plots (c) and (d)).

that we computed for $\varepsilon = 0.5$ as in this case all eigenfunctions are not singular. Instead, for $\varepsilon = 0.1$ a slower convergence rate is seen, as expected, for the eigenvalues $\lambda = 6.2503$ and $\lambda = 26.0952$ since the latters correspond to eigenfunctions that are singular in $(0,0)$. This behavior is visible in the plots in the middle of Fig. 7 (electric formulation) and Fig. 8 (magnetic formulation). A slower convergence is also shown for the eigenvalues $\lambda = 15.5369$ and $\lambda = 29.6466$ in the right plots of Fig. 7 (electric formulation) and Fig. 8 (magnetic formulation). As outlined in the benchmark description [46], an accurate approximation of these eigenvalues is difficult for the presence of a singularity in $(0,0)$ in the asymptotics of the corresponding eigenvectors. Indeed, the number of digits reported as correct on the benchmark webpage is half that of the other eigenvalues. This difficulty is well reflected by the smaller rate of convergence of the corresponding error curves. However, from these experimental results we conclude that the method is robust with respect to discontinuities in the magnetic permeability.

Table 7
Maxwell eigenvalues calculated on the L-shaped domain by the mimetic discretization (83) that approximates the electric formulation (79). Column "Slope" refers to the last refinement and the results are computed with respect to the number of degrees of freedom reported in each row labeled by "D.o.f.".

Exact	Computed				Slope
	n = 4	8	16	32	
Square mesh					
1.475622	1.49874	1.48081	1.47668	1.47579	2.66
3.534031	3.63671	3.55930	3.54032	3.53560	2.03
9.869604	10.94310	10.12090	9.93144	9.88500	2.04
9.869604	10.94310	10.12090	9.93144	9.88500	2.04
11.38948	12.48140	11.64570	11.45260	11.40520	2.04
D.o.f.	112	416	1600	6272	
Mainly-hexagonal mesh					
1.475622	1.54311	1.50056	1.48489	1.47912	1.47
3.534031	3.66439	3.56595	3.54196	3.53602	2.09
9.869604	10.54050	10.04700	9.91550	9.88124	2.07
9.869604	11.09850	10.17050	9.94470	9.88842	2.09
11.38948	12.84460	11.74970	11.47920	11.41200	2.09
D.o.f.	224	736	2624	9856	
Non-convex mesh					
1.475622	1.63327	1.54855	1.50674	1.48845	1.3
3.534031	3.85630	3.63434	3.56180	3.54131	1.96
9.869604	10.93010	10.11620	9.92994	9.88458	2.04
9.869604	10.98190	10.12550	9.93207	9.88510	2.04
11.38948	17.15650	12.81140	11.74490	11.47850	2.03
D.o.f.	224	832	3200	12 544	

Table 8
Maxwell eigenvalues calculated on the L-shaped domain by the mimetic discretization (88) that approximates the magnetic formulation (80). Column "Slope" refers to the last refinement and the results are computed with respect to the number of degrees of freedom reported in each row labeled by "D.o.f.".

Exact	Computed				Slope
	n = 4	8	16	32	
Square mesh					
1.475622	1.50729	1.48410	1.47797	1.47630	1.84
3.534031	3.63870	3.55978	3.54044	3.53563	2.06
9.869604	10.96190	10.12490	9.93241	9.88524	2.06
9.869604	10.96190	10.12490	9.93241	9.88524	2.06
11.38948	12.50520	11.65090	11.45380	11.40550	2.06
D.o.f.	65	225	833	3201	
Mainly-hexagonal mesh					
1.475622	1.40500	1.44825	1.46455	1.47113	1.37
3.534031	3.57303	3.54755	3.53809	3.53516	1.95
9.869604	9.83194	9.92967	9.89199	9.87600	1.91
9.869604	10.52540	10.05810	9.92096	9.88303	2.04
11.38948	11.82700	11.58200	11.44620	11.40470	2.01
D.o.f.	160	512	1792	6656	
Non-convex mesh					
1.475622	1.12073	1.34261	1.42846	1.45868	1.51
3.534031	3.18295	3.43579	3.50772	3.52717	1.98
9.869604	6.03331	8.46654	9.47429	9.76780	2.00
9.869604	6.03955	8.46970	9.47591	9.76827	2.00
11.38948	8.16247	10.50670	11.13800	11.32390	1.98
D.o.f.	177	641	2433	9473	

4.3.3. Three-dimensional mimetic inner products

Test 4: *Cubic domain, Dirichlet boundary, constant magnetic permeability and electric permittivity.*

In this test case, we calculate the Maxwell eigenvalues by solving the electric variational formulation (79) on the cubic domain $\Omega = (0,\pi) \times (0,\pi) \times (0,\pi)$ through the mimetic approximation (83). According to [44], the eigenvalues of this problem are given by $\lambda = m_x^2 + m_y^2 + m_z^2$ where the triplet (m_x, m_y, m_z) is repeated once when $m_x, m_y, m_z \geqslant 0$ with only one number that may be chosen equal to zero, and twice when $m_x, m_y, m_z \geqslant 1$. The corresponding eigenfunctions are (sum of) products of two sine terms like $\sin(m\zeta)$ and one cosine term like $\cos(m\zeta)$ for $m \in \{m_x, m_y, m_z\}$ and $\zeta \in (0,\pi)$. We solve this eigenvalue problem on a sequence of meshes formed by random hexahedra, which are obtained by cutting the cells of a tetrahedral mesh provided by the mesh generator TetGen [84]. The first mesh of this mesh sequence is shown in Fig. 9; a portion of the mesh around the corner $(1,1,1)$ has been removed to show the interior structure. Table 9

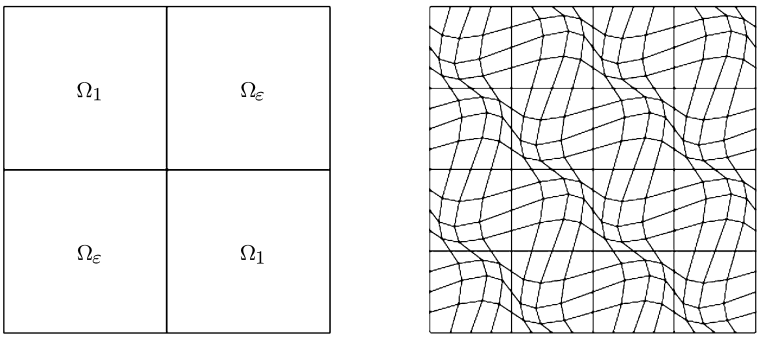

Fig. 6. Test 3. Left plot: subdivision of Ω in a checked-board fashion. Right plot: locally unstructured quadrilateral mesh corresponding to n = 8.

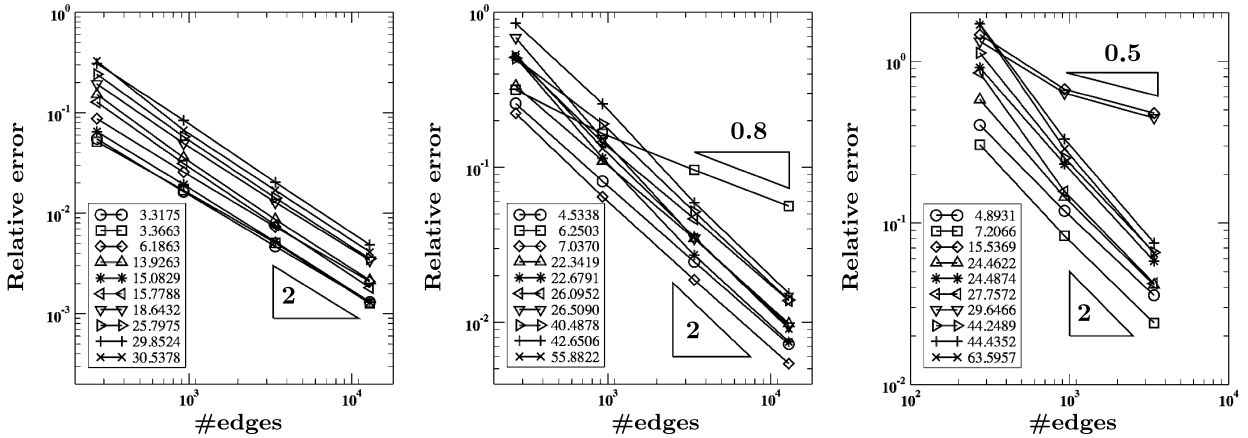

Fig. 7. Test 3, electric formulation, Neumann boundary, discontinuous magnetic permeability, mainly-hexagonal mesh, $\varepsilon = 0.50$ (left), 0.10 (middle), 0.01 (right).

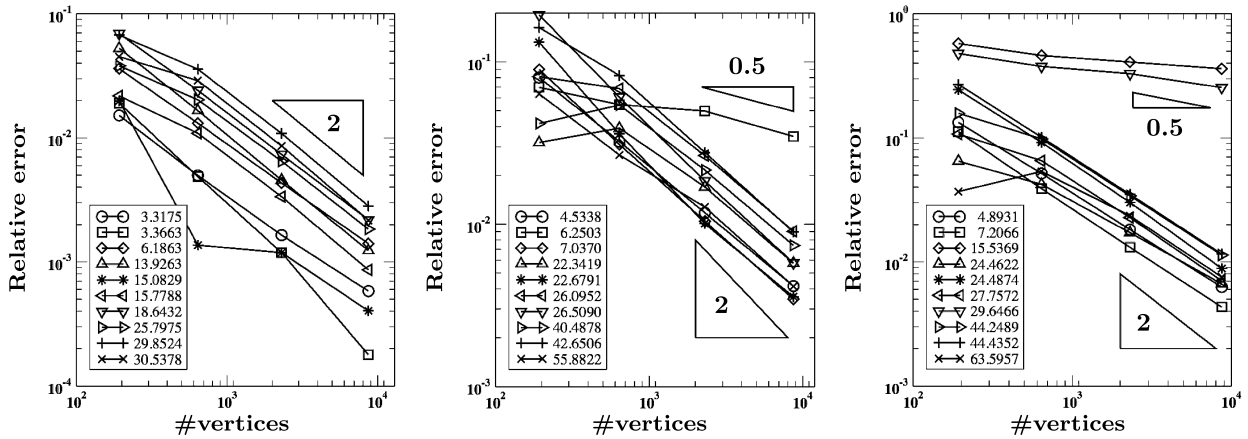

Fig. 8. Test 3, magnetic formulation, Neumann boundary, discontinuous diffusivity, mainly-hexagonal mesh, $\varepsilon = 0.50$ (left), 0.10 (middle), 0.01 (right).

reports the results for the calculations of the first four eigenvalues 2, 3, 5 and 6, which have multiplicities 3, 2, 6, and 6, respectively. The last column labeled by Slope shows the convergence rate for the last refinement with respect to the mesh size parameter h reported in the last table row. These results confirm the second order of accuracy of the mimetic approximation.

Test 5: *Thick L-shaped domain, Neumann boundary, constant magnetic permeability and electric permittivity.*

In this test case, we calculate the Maxwell eigenvalues on the "thick L-shaped domain" that is given by tensor product of the 2-D "L-shaped" domain of Test 2 and the interval $(0, 1)$ along the z-axis. To such purpose, we use the mimetic approximation (83) of the electric variational formulation (79) on two different mesh sequences. The first mesh sequence is formed by regular partitions of the computational domain in regular hexahedra. The second mesh sequence is formed

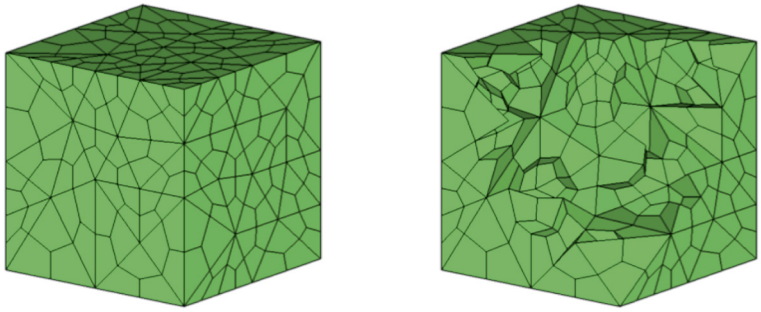

Fig. 9. Cubic domain $(0,\pi)\times(0,\pi)\times(0,\pi)$: mesh of random hexahedra used in refinement ref. $=2$ (right plot); a portion of the mesh near the corner (π,π,π) has been removed in the plot on the left to show the interior structure; refinement ref. $=1$.

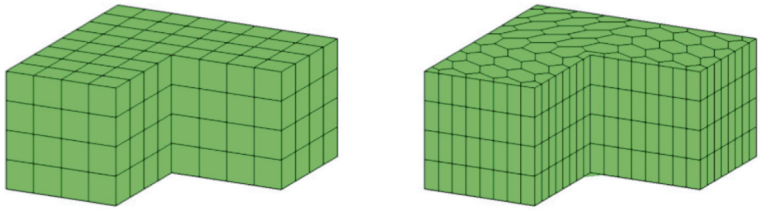

Fig. 10. Thick L-shaped domain: regular hexahedral mesh (left) and prismatic mesh with main-hexagonal base (right); refinement ref. $=1$.

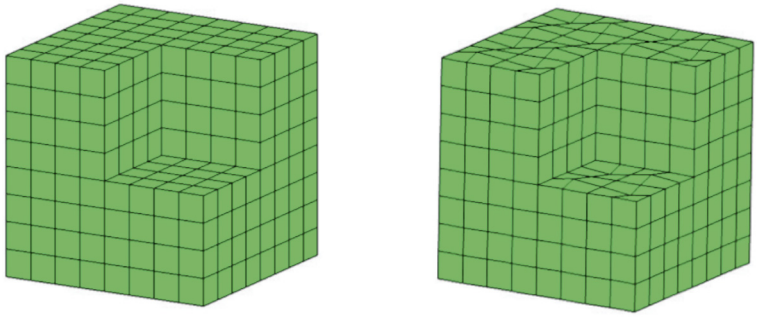

Fig. 11. Fichera's corner domain: regular hexahedral mesh (left) and prismatic mesh with general quadrilateral base (right); refinement ref. $=1$.

by prismatic cells with the polygonal (mainly-hexagonal) base meshes considered in Test 2. Fig. 10 shows the first mesh of each mesh sequence. Table 10 reports the first nine eigenvalues from [46]; the eigenvalue approximation provided by the first four mesh refinement; the convergence rate calculated on the last refinement with respect to the number of degrees of freedom shown in the last table row. These results confirm the second order of accuracy of the mimetic approximation for this eigenvalue calculation.

Test 6: *Fichera's corner domain, Neumann boundary*.

In this test case, we calculate the Maxwell eigenvalues on the *Fichera's corner* domain $\Omega=\Omega'\backslash\Omega''$ where $\Omega'=(-1,1)\times(-1,1)\times(-1,1)$ and $\Omega''=(0,1)\times(0,1)\times(0,1)$. To such purpose, we use the mimetic approximation (83) of the electric variational formulation (79) on two different mesh sequences. The first mesh sequence is formed by regular partitions of the computational domain in regular hexahedra. The second mesh sequence is formed by prismatic cells with a quadrilateral base. Fig. 11 shows the first mesh of each mesh sequence. For this test case, the exact eigenvalues and eigenfunctions are not known, although it is known that some eigenfunctions have singularities at the origin, which makes the problem difficult to approximate. For comparison, error evaluation is performed against the numerical results posted by M. Dauge on the benchmark webpage [46]. Table 11 reports the first eight eigenvalues, the number of reliable estimated digits and the conjecture eigenvalues in the first three columns. Columns 4 to 7 show our eigenvalue approximation on the first four mesh refinements. The last column reports the convergence rate, which calculated on the last refinement with respect to the mesh size parameter h. Assuming that at least the first two digits of the eigenvalues conjectured in the benchmark specifications are exact, our results confirm the second order of accuracy of the mimetic approximation in this eigenvalue calculation.

Table 9
Maxwell eigenvalues on the cube $[0,\pi]\times[0,\pi]\times[0,\pi]$ calculated using the mimetic discretization of the electric formulation. Column "Slope" refers to the last refinement and is computed with respect to the mesh size parameter h.

Exact	Computed				Slope
	ref. = 1	2	3	4	
Hexahedral mesh					
2	2.20957	2.06441	2.01154	2.00276	1.93
2	2.23441	2.06700	2.01160	2.00276	1.93
2	2.23756	2.06912	2.01176	2.00279	1.94
3	3.50981	3.13426	3.02572	3.00613	1.93
3	3.56312	3.14459	3.02606	3.00620	1.93
5	5.78111	5.38253	5.07073	5.01702	1.92
5	5.86490	5.38954	5.07141	5.01706	1.93
5	5.95741	5.41263	5.07325	5.01718	1.95
5	6.23026	5.42093	5.07395	5.01734	1.95
5	6.61963	5.42634	5.07409	5.01744	1.95
5	6.67565	5.43952	5.07485	5.01763	1.95
6	7.34328	6.51181	6.09957	6.02428	1.90
6	7.49230	6.52719	6.10096	6.02456	1.90
6	7.64339	6.54744	6.10354	6.02458	1.94
6	7.75005	6.56439	6.10525	6.02473	1.95
6	8.16632	6.58070	6.10634	6.02490	1.95
6	8.30883	6.62644	6.10750	6.02510	1.96
D.o.f.	698	3153	37 495	299 613	
h	1.666	1.091	$5.505\,10^{-1}$	$2.618\,10^{-1}$	

Table 10
Maxwell eigenvalues on the thick L-shaped domain calculated using the mimetic discretization of the electric formulation. Column "Slope" refers to the last refinement and is computed with respect to the mesh size parameter h.

Exact	Computed				Slope
	ref. = 1	2	3	4	
Cubic mesh					
9.639724	12.88120	10.27030	9.78515	9.67375	2.10
11.34523	17.01880	12.42800	11.60100	11.40860	2.01
13.40364	19.47490	14.55880	13.67580	13.47070	2.02
15.19725	24.06730	16.83450	15.58040	15.29150	2.02
19.50933	27.59560	21.17320	19.90080	19.60410	2.04
19.73921	31.06800	21.84890	20.23380	19.86100	2.02
19.73921	31.06800	21.84890	20.23380	19.86100	2.02
D.o.f.	138	820	5544	40 528	
h	$8.660\,10^{-1}$	$4.330\,10^{-1}$	$2.165\,10^{-1}$	$1.083\,10^{-1}$	
Prismatic mesh					
9.639724	14.39960	11.08380	10.05740	9.77014	1.68
11.34523	15.98290	12.40610	11.61310	11.41560	1.93
13.40364	17.23230	14.50870	13.66970	13.46960	2.01
15.19725	18.96910	18.57780	15.91850	15.36090	2.14
19.50933	19.90790	20.85840	20.06990	19.71910	1.42
19.73921	22.07360	21.32910	20.14500	19.82620	2.22
19.73921	22.56630	21.97340	20.21420	19.84270	2.20
D.o.f.	340	1760	10 720	73 280	
h	$8.975\,10^{-1}$	$4.488\,10^{-1}$	$2.244\,10^{-1}$	$1.122\,10^{-1}$	

5. Conclusions

In this paper, we developed a family of mimetic inner products that are suitable to the construction of mimetic schemes for the numerical treatment of partial differential equations on polygonal and polyhedral meshes. Our mimetic formulations may associate the degrees of freedom to the most basic geometric objects forming a mesh: vertices, edges, faces and cells. These degrees of freedom are represented as linear spaces of grid functions, also called cochains, that are formally equipped with inner products. A fundamental ingredient in the definition of the inner products is the reconstruction of scalar and vector fields from grid functions. However, such a reconstruction is only a theoretical tool as the implementation of our mimetic inner products does not require the explicit knowledge of the reconstructed fields. In our mimetic setting, we employ the natural discrete operators that mimic the behavior of the gradient, the curl and the divergence operators on the grid functions. Mimetic discretization are easily designed by combining the discrete gradient, curl and divergence operators acting on the cochain spaces with the mimetic inner products defined for such discrete spaces. The accuracy of the numerical schemes that can be derived through this strategy is illustrated by applying these techniques to a set of problems related to the Maxwell equations.

Table 11
Maxwell eigenvalues on the Fichera's corner domain calculated using the mimetic approximation to the electric formulation. Column "Benchmark" reports, for comparison, the results of M. Dauge in the benchmark page [46]; column "#" reports the number of reliable digits after the first one in the first column; column "Conj." reports the conjectured eigenvalues and the question mark symbol "?" stands for the unknown digits.

Benchmark	#	Conj.	Computed				
			ref. = 1	2	3	4	5
Cubic mesh							
3.313805	1	3.2???	4.09849	3.48201	3.29328	3.24067	3.22606
5.88635	3	5.88??	9.54785	6.59034	6.04703	5.92130	5.89053
5.88635	3	5.88??	9.54785	6.59034	6.04703	5.92130	5.89053
10.69451	4	10.694	9.75421	14.05700	11.37130	10.85250	10.73020
10.69451	4	10.694	9.75421	14.05700	11.37130	10.85250	10.73150
10.70058	2	10.7??	10.50190	14.59540	11.47210	10.87070	10.73150
12.33455	3	12.32?	12.00000	18.22020	13.44160	12.58190	12.38220
12.33455	3	12.32?	12.00000	18.22020	14.56130	12.58190	12.38220
D.o.f.			51	276	1752	12 336	92 256
h			1.732	$8.660\,10^{-1}$	$4.330\,10^{-1}$	$2.165\,10^{-1}$	$1.083\,10^{-1}$
Prismatic mesh							
3.313805	1	3.2???	4.09849	3.48201	3.29306	3.24464	3.22767
5.88635	3	5.88??	9.54785	6.59034	6.06367	5.92983	5.89309
5.88635	3	5.88??	9.54785	6.59034	6.08428	5.93502	5.89440
10.69451	4	10.694	9.75421	14.05700	11.39120	10.86330	10.73470
10.69451	4	10.694	9.75421	14.05700	11.43770	10.87890	10.73720
10.70058	2	10.7??	10.50190	14.59540	11.61040	10.92530	10.74890
12.33455	3	12.32?	12.00000	18.22020	13.60610	12.62190	12.39350
12.33455	3	12.32?	12.00000	18.22020	14.55570	12.65530	12.40340
D.o.f.			51	276	1752	12 336	92 256
h			1.732	$8.660\,10^{-1}$	$5.545\,10^{-1}$	$3.037\,10^{-1}$	$1.556\,10^{-1}$

Acknowledgements

The work of the third author was partially supported by the National Nuclear Security Administration of the U.S. Department of Energy at Los Alamos National Laboratory under Contract No. DE-AC52-06NA25396 and the DOE Office of Science Advanced Scientific Computing Research (ASCR) Program in Applied Mathematics.

Appendix A. Minimal reconstructions

Here, we provide an example of a complete set of reconstructions, that we call *minimal reconstructions*, and, at the same time, several families of admissible reconstruction operators. As we shall see, in most cases *local orthogonality*, which comes along property (R4), is the crucial condition to be satisfied and deserves a careful treatment.

A.1. One-dimensional case

The one-dimensional case for the reconstruction operator $R_{\mathsf{e}}^{\mathcal{V}}$ is completely uniquely determined by property (R3). In fact, in such a case the gradient operator is the derivative with respect to the one-dimensional coordinate ξ defined along e. Using the commuting property (R3) and the definition of the discrete gradient in (3) we observe that

$$\forall \varphi \in \mathcal{V}_{\mathsf{e}}^h: \quad \frac{d}{d\xi}\big(R_{\mathsf{e}}^{\mathcal{V}}(\varphi)\big) = \mathcal{GRAD}\big(R_{\mathsf{v}}^{\mathcal{V}}(\varphi)\big)_{|\mathsf{e}} = \varphi_{\mathsf{v}_2} - \varphi_{\mathsf{v}_1},$$

which implies that $R_{\mathsf{e}}^{\mathcal{V}}(\varphi)$ is a linear function since the right-most quantity is a constant over the edge e. The trace commuting property (R5) requires that $R_{\mathsf{e}}^{\mathcal{V}}(\varphi)(\xi_{\mathsf{v}_1}) = \varphi_{\mathsf{v}_1}$ and $R_{\mathsf{e}}^{\mathcal{V}}(\varphi)(\xi_{\mathsf{v}_2}) = \varphi_{\mathsf{v}_2}$. Thus, the reconstructed function $R_{\mathsf{e}}^{\mathcal{V}}(\varphi)$ linearly interpolates the values taken by φ at the edge vertices v_1 and v_2.

A.2. Two-dimensional case

A.2.1. The reconstruction operator $R_{\mathsf{f}}^{\mathcal{V}}$

Let us consider a face f and a 0-cochain $\varphi \in \mathcal{V}_{\mathsf{f}}^h$. We first remark that the value of every admissible reconstruction $R_{\mathsf{f}}^{\mathcal{V}}$ on $\partial\mathsf{f}$ is, in a sense, already fixed by (R4) and by the unique possible choice for the one-dimensional operator $R_{\mathsf{e}}^{\mathcal{V}}$. We recall that all this means that we start from the values of φ at the couple of vertices of each edge e and we interpolate linearly along the edge. For every admissible reconstruction operator $R_{\mathsf{f}}^{\mathcal{E}}$, we can then construct an admissible reconstruction $R_{\mathsf{f}}^{\mathcal{V}}$ by taking

$$\mathbf{grad}\big(R_{\mathsf{f}}^{\mathcal{V}}(\varphi)\big) = R_{\mathsf{f}}^{\mathcal{E}}\big(\mathcal{GRAD}(\varphi)\big) \tag{A.1}$$

and note that this will be compatible with the boundary value already assigned to $R^{\mathcal{V}}_{\mathsf{f}}(\varphi)$ automatically. We indicate by $\overline{R}^{\mathcal{V}}_{\mathsf{f}}(u)$ the reconstruction operator obtained from (A.1) when, for $R^{\mathcal{E}}_{\mathsf{f}}$, we take the minimal reconstruction $\overline{R}^{\mathcal{E}}_{\mathsf{f}}$. We will call $\overline{R}^{\mathcal{V}}_{\mathsf{f}}(\varphi)$ *a minimal reconstruction* as well.

A.2.2. The reconstruction operator $R^{\mathcal{E}}_{\mathsf{f}}$

Let us consider a face f, a 1-cochain $\varphi \in \mathcal{E}^h_{\mathsf{f}}$, and the two-dimensional vector field $\boldsymbol{\phi} \in \mathcal{H}^{\mathcal{E}}(\mathsf{f})$ that is such that

$$\mathbf{rot}(\boldsymbol{\phi}) = R^{\mathcal{E}}_{\mathsf{f}}\big(\mathcal{CURL}(\varphi)\big) = \mathcal{CURL}(\varphi)/|\mathsf{f}| \quad \text{in } \mathsf{f}, \tag{A.2}$$

$$\operatorname{div}(\boldsymbol{\phi}) = 0 \quad \text{in } \mathsf{f}, \tag{A.3}$$

$$\gamma_{t,\mathsf{e}}(\boldsymbol{\phi}) = R^{\mathcal{E}}_{\mathsf{e}}\big(\gamma_{h,\mathsf{e}}(\varphi)\big) = \varphi_{\mathsf{e}}/|\mathsf{e}| \quad \text{on } \mathsf{e} \in \partial\mathsf{f}. \tag{A.4}$$

Note that (A.2) and (A.4) are necessary to ensure (R1), (R3) and (R5), while condition (A.3) is introduced just to ensure that the three conditions (A.2)–(A.4) imply the existence and the uniqueness of ϕ. Let Φ denote the mapping $\varphi \to \phi =: \Phi(\varphi)$ constructed by means of (A.2)–(A.4). Whenever $\varphi = \Pi^{\mathcal{E}}_{\mathsf{f}}\mathbf{c}$ for some constant vector $\mathbf{c}$, the unique solution to (A.2)–(A.4) is $\boldsymbol{\phi} = \mathbf{c}$, so that it holds

$$\Phi\big(\Pi^{\mathcal{E}}_{\mathsf{f}}\mathbf{c}\big) = \mathbf{c}, \tag{A.5}$$

which is a crucial step towards (R2). In general, it holds that

$$\int_{\mathsf{f}} \phi \cdot (\boldsymbol{\xi} - \boldsymbol{\xi}_{\mathsf{f}})\, dS \neq 0,$$

which implies that the orthogonality condition required by (R4) is not satisfied. Consequently, we cannot take $R^{\mathcal{E}}_{\mathsf{f}} := \Phi$ but we need to add a correction term to it. In doing this, we are allowed to give up condition (A.3), but we must preserve (A.2), (A.4) and (A.5). To take care of (A.2) and (A.4) we use a correction of the form $\mathbf{grad}(q)$ for some $q \in H^1_0(\mathsf{f})$: indeed, for every $q \in H^1_0(\mathsf{f})$ we have that $\mathbf{grad}(q)$ is rot-free and q has, obviously, a zero tangential trace on the boundary $\partial\mathsf{f}$, i.e. $q_{|\partial\mathsf{f}} = 0$. The orthogonality condition (R4) on $\phi + \mathbf{grad}(q)$ and the fact that $q_{|\partial\mathsf{f}} = 0$ implies that

$$\int_{\mathsf{f}} \phi \cdot (\boldsymbol{\xi} - \boldsymbol{\xi}_{\mathsf{f}})\, dS = -\int_{\mathsf{f}} \mathbf{grad}(q) \cdot (\boldsymbol{\xi} - \boldsymbol{\xi}_{\mathsf{f}})\, dS = 2\int_{\mathsf{f}} q\, dS. \tag{A.6}$$

Eq. (A.6) gives us a necessary condition to be followed in choosing q as a function of ϕ. In principle, every linear operator $M : \phi \to q$ that respect (A.6) and such that $M(\mathbf{c}) = 0$ for every constant vector $\mathbf{c}$, will produce an *admissible reconstruction* operator

$$R^{\mathcal{E}}_{\mathsf{f}}(\varphi) := \Phi(\varphi) + \mathbf{grad}\big(M\big(\Phi(\varphi)\big)\big). \tag{A.7}$$

Let us build one of them. Let $\chi := \frac{1}{2}\int_{\mathsf{f}} \phi \cdot (\boldsymbol{\xi} - \boldsymbol{\xi}_{\mathsf{f}})\, dS$ and let $p \in H^1_0(\mathsf{f})$ be the unique solution of the minimization problem:

$$\min_{\substack{q \in H^1_0(\mathsf{f}) \\ \int_{\mathsf{f}} q\, dS = \chi}} \int_{\mathsf{f}} \big|\mathbf{grad}(q)\big|^2\, dS.$$

Then, we take $M(\phi) := p$ and, according to (A.7), the vector field $\overline{R}^{\mathcal{E}}_{\mathsf{f}}(\varphi) = \phi + \mathbf{grad}(p)$ is an admissible reconstruction of φ.

A.3. Three-dimensional case

A.3.1. The reconstruction operator $R^{\mathcal{V}}_{\mathsf{P}}$

Let us consider the 0-cochain $\varphi \in \mathcal{V}^h_{\mathsf{P}}$. As in the two-dimensional case, the natural choice for the minimal reconstruction $\overline{R}^{\mathcal{V}}_{\mathsf{P}}(\varphi)$ is to require

$$\mathbf{grad}\big(\overline{R}^{\mathcal{V}}_{\mathsf{P}}(\varphi)\big) := \overline{R}^{\mathcal{E}}_{\mathsf{P}}\big(\mathcal{GRAD}(\varphi)\big), \tag{A.8}$$

with the boundary conditions:

$$\gamma_{t,\mathsf{f}}\big(R^{\mathcal{V}}_{\mathsf{P}}(\varphi)\big) = R^{\mathcal{V}}_{\mathsf{f}}(\varphi) \quad \forall \mathsf{f} \in \partial\mathsf{P}, \tag{A.9}$$

that, due to the two-dimensional construction (A.1), are compatible with the above choice (A.8).

A.3.2. The reconstruction operator $R_{\mathsf{P}}^{\mathcal{E}}$

Let us consider the 1-cochain $\varphi \in \mathcal{E}_{\mathsf{P}}^h$. Taking into account (R3)–(R5) and what has been done in two dimensions, we define the vector field $\boldsymbol{\phi}$ such that

$$\mathbf{curl}(\boldsymbol{\phi}) = \overline{R}_{\mathsf{P}}^{\mathcal{F}}\left(\mathcal{CURL}(\varphi)\right) \quad \text{in } \mathsf{P}, \tag{A.10}$$

$$\operatorname{div}(\boldsymbol{\phi}) = 0 \quad \text{in } \mathsf{P}, \tag{A.11}$$

$$\gamma_{t,\mathsf{f}}(\boldsymbol{\phi}) = \overline{R}_{\mathsf{f}}^{\mathcal{E}}(\varphi_{|\mathsf{f}}) \quad \forall \mathsf{f} \in \partial\mathsf{P}. \tag{A.12}$$

Again, we define the mapping $\varphi \to \boldsymbol{\phi} =: \Phi(\varphi)$ and, as in the previous cases, we need to impose the orthogonality condition (R4) explicitly, since, general, (R4) is not automatically satisfied by this choice. To do so, we consider a correction of the form $\boldsymbol{\phi} + \mathbf{grad}(\varphi)$, with $q \in H_0^1(\mathsf{P})$. Indeed, $\mathbf{grad}(q)$ is curl-free and q has zero tangential traces, so that this correction cannot alter (A.10) and (A.12), and modifies only (A.11). Now, imposing the orthogonality condition (R4) on $\boldsymbol{\phi} + \mathbf{grad}(\varphi)$ and using the integration by parts yield:

$$-\int_{\mathsf{P}} \boldsymbol{\phi} \cdot (\mathbf{x} - \mathbf{x}_{\mathsf{P}})\, dV = \int_{\mathsf{P}} \mathbf{grad}(q) \cdot (\mathbf{x} - \mathbf{x}_{\mathsf{P}})\, dV = 3\int_{\mathsf{P}} q\, dV. \tag{A.13}$$

Let $\chi := \int_{\mathsf{P}} \boldsymbol{\phi} \cdot (\mathbf{x} - \mathbf{x}_{\mathsf{P}})\, dV$ and p be the unique solution of the minimization problem:

$$\min_{\substack{q \in H_0^1(\mathsf{P}) \\ \int_{\mathsf{P}} q\, dV = \chi}} \int_{\mathsf{P}} \left|\mathbf{grad}(q)\right|^2 dV. \tag{A.14}$$

The *minimal reconstruction* is given by $\overline{R}_{\mathsf{P}}^{\mathcal{E}}(\varphi) = \boldsymbol{\phi} + \mathbf{grad}(p)$. Note that if $\varphi \in (\Pi^{\mathcal{E}}(\mathbb{P}_0(\mathsf{P})))^3$ then $\boldsymbol{\phi} = \mathbf{c}$ and $p = 0$. Thus, constant fields are left invariant, i.e., condition (R3) is satisfied.

A.3.3. The reconstruction operator $R_{\mathsf{P}}^{\mathcal{F}}$

Given $\varphi \in \mathcal{F}^h$, we construct the vector field $\boldsymbol{\phi} \in H(\operatorname{div}, \mathsf{P})$ such that

$$\operatorname{div}(\boldsymbol{\phi}) = R_{\mathsf{P}}^{\mathcal{P}}\mathcal{DIV}(\varphi) = \mathcal{DIV}(\varphi)/|\mathsf{P}| \quad \text{in } \mathsf{P}, \tag{A.15}$$

$$\mathbf{curl}(\boldsymbol{\phi}) = 0 \quad \text{in } \mathsf{P}, \tag{A.16}$$

$$\gamma_{h,\mathsf{f}}(\boldsymbol{\sigma}) = R_{\mathsf{f}}^{\mathcal{F}}\left(\gamma_{h,F}(\sigma)\right) = \sigma_{\mathsf{f}}/|\mathsf{f}| \quad \forall \mathsf{f} \in \partial\mathsf{P}. \tag{A.17}$$

Since the problem defined by (A.15)–(A.17) characterizes $\boldsymbol{\phi}$ in a unique way and this fact allows us to introduce the mapping $\varphi \to \boldsymbol{\phi} =: \Phi(\varphi)$. However, orthogonality property (R4) does not hold for $\Phi(\varphi)$ and we cannot choose $R_{\mathsf{P}}^{\mathcal{F}}(\varphi) = \boldsymbol{\phi}$. Nonetheless, we can fix this issue by introducing a correction of the form

$$R_{\mathsf{P}}^{\mathcal{F}}(\varphi) = \boldsymbol{\phi} + \mathbf{curl}(\boldsymbol{\xi}) \tag{A.18}$$

with $\boldsymbol{\xi} \in H_0(\mathbf{curl}, \mathsf{P})$. Indeed, such a correction does not interfere with (A.15) and (A.17) (which are essential) but only with (A.16). Integrating by parts, orthogonality condition (R4) for the vector field $\boldsymbol{\phi} + \mathbf{curl}(\boldsymbol{\xi})$ reads as:

$$\forall \mathbf{a} \in \mathbb{R}^3: \quad \mathbf{a} \cdot \int_{\mathsf{P}} \boldsymbol{\phi} \times (\mathbf{x} - \mathbf{x}_{\mathsf{P}})\, dV = \int_{\mathsf{P}} \mathbf{curl}(\boldsymbol{\xi}) \cdot \left(\mathbf{a} \times (\mathbf{x} - \mathbf{x}_{\mathsf{P}})\right) dV = 2\int_{\mathsf{P}} \boldsymbol{\xi} \cdot \mathbf{a}\, dV. \tag{A.19}$$

We set $\boldsymbol{\chi} := \frac{1}{2}\int_{\mathsf{P}} \boldsymbol{\phi} \times (\mathbf{x} - \mathbf{x}_{\mathsf{P}})\, dV$ and we denote by $\boldsymbol{\lambda}$ the unique solution of the minimization problem:

$$\min_{\substack{\boldsymbol{\xi} \in H_0(\mathbf{curl}, \mathsf{P}) \\ \int_{\mathsf{P}} \boldsymbol{\xi}\, dS = \boldsymbol{\chi}}} \int_{\mathsf{P}} \left|\mathbf{curl}(\boldsymbol{\xi})\right|^2 dV. \tag{A.20}$$

The *minimal reconstruction operator* is, then, defined as $\overline{R}_{\mathsf{P}}^{\mathcal{F}}(\varphi) := \boldsymbol{\phi} + \mathbf{curl}(\boldsymbol{\lambda})$. Note that if $\varphi = \Pi^{\mathcal{F}}(\mathbf{c})$ for some constant vector field $\mathbf{c} \in \mathbb{R}^3$ then $\boldsymbol{\phi} = \mathbf{c}$ and $\boldsymbol{\lambda} = 0$. Thus, constants are left invariant.

References

[1] J.E. Aarnes, S. Krogstad, K.-A. Lie, Multiscale mixed/mimetic methods on corner-point grids, Comput. Geosci. 12 (3) (2007) 297–315.

[2] B. Andreianov, F. Boyer, F. Hubert, Discrete duality finite volume schemes for Leray–Lions type elliptic problems on general 2D-meshes, Numer. Methods Partial Differ. Equ. 23 (1) (2007) 145–195.

[3] P.F. Antonietti, L. Beirão da Veiga, M. Verani, Hierarchical a posteriori error estimators for the mimetic discretization of elliptic problems, SIAM J. Numer. Anal. 51 (2013) 654–675.

[4] P.F. Antonietti, L. Beirão da Veiga, M. Verani, A mimetic discretization of elliptic obstacle problems, Math. Comput. 82 (2013) 1379–1400.

[5] D.N. Arnold, R.S. Falk, R. Winther, Finite element exterior calculus, homological techniques, and applications, Acta Numer. 15 (2006) 1–155.
[6] D.N. Arnold, R.S. Falk, R. Winther, Finite element exterior calculus: from Hodge theory to numerical stability, Bull. Am. Math. Soc. (N.S.) 47 (2) (2010) 281–354.
[7] E.D. Batista, J.E. Castillo, Mimetic schemes on non-uniform structured meshes, Electron. Trans. Numer. Anal. 34 (2009) 152–162.
[8] L. Beirão da Veiga, A residual based error estimator for the mimetic finite difference method, Numer. Math. 108 (3) (2008) 387–406.
[9] L. Beirão da Veiga, A mimetic discretization method for linear elasticity, Math. Model. Numer. Anal. 44 (2) (2010) 231–250.
[10] L. Beirão da Veiga, F. Brezzi, A. Cangiani, G. Manzini, L.D. Marini, A. Russo, Basic principles of virtual element methods, Math. Models Methods Appl. Sci. 23 (01) (2013) 199–214.
[11] L. Beirão da Veiga, J. Droniou, G. Manzini, A unified approach to handle convection term in finite volumes and mimetic discretization methods for elliptic problems, IMA J. Numer. Anal. 31 (4) (2011) 1357–1401.
[12] L. Beirão da Veiga, V. Gyrya, K. Lipnikov, G. Manzini, Mimetic finite difference method for the Stokes problem on polygonal meshes, J. Comput. Phys. 228 (19) (2009) 7215–7232.
[13] L. Beirão da Veiga, K. Lipnikov, A mimetic discretization of the Stokes problem with selected edge bubbles, SIAM J. Sci. Comput. 32 (2) (2010) 875–893.
[14] L. Beirão da Veiga, K. Lipnikov, G. Manzini, Convergence analysis of the high-order mimetic finite difference method, Numer. Math. 113 (3) (2009) 325–356.
[15] L. Beirão da Veiga, K. Lipnikov, G. Manzini, Arbitrary order nodal mimetic discretizations of elliptic problems on polygonal meshes, SIAM J. Numer. Anal. 49 (5) (2011) 1737–1760.
[16] L. Beirão da Veiga, K. Lipnikov, G. Manzini, Error analysis for a mimetic discretization of the steady Stokes problem on polyhedral meshes, SIAM J. Numer. Anal. 48 (2011) 1419–1443.
[17] L. Beirão da Veiga, G. Manzini, An a posteriori error estimator for the mimetic finite difference approximation of elliptic problems, Int. J. Numer. Methods Eng. 76 (11) (2008) 1696–1723.
[18] L. Beirão da Veiga, G. Manzini, A higher-order formulation of the mimetic finite difference method, SIAM J. Sci. Comput. 31 (1) (2008) 732–760.
[19] L. Beirão da Veiga, D. Mora, A mimetic discretization of the Reissner–Mindlin plate bending problem, Numer. Math. 117 (3) (2011) 425–462.
[20] E. Bertolazzi, G. Manzini, A second-order maximum principle preserving finite volume method for steady convection–diffusion problems, SIAM J. Numer. Anal. 43 (5) (2005) 2172–2199.
[21] E. Bertolazzi, G. Manzini, On vertex reconstructions for cell-centered finite volume approximations of 2-D anisotropic diffusion problems, Math. Models Methods Appl. Sci. 17 (1) (2007) 1–32.
[22] P. Bochev, J.M. Hyman, Principle of mimetic discretizations of differential operators, in: D. Arnold, P. Bochev, R. Lehoucq, R. Nicolaides, M. Shashkov (Eds.), Compatible Discretizations. Proceedings of IMA Hot Topics Workshop on Compatible Discretizations, in: The IMA Volumes in Mathematics and its Applications Series, vol. 142, Springer-Verlag, 2006, pp. 89–120.
[23] D. Boffi, P. Fernandes, L. Gastaldi, I. Perugia, Computational models of electromagnetic resonators: analysis of edge element approximation, SIAM J. Numer. Anal. 36 (1999) 1264–1290.
[24] A. Bossavit, Mixed finite elements and the complex of Whitney forms, in: The Mathematics of Finite Elements and Applications, VI, Uxbridge, 1987, Academic Press, London, 1988, pp. 137–144.
[25] A. Bossavit, Whitney forms: a class of finite elements for three dimensional computation in electromagnetism, IEE Proc. 135 (1988) 493–500.
[26] A. Bossavit, Differential forms and the computation of fields and forces in electromagnetism, Eur. J. Mech. B, Fluids 10 (5) (1991) 474–488.
[27] A. Bossavit, Mixed methods and the marriage between “mixed” finite elements and boundary elements, Numer. Methods Partial Differ. Equ. 7 (4) (1991) 347–362.
[28] A. Bossavit, Computational Electromagnetism, Academic Press, San Diego, CA, 1998.
[29] F. Brezzi, A. Buffa, Innovative mimetic discretizations for electromagnetic problems, J. Comput. Appl. Mech. 234 (6) (2010) 1980–1989.
[30] F. Brezzi, M. Fortin, Mixed and Hybrid Finite Element Methods, Springer-Verlag, 1991.
[31] F. Brezzi, K. Lipnikov, M. Shashkov, Convergence of the mimetic finite difference method for diffusion problems on polyhedral meshes, SIAM J. Numer. Anal. 43 (5) (2005) 1872–1896.
[32] F. Brezzi, K. Lipnikov, V. Simoncini, A family of mimetic finite difference methods on polygonal and polyhedral meshes, Math. Models Methods Appl. Sci. 15 (10) (2005) 1533–1551.
[33] A. Buffa, Remarks on the discretization of some noncoercive operator with applications to heterogeneous Maxwell equations, SIAM J. Numer. Anal. 43 (1) (2006) 1–18.
[34] A. Buffa, S.H. Christiansen, A dual finite element complex on the barycentric refinement, Math. Comput. 76 (260) (2007) 1743–1769.
[35] J. Campbell, M. Shashkov, A tensor artificial viscosity using a mimetic finite difference algorithm, J. Comput. Phys. 172 (2001) 739–765.
[36] A. Cangiani, F. Gardini, G. Manzini, Convergence of the mimetic finite difference method for eigenvalue problems in mixed form, Comput. Methods Appl. Mech. Eng. 200 (9–12) (2011) 1150–1160.
[37] A. Cangiani, G. Manzini, Flux reconstruction and pressure post-processing in mimetic finite difference methods, Comput. Methods Appl. Mech. Eng. 197 (9–12) (2008) 933–945.
[38] A. Cangiani, G. Manzini, A. Russo, Convergence analysis of the mimetic finite difference method for elliptic problems, SIAM J. Numer. Anal. 47 (4) (2009) 2612–2637.
[39] J. Castillo, J. Hyman, M. Shashkov, S. Steinberg, The sensitivity and accuracy of fourth order finite-difference schemes on nonuniform grids in one dimension, Comput. Math. Appl. 30 (8) (1995) 41–55.
[40] J. Castillo, J. Hyman, M. Shashkov, S. Steinberg, Fourth- and sixth-order conservative finite-difference approximations of the divergence and gradient, Appl. Numer. Math. 37 (2001) 171–187.
[41] J.E. Castillo, R.D. Grone, A matrix analysis approach to higher-order approximations for divergence and gradients satisfying a global conservation law, SIAM J. Matrix Anal. Appl. 25 (1) (2003) 128–142.
[42] J.E. Castillo, J.M. Hyman, M.J. Shashkov, S. Steinberg, High-order mimetic finite difference methods on nonuniform grids, in: A.V. Ilin, L.R. Scott (Eds.), Houston J. Math. (Special Issue) (1995) 347–361.
[43] P.G. Ciarlet, The Finite Element Method for Elliptic Problems, North-Holland, Amsterdam, 1978.
[44] M. Costabel, M. Dauge, Maxwell eigenmodes in tensor product domain, 2006. Available at http://perso.univ-rennes1.fr/monique.dauge/publis/CoDa06MaxTens.pdf.
[45] Y. Coudière, G. Manzini, The discrete duality finite volume method for convection–diffusion problems, SIAM J. Numer. Anal. 47 (6) (2010) 4163–4192.
[46] M. Dauge, Benchmark computations for Maxwell equations. Available at http://perso.univ-rennes1.fr/monique.dauge/benchmax.html.
[47] J. Dodziuk, Finite-difference approach to the Hodge theory of harmonic forms, Am. J. Math. 98 (1) (1976) 79–104.
[48] K. Domelevo, P. Omnes, A finite volume method for the Laplace equation on almost arbitrary two-dimensional grids, M2AN Math. Model. Numer. Anal. 39 (6) (2005) 1203–1249.
[49] R. Eymard, G. Henry, R. Herbin, F. Hubert, R. Klöfkorn, G. Manzini, 3D benchmark on discretization schemes for anisotropic diffusion problems on general grids, in: J. Fořt, J. Fürst, J. Halama, R. Herbin, F. Hubert (Eds.), FVCA6: Finite Volume for Complex Applications VI, Prague, Czech Republic, March 2011, in: Springer Proceedings in Mathematics, Springer, 2011.

[50] C. Gallo, G. Manzini, 2-D numerical modeling of bioremediation in heterogeneous saturated soils, Transp. Porous Media 31 (1) (1998) 67–88.
[51] C. Gallo, G. Manzini, A mixed finite element/finite volume approach for solving biodegradation transport in groundwater, Int. J. Numer. Methods Fluids 26 (5) (1998) 533–556.
[52] P.W. Gross, P.R. Kotiuga, Data structures for geometric and topological aspects of finite element algorithms, in: F.L. Teixeira (Ed.), Geometric Methods in Computational Electromagnetics, PIER 32, EMW Publishing, Cambridge, MA, 2001, pp. 151–169.
[53] P.W. Gross, P.R. Kotiuga, Finite element-based algorithms to make cuts for magnetic scalar potentials: topological constraints and computational complexity, in: F.L. Teixeira (Ed.), Geometric Methods in Computational Electromagnetics, PIER 32, EMW Publishing, Cambridge, MA, 2001, pp. 207–245.
[54] V. Gyrya, K. Lipnikov, High-order mimetic finite difference method for diffusion problems on polygonal meshes, J. Comput. Phys. 227 (2008) 8841–8854.
[55] R. Hiptmair, Canonical construction of finite elements, Math. Comput. 68 (228) (1999) 1325–1346.
[56] R. Hiptmair, Finite elements in computational electromagnetism, Acta Numer. 11 (2002) 237–339.
[57] J.M. Hyman, J.C. Scovel, Deriving mimetic difference approximations to differential operators using algebraic topology, Los Alamos National Laboratory, Los Alamos, NM, 1988.
[58] J.M. Hyman, M.J. Shashkov, Adjoint operators for the natural discretizations of the divergence, gradient and curl on logically rectangular grids, Appl. Numer. Math. 25 (4) (1997) 413–442.
[59] J.M. Hyman, M.J. Shashkov, Natural discretizations for the divergence, gradient, and curl on logically rectangular grids, Comput. Math. Appl. 33 (4) (1997) 81–104.
[60] J.M. Hyman, M.J. Shashkov, Mimetic finite difference methods for Maxwell's equations and the equations of magnetic diffusion, in: F.L. Teixeira (Ed.), Geometric Methods in Computational Electromagnetics, PIER 32, EMW Publishing, Cambridge, MA, 2001, pp. 89–121.
[61] J.M. Hyman, M.J. Shashkov, S. Steinberg, The numerical solution of diffusion problems in strongly heterogeneous non-isotropic materials, J. Comput. Phys. 132 (1) (1997) 130–148.
[62] J.M. Hyman, M.J. Shashkov, S. Steinberg, The effect of inner products for discrete vector fields on the accuracy of mimetic finite difference methods, Comput. Math. Appl. 42 (12) (2001) 1527–1547.
[63] K. Lipnikov, G. Manzini, F. Brezzi, A. Buffa, The mimetic finite difference method for 3D magnetostatics fields problems, J. Comput. Phys. 230 (2) (2011) 305–328.
[64] K. Lipnikov, G. Manzini, D. Svyatskiy, Analysis of the monotonicity conditions in the mimetic finite difference method for elliptic problems, J. Comput. Phys. 230 (7) (2011) 2620–2642.
[65] K. Lipnikov, J. Morel, M. Shashkov, Mimetic finite difference methods for diffusion equations on non-orthogonal non-conformal meshes, J. Comput. Phys. 199 (2004).
[66] K. Lipnikov, J.D. Moulton, D. Svyatskiy, A multilevel multiscale mimetic (M^3) method for two-phase flows in porous media, J. Comput. Phys. 227 (2008) 6727–6753.
[67] G. Manzini, A. Russo, A finite volume method for advection–diffusion problems in convection-dominated regimes, Comput. Methods Appl. Mech. Eng. 197 (13–16) (2008) 1242–1261.
[68] L. Margolin, M. Shashkov, P. Smolarkiewicz, A discrete operator calculus for finite difference approximations, Comput. Methods Appl. Mech. Eng. 187 (2000) 365–383.
[69] C. Mattiussi, An analysis of finite volume, finite element, and finite difference methods using some concepts from algebraic topology, J. Comput. Phys. 133 (2) (1997) 289–309.
[70] C. Mattiussi, The finite volume, finite difference and finite elements methods as numerical methods for physical field problems, Online publication available at: http://www.scribd.com, 2000.
[71] J. Morel, R. Roberts, M. Shashkov, A local support-operators diffusion discretization scheme for quadrilateral $r-z$ meshes, J. Comput. Phys. 144 (1998) 17–51.
[72] J. Munkres, Elements of Algebraic Topology, 2nd edition, Prentice Hall, January 1984.
[73] R.A. Nicolaides, K.A. Trapp, Covolume discretizations of differential forms, in: D. Arnold, P. Bochev, R. Lehoucq, R. Nicolaides, M. Shashkov (Eds.), Compatible Discretizations. Proceedings of IMA Hot Topics Workshop on Compatible Discretizations, in: The IMA Volumes in Mathematics and its Applications Series, vol. 142, Springer-Verlag, 2006, pp. 161–172.
[74] R.A. Nicolaides, D.-Q. Wang, Convergence analysis of a covolume scheme for Maxwell's equations in three dimensions, Math. Comput. 67 (223) (1998) 947–963.
[75] R.A. Nicolaides, Direct discretization of planar div–curl problems, SIAM J. Numer. Anal. 29 (1) (1992) 32–56.
[76] R.A. Nicolaides, X. Wu, Covolume solutions of three-dimensional div–curl equations, SIAM J. Numer. Anal. 34 (6) (1997) 2195–2203.
[77] J.B. Perot, V. Subramanian, Discrete calculus methods for diffusion, J. Comput. Phys. 224 (1) (2007) 59–81.
[78] J.B. Perot, D. Vidovic, P. Wesseling, Mimetic reconstructions of vectors, in: D. Arnold, P. Bochev, R. Lehoucq, R. Nicolaides, M. Shashkov (Eds.), Compatible Discretizations. Proceedings of IMA Hot Topics Workshop on Compatible Discretizations, in: The IMA Volumes in Mathematics and its Applications Series, vol. 142, Springer-Verlag, 2006, pp. 173–188.
[79] N. Robidoux, Numerical solution of the steady diffusion equation with discontinuous coefficients, PhD thesis, University of New Mexico, Albuquerque, NM, May 2002.
[80] M. Shashkov, S. Steinberg, Support-operator finite-difference algorithms for general elliptic problems, J. Comput. Phys. 118 (1) (1995) 131–151.
[81] M. Shashkov, S. Steinberg, Solving diffusion equations with rough coefficients in rough grids, J. Comput. Phys. 129 (2) (1996) 383–405.
[82] J.R. Shewchuk, Triangle: Engineering a 2D quality mesh generator and Delaunay triangulator, in: Ming C. Lin, Dinesh Manocha (Eds.), Applied Computational Geometry: Towards Geometric Engineering, in: Lecture Notes in Computer Science, vol. 1148, Springer-Verlag, Berlin, May 1996, pp. 203–222.
[83] J.R. Shewchuk, Delaunay refinement algorithms for triangular mesh generation, Comput. Geom. 22 (1–3) (May 2002) 21–74.
[84] H. Si, A quality tetrahedral mesh generator and a 3D Delaunay triangulator, Weierstrass Institute for Applied Analysis and Stochastics (WIAS), http://wias-berlin.de/software/tetgen.
[85] E. Tonti, A mathematical model for physical theories. I, Atti Accad. Naz. Lincei, Rend. Cl. Sci. Fis. Mat. Nat. 8 (52) (1972) 175–181;
E. Tonti, A mathematical model for physical theories. II, Atti Accad. Naz. Lincei, Rend. Cl. Sci. Fis. Mat. Nat. 8 (52) (1972) 350–356.
[86] E. Tonti, On the formal structure of the physical theories, in: Quaderno dei Gruppi di Ricerca Matematica del CNR, Consiglio Nazionale delle Ricerche, Istituto di Matematica del Politecnico di Milano, 1975. Available online at: http://www.dic.univ.trieste.it/perspage/tonti/DEPOSITO/CNR.pdf.
[87] K.A. Trapp, Inner products in covolume and mimetic methods, M2AN Math. Model. Numer. Anal. 42 (2008) 941–959.
[88] H. Whitney, Geometric Integration Theory, Princeton University Press, Princeton, NJ, 1957.
[89] K.S. Yee, Numerical solution of initial boundary value problems involving Maxwell's equations in isotropic media, IEEE Trans. Antennas Propag. AP-14 (3) (1966) 302–307.